Final Report *June 1971*

THE KINETICS OF REACTION OF THE BY-PRODUCTS OF ABLATIVE MATERIALS AT HIGH TEMPERATURES AND THE RATE OF HEAT TRANSFER BETWEEN HOT SURFACES AND REACTIVE GASES

By: G. N. SPOKES, P. C. BEADLE, N. A. GAC,
D. M. GOLDEN, K. D. KING, and S. W. BENSON

Prepared for:

NATIONAL AERONAUTICS AND SPACE ADMINISTRATION
AMES RESEARCH CENTER
MOFFETT FIELD, CALIFORNIA 94035

CONTRACT NAS7-472

STANFORD RESEARCH INSTITUTE
Menlo Park, California 94025 · U.S.A.

STANFORD RESEARCH INSTITUTE
Menlo Park, California 94025 • U.S.A.

Final Report *June 1971*

THE KINETICS OF REACTION OF THE BY-PRODUCTS OF ABLATIVE MATERIALS AT HIGH TEMPERATURES AND THE RATE OF HEAT TRANSFER BETWEEN HOT SURFACES AND REACTIVE GASES

By: G. N. SPOKES, P. C. BEADLE, N. A. GAC,
D. M. GOLDEN, K. D. KING, and S. W. BENSON

Prepared for:

NATIONAL AERONAUTICS AND SPACE ADMINISTRATION
AMES RESEARCH CENTER
MOFFETT FIELD, CALIFORNIA 94035

CONTRACT NAS7-472

SRI Project 6098

Approved by:

SIDNEY W. BENSON, *Group Manager*
Thermochemistry and Chemical Kinetics

M. E. HILL, *Director*
Physical Sciences, Chemistry Laboratory

C. J. COOK, *Executive Director*
Physical Sciences Division

Copy No. 26

PREFACE

The work reported here is the result of the efforts of many contributors. The program was under the general supervision of Dr. Sidney W. Benson, Manager of the Thermochemistry and Chemical Kinetics Group in the Chemistry Laboratory. Dr. Benson also contributed directly to the work. Dr. G. Neil Spokes and Dr. David M. Golden were project leaders.

Postdoctoral research fellows who contributed to the program include: Dr. Peter C. Beadle, Dr. Norman A. Gac,* Dr. Keith D. King,† and Dr. Richard K. Solly.**

Roland S. Jackson was responsible for much of the technical work on the project.

The authors of this report wish to thank Elaine Adkins who so willingly labored over the typing of the various manuscripts generated by the group during the course of the work.

The work was carried out in the Stanford Research Institute (SRI) Chemistry Laboratory, M. E. Hill, Director. The Chemistry Laboratory is part of the Physical Sciences Division of which Dr. Charles J. Cook is Executive Director.

---

*Present Address: Raychem Corporation, 300 Constitution Drive, Menlo Park, California 94025.

†Present Address: Department of Chemical Engineering, University of Adelaide, Adelaide, S.A. 5001, Australia.

**Present Address: Department of Physical Chemistry, University of New South Wales, Box 1, P.O. Kensington, New South Wales, 2033, Australia.

CONTENTS

FIGURES

FIGURES (Continued)

TABLES

I INTRODUCTION

The use by NASA of charring ablative heat shields on reentry capsules for manned space flight is now standard practice. The first manned capsules to use these protective heat shields are currently on display in the Smithsonian Institution in Washington, D.C. The proposed Space Shuttle will include some ablative materials as part of its thermal protection system.

The purpose of this SRI program was to add to the stock of basic knowledge that may be needed by chemists and engineers in their solution of future heat shield design problems. The program has covered the time period May 1966 to May 1971. During this time we have examined in detail the fundamentals of many of the significant phenomena that occur in the heat shield during the reentry phase.

Much of the research generated under the support of this contract has already appeared in the open literature. To be consistent with NASA policy regarding avoidance of dual publication, we will not attempt to again present this material in detail in this report. We have included summaries of published work and additional details that have not yet been reported. In addition to this, we present the results of work not yet submitted for publication in professional journals.

Objectives

The objectives of the research were to perform laboratory experiments to enhance understanding of the fundamental mechanisms of heterogeneous and homogeneous chemical reactions taking place during the

ablative processes that accompany the reentry of manned space vehicles into planetary atmospheres.

The intent of the program was to examine the fundamental mechanisms of those chemical reactions believed to be important in the thermal degradation of ablative plastic heat shield materials.[1] Our concern has been primarily with the gases that are evolved as a consequence of thermal degradation of the plastic. Our knowledge of the details of the chemical behavior of gases in the char zone is sparse.[2] Several workers have studied the evolution of gases by polymers as they are pyrolyzed.[3] Some work has been done on the reactions of the gases leaving a char surface and mingling with hot air in a boundary layer. Heicklen[4] has

---

[1]The general problem of ablative plastics was discussed at an American Chemical Society symposium in San Francisco in March 1968. The proceedings of this symposium are reported in J. Macromol. Sci.-Chem., A3, 325, 573 (1969).

[2]A common working assumption is that the gases evolved by the ablative materials are either chemically frozen or are in equilibrium at some temperature. April et al. have considered partial reaction kinetics but have ignored bimolecular reactions involving free radicals. Heterogeneous reactions cannot be characterized, but our evidence is that they can be very fast (see Section VI this report). G. C. April, R. W. Pike, and E. G. Del Valli, J. Macromol. Sci.-Chem., A3, 685 (1969); J. D. Seader, J. F. Larsen, R. W. Thompson, and J. D. Chidley, J. Spacecraft and Products, 5, 1362 (1968).

[3]E. M. Liston, J. Macromol. Sci.-Chem., A3, 705 (1969) and L.-H. Lee, J. Polym. Sci., A3, 859 (1965). C. A. Gaudin, F. M. Wachi, and D. E. Gilmartin, "Mass-thermal Method for Studying Ablation Polymer Degradation Mechanisms," U.S. Clearing House, Federal Scientific Technical Information, 1968, AD-670535. N. A. Gac, G. N. Spokes, and S. W. Benson, J. Polym. Sci., A1, 593 (1970).

[4]J. Heicklen, "Gas Phase Chemistry of Reaction," Aerospace Corporation Report No. TDR-669(6250-40)-7 on Contract AF-04(695)-669, May 1966.

considered the general gas-phase reactions problem related to ablation. Several workers[5] have considered the reaction between oxygen and char layer of charring ablative materials as affected by gases that are evolved by the ablative process.

The major gaps in our knowledge lie in understanding the chemistry that takes place in the zone between the decomposing virgin polymer and the char surface. The general objectives of our program were thus to study the reactions of hydrocarbons and other gases in contact with char-like materials and char-support materials including carbon and with quartz, metals, and other refractories that are sometimes used to strengthen the heat shield. The reactions that occur in chars must occur in the pores of the char. Gases will make very many collisions with the pore walls. In our systems we have simulated the pore experimentally by using a tube of 2- to 5-cm diameter. The number of gas-gas collisions, however, has been reduced by going to very low pressure. Since we expect that the walls in the char pores become more reactive as temperatures rise, we have made studies at temperatures up to 1900°K.

---

[5]R. M. Wakefield, G. H. Lundell, R. M. Dickey, J. Spacecraft and Rockets, 6, 122 (1968); J. R. Roland and M. C. Gischke, AIAA Journal, 8, 1516 (1970); D. E. Rosner and H. D. Allendorf, AIAA Journal, 6, 650 (1968); W. D. Brown, C. W. Strand, and R. K. Clark, "Effect of Chemical State of Pyrolysis Gases on the Heat Shield Mass," NASA Technical Note TND-4975, December 1968; G. D. Walburg, "Analytical Study of Diffusion-controlled Char Oxidation and Its Effects on Steady State Ablation of Plastic Materials," NASA Technical Report TRR-244, July 1966.

We have also studied chemical reactions of gases other than those connected with charring ablators. For example, we have studied pyrolysis of C_2F_4 (of importance in Teflon ablation). We have studied reactions of oxygen with char and have examined reactions of importance in combustion and in flames. We have also measured the rate constants of chemical reactions that involve moieties of fundamental importance in the general problems of hydrocarbon pyrolysis.

The Rationale for Use of Very Low-Pressure Pyrolysis as a Tool for Simulation of Gas Flow in Charring Ablative Heat Shields

The chief tool that we have used to explore the fundamental mechanisms taking place during ablative reentry of manned space vehicles has been a newly developed technique known as very low-pressure pyrolysis (VLPP). Figure 1 illustrates the basis for the simulation. The chemical reactions that we study in our low-pressure reactors are the same as those taking place in the pores of the char layer even though there is a big difference in gas pressure.

Figure 2 shows a model that we have developed to explain qualitatively the mode of operation of the ablative heat shield. Gases are evolved by pyrolysis of the polymer of the heat shield at some depth inside the surface. The gases pass through the porous char layer to mix with shock-heated air in the boundary layer. We will describe in more detail later in the report other features shown in Figure 2.

We have attempted to break down into its component parts the operation of the charring ablative heat shield so as to make the system more amenable to analysis. Let us ignore for the moment the start-up

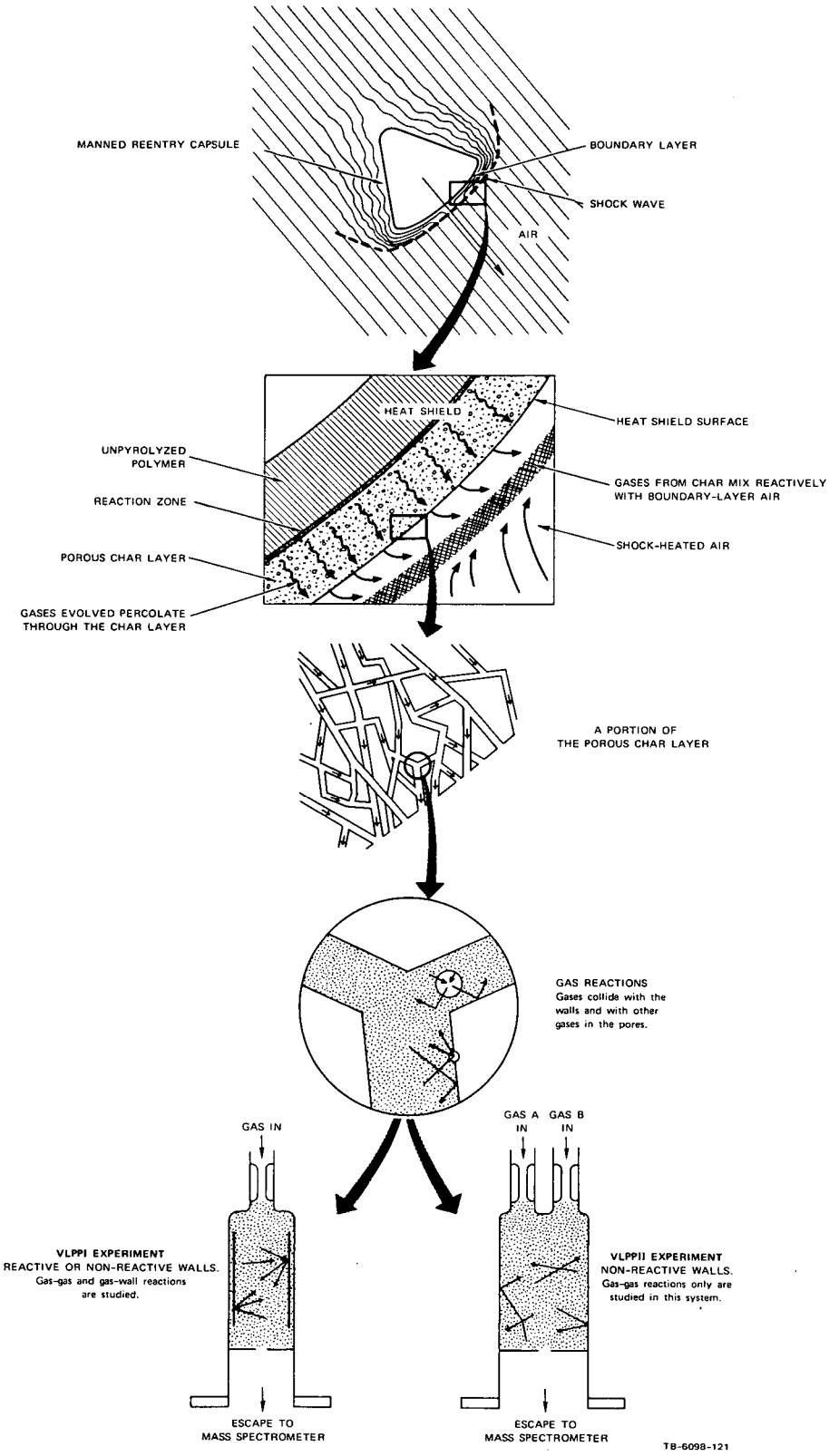

FIGURE 1 LABORATORY PORE SIMULATION EXPERIMENTS VLPP-I AND VLPP-II

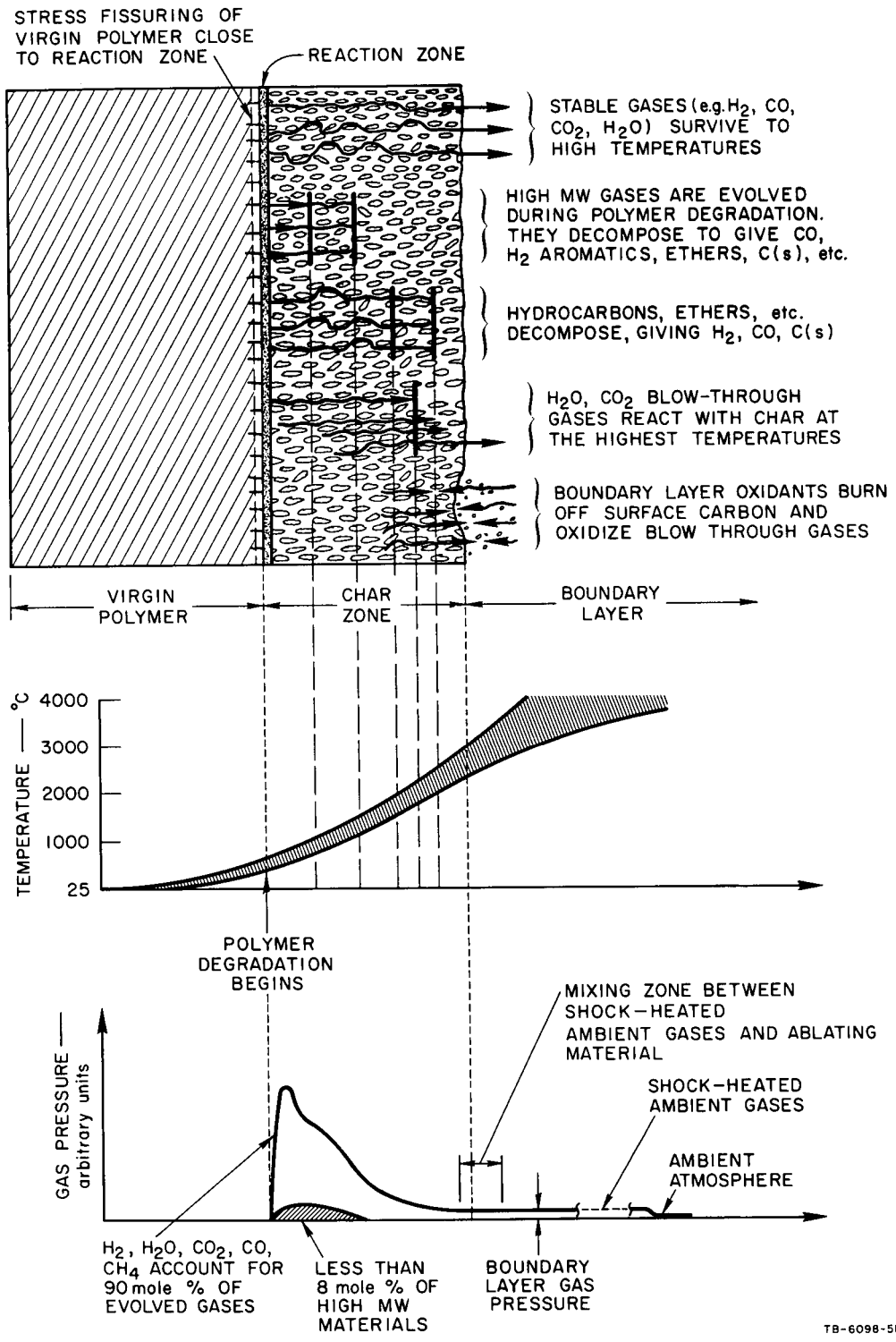

FIGURE 2 SCHEMATIC MODEL OF A CHAR-FORMING ABLATIVE HEAT SHIELD. No account is taken of the effects of including glass or quartz fibers.

transient and consider the steady state ablation process as illustrated in Figure 2. The char surface is heated by conduction, by radiation, and by chemical heat release at the char surface. Gases that percolate through the char are pyrolyzed as they travel from their point of generation at the polymer reaction zone to the surface of the char. At the char surface the emerging gases are oxidized as they mix with the hot boundary layer air. During their passage from their point of generation the gases change composition markedly. As will be detailed later, we have shown that the gases start out primarily as high-molecular-weight tarry or monomer-like substances. Pyrolysis and heterogeneous reaction change these substances to carbon, hydrogen, carbon monoxide, lower hydrocarbons, and aromatics during their passage to higher temperature zones in the char. The carbon that is deposited as a result of gas pyrolysis may be expected to lead to partial pore-clogging--a phenomenon that may in extreme cases lead to total sealing off of the char layer. (This may lead to the highly disruptive spallation of the char layer reported by Liston.[6])

To learn the natures of the gases involved in the polymer pyrolysis, we studied the vacuum pyrolysis of an epoxy novolac (DEN438 cured by NMA). The gases evolved during this pyrolysis were condensed and analyzed in detail. Our results guided our choice of experimental gases for subsequent study.

---

[6]E. M. Liston, "Experimental and Analytical Studies of Radiation-Only Pyrolysis of Model Char-forming Polymers." Final Report on Contract NAS7-341, December 1968.

The processes that occur under ablative conditions may be divided into several categories:

- Anaerobic, high-temperature decomposition of the polymer to yield char and volatiles.
- Pyrolysis of the volatile materials by homogeneous and heterogeneous chemical reactions to yield carbon deposits and lower MW volatiles.
- Graphitization of the char and of the charry deposits caused by in-pore pyrolysis of blow-through gases.
- Chemical reactions of the char and gases with support materials.
- Interaction of boundary layer gases with char layer and with pyrolysis gases:
  - — Combustion of char
  - — Spallation of char
  - — Combustion of pyrolysis gases.
- Other ablative systems.
- Other high-temperature systems.

Let us use a few thumbnail calculations to help us understand the ablation process in broad outline.

The surface recession rate of an epoxy novolac ablating material used on the polymer heat shield may be as high as 0.025 cm/sec. Gas generation by this material is about 250 $cm^3/sec/cm^2$ at 2000^oK at

1/2 atmosphere pressure.[7] The Apollo vehicle speeds into the earth's atmosphere at, say 4 km/sec, to give a boundary layer pressure of about 1/2 atmosphere. The amount of air swept per second is about 3000 $cm^3/sec/cm^2$.[8] The emitted volume of gas is thus a significant fraction (10%) of the boundary layer gas flow.[9]

As a consequence of reactions with hydrocarbons present in the ablative by-product gases, we can expect that the atomic oxygen in the boundary layer close to the char surface will be nearly zero. Because of this, chemical erosion of the char layer will be less than would be the case if the char layer were ablating without blow-through gases such as hydrocarbon (Rosner and coworkers[10] have pointed out that oxygen atoms attack carbon with very high probability). Some molecular oxygen may survive the burning zone and react with the char. We have studied the reactions of molecular oxygen with typical chars and find the reaction rate is much higher than with graphitized material.

---

[7]Based on 20% char yield and excluding CO produced as a result of char oxidation. Products are assumed to be H_2 - 5% (by weight), CH_4 - 2%, H_2O - 1.5%, C_2H_2 - 13.2%, C_2H_4 - 4.2%, C_2H_6 - 1.3%, CO - 42%, CO_2 - 22%, C_3^+ - 7%, C_6H_6 - 1.7%. Gas composition is based on results reported in footnote 6.

[8]Based on 120-fold shock compression of gas in the boundary layer.

[9]A stoichiometric mixture for combustion to CO_2 and H_2O would be 8.3 parts by volume of air to 1 part evolved gases.

[10]D. E. Rosner and H. D. Allendorf, AIAA Journal, 6, 650 (1968).

Summary

We have explored a large variety of reactions and have done work closely related to the practical problems. As a result of our work we have a better understanding of some of these fundamental reactions. It is clear that in each of the several zones of the ablative layer of a reentry heat shield different chemical phenomena will be significant. Our experimental data have given qualitative and quantitative evidence about these phenomena. Significant new ideas have emerged from this work, and many breakthroughs have been achieved. Some of these breakthroughs are summarized here.

The first relates to our studies of the vacuum pyrolysis of DEN438 epoxy novolac polymer. Our findings showed that a very significant amount of the weight loss occurring in the pyrolyzing polymer was due to the elimination of high-molecular-weight tarry polymers. These polymers were found to carbonize with great ease during subsequent pyrolysis reactions. These high-molecular-weight materials accounted for two-thirds of the weight loss of the decomposing polymer.

A second breakthrough occurred as we began our studies of the chemical kinetics of reaction of gases at temperatures up to 1900°K. We found that very stable hydrocarbons, such as benzene and ethylene, underwent very rapid heterogeneous reactions at temperatures above 1600°K. The results showed that a mechanism existed for the achievement of equilibrium between gas and char as gases produced by pyrolysis of virgin polymer percolated through the porous char layer toward the very high-temperature surface. Our previous calculations, based on homogeneous kinetics, indicated that there was little hope of achieving equilibrium

in these gases. We should note that our experiments were carried out at a much lower pressure than those expected to be found in the practical case. For this reason it would be unwise to extrapolate our observed rate constants to high-pressure rate constants without careful further examination of the order of the reaction at much higher pressures. We find, for example, that during heterogeneous reaction between oxygen and chars the reaction is lower than first order in oxygen.

Our studies have also shown that at temperatures above 1600°K hydrocarbons such as benzene, ethylene, and ethane reacted with refractory oxides such as quartz and alumina at a very rapid rate (faster than 0.001 per collision). Products included carbon monoxide. The rapid attack by hydrocarbons on these refractory materials may be significant under ablative conditions. The high endothermicity of these reactions may make them desirable as additional heat blocking reactions for practical ablative materials.

We have achieved some significant breakthroughs as a result of our studies of the fundamental aspects of the basics of ablative chemistry. Our values of the thermodynamic properties of important chemical moieties, such as the free methyl radical and the very important allyl radical, have received publicity.[11]

---

[11]Chem. Eng. News, "Tool Predicts Yields," March 1, 1971, p. 5.

II VERY LOW-PRESSURE PYROLYSIS (VLPP)

The use of VLPP as an experimental tool for the study of the basics of chemical reactions has been pioneered by the authors during the last six years at SRI. The funding for this work was derived in large part from a continuing contract between SRI and NASA. At the same time that we have been bringing this important new chemical kinetic tool to bear on problems of interest to NASA, we have been able to advance the VLPP technique to a high general level of applicability to many new problems.

The development of VLPP has made an important change in the state of the kinetic art. It now provides the general, exciting possibility of studying, in a fairly direct way, the absolute rate constants for large numbers of elementary gas-phase reactions. We have studied unimolecular, radical-molecule, radical-radical, molecule-molecule, and molecule-surface reactions.[12,13]

The reaction vessel is an electrically heated cylindrical Knudsen cell made of quartz, sapphire, or other appropriate material (see Figure 3). Reactant flows into it through a capillary leak. The cell has an escape aperture leading to a mass spectrometer detector. The flow conditions are such that the pressure inside the cell is $\leq$ 10 microns,

---

[12]a. G. N. Spokes and S. W. Benson, J. Amer. Chem. Soc., 89, 6030 (1967);
b. S. W. Benson and G. N. Spokes, J. Amer. Chem. Soc., 89, 2525 (1967);
c. S. W. Benson and G. N. Spokes, 11th Symposium (International) on Combustion, 1967, pp. 95-103;
d. S. W. Benson and G. N. Spokes, J. Phys. Chem., 72, 1182 (1968).

[13]a. D. M. Golden, N. A. Gac, and S. W. Benson, J. Amer. Chem. Soc., 91, 2136 (1969);
b. D. M. Golden, N. A. Gac, and S. W. Benson, J. Amer. Chem. Soc., 91, 3091 (1969);
c. See, also, Chem. Eng. News, April 15, 1968, p. 45 and Chem. Eng. News, November 23, 1970, pp. 31, 32.

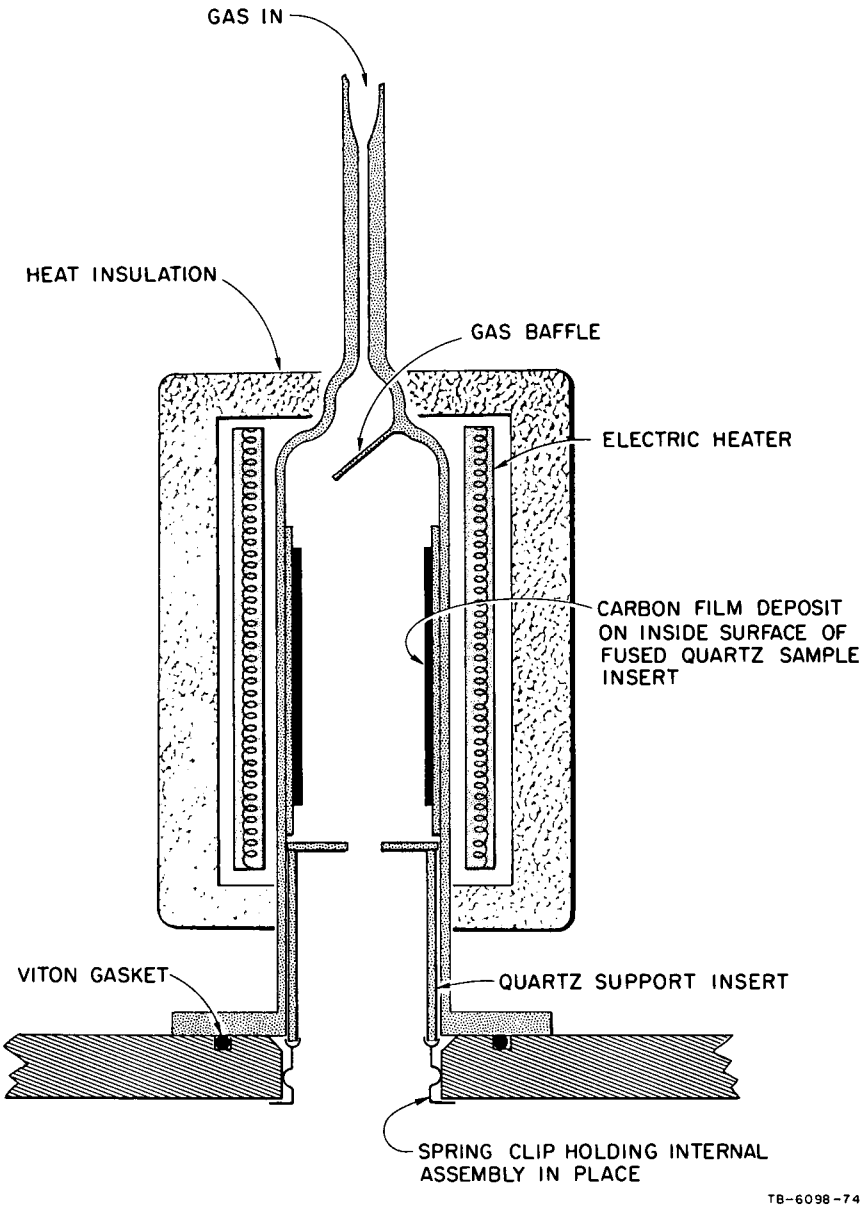

FIGURE 3 ALL-QUARTZ VLPP REACTOR FOR STUDIES OF HOMOGENEOUS AND HETEROGENEOUS CHEMICAL REACTIONS AT LOW PRESSURE

so that the mean free path is $\geq$ the cell diameter. Most collisions, thus, take place between gas molecules and the vessel walls.

In a typical experiment, gas-phase molecules will make on the average Z collisions with the vessel walls before escaping; Z is equal to the ratio of the area of the escape orifice to the total area of the vessel wall. By using different escape apertures, we can vary A from 20 to 20,000 wall collisions.

Unimolecular Reactions

The method lends itself uniquely to the study of unimolecular reactions in that the initial product of the reaction can be detected. We were able to demonstrate that the pyrolyses of both 1- and 2-nitropropane yield the same products,[12a] namely, $HNO_2 + C_3H_6$ in a single step, and not free radicals. This settled a controversy of some 25 years standing.

In similar fashion, we were able to demonstrate that the pyrolysis of $MeNH\text{-}NH_2$ does not give radicals but gives, instead, $CH_2{=}NH + NH_3$ in a concerted step. This work and some pyrolysis work on $\emptyset CH_2NH_2$, $\emptyset CH_2NHCH_3$, and $\emptyset CH_2N(CH_3)_2$, which give amino radicals, have led to a drastic revision of the N-H bond strengths in amines and of the N-N bond strengths in hydrazines.[14] It appears at the moment that the published details of oxidation of NH_3, amines, and hydrazines are in need of serious change; none of the published kinetic schemes is correct.

[14] a. David M. Golden, Richard K. Solly, and Norman A. Gac, Special Report No. AFRPL-TR-132-70, AF Contract F04611-69-C-0096, December 1, 1970.

b. R. K. Solly, D. M. Golden, and S. W. Benson, paper presented at American Chemical Society Meeting, Chicago, 1969.

The kinetics of VLPP follow the characteristics of a well-stirred flow reactor. Because of the low pressure, it takes from 1 to 10 collisions times ($\sim 10^{-4}$ sec) to achieve complete mixing of reactants, products, and any independently added gases in the reactor. These mixing times are always less than 1% of the residence times used and, hence, negligible.

Unimolecular rate data obtained with VLPP are usually in the fall-off, pressure-dependent region. We have demonstrated[15] that the use of the appropriate theory permits us to obtain high-pressure Arrhenius parameters from such data with excellent precision (E_{act} to within ± 1 kcal). This, of course, has no effect on bimolecular reactions.

Early fears were expressed that in VLPP the walls would behave catalytically. We pointed out then, and have since amply confirmed for many very "wall-sensitive" reactions, that at the temperatures and residence times employed, quartz and carbon-covered walls act as inert third bodies, and most catalytic reactions are too "slow" to be seen.[12]

Bimolecular Reactions

By introducing a second reactant gas, either premixed with the first gas or independently through a second inlet (Figure 4), it is possible to

[15]Keith D. King, David M. Golden, G. Neil Spokes, and Sidney W. Benson, Int. J. Chem. Kinetics, 3, 0000 (1971).

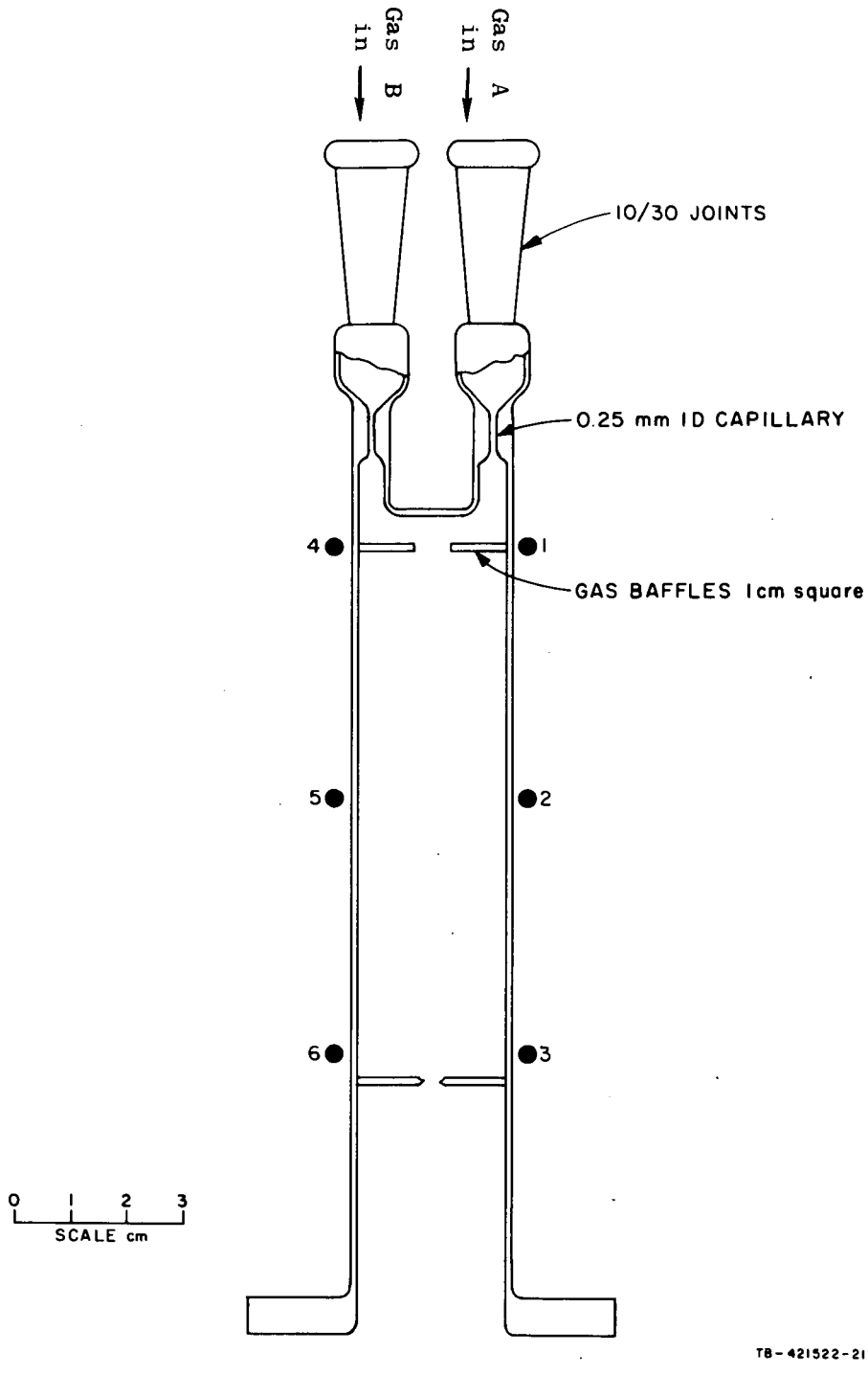

FIGURE 4 VLPP KNUDSEN CELL FOR STUDYING BIMOLECULAR REACTIONS

study very rapid bimolecular reactions. For example, in a recent study we were able to measure the absolute rate constant for the reaction:[13b]

$$CH_3 + DBr \rightarrow CH_3D + Br$$

Since the reverse reaction had been measured, this permitted us to verify to $\pm$ 1 kcal the $\Delta H_f^0(CH_3)$ and the absolute entropy of the CH_3 radical. Both of these were in excellent agreement with independent studies and represented the first direct experimental measurements of ΔH_f^0 and S^0 for a complex organic radical.

In a similar fashion, we were able to study the reactions of CH_3 with added O_2 and showed that from 800 to 1500°K in 10^4 collisions there was no measurable reaction. This put a lower limit of 24 kcal for the often proposed, but suspect, reaction $CH_3 + O_2 \rightarrow CH_2O + OH$. This value of 24 kcal completely rules out this reaction as a significant flame step. The competing step $CH_3 + O_2 \rightarrow CH_3O + O$ with E_a = 29 kcal has a higher A-factor and should be faster.

By adding NO_2, it was possible to show that, over the same temperature range, $CH_3 + NO_2 \rightarrow CH_3O + NO$ occurs at every tenth collision; hence, $E_{act} = 0$!

The same study also showed that allyl radicals did not react with O_2 from 800 to 1300°K in 10^4 collisions but did react with NO_2.

In a very recent study,[13a] allyl radicals were generated from the pyrolysis of biallyl oxalate, and it was possible to study the reversible formation of biallyl:

$$2 \text{ allyl} \underset{}{\overset{1}{\rightleftharpoons}} \text{biallyl}$$

In this way the equilibrium constant k_1 was measured at 800 and 1100°K. From this it was possible to obtain the heat of formation and entropy of allyl radicals, again in excellent agreement with independent and very different studies.[13a]

Among the most impressive results achieved with VLPP has been the recent, direct observation of two competing unimolecular pathways, one radical and one molecular. Indirect evidence for such events from product and rate studies has been available for some time. However, it has never been possible to obtain accurate measurements of the two pathways separately because of the chemical complexity of the secondary reactions. In the present instance, n-propyl iodide decomposes as follows:

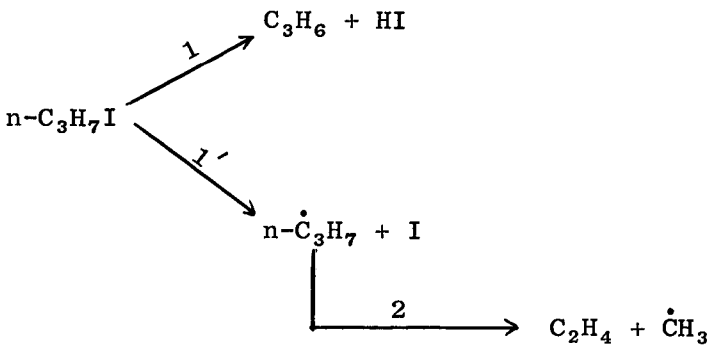

By running the experiment at temperatures and residence times so that n-$\dot{C}_3H_7$ always decompose into C_2H_4 before escaping from the reactor, we can use C_2H_4 and C_3H_6 as measures of the two competing paths. Mass balances check out very well for such an assumption. Perhaps the most interesting feature of the experiment is that each reaction perturbs the distribution of energized states for the other pathway. This result follows directly from the treatment of the data,

which shows anomalous falloff in rates of decomposition at higher temperatures.[16]

An additional breakthrough has been the kinetic work done at temperatures in excess of 1000°C. Careful reactor design has permitted us to extend the range of meaningful chemical kinetic experiments up to 1900°K. Severe problems of materials reactivity were overcome and very significant results achieved in this new temperature region. Details are presented in the next section.

[16]K. D. King, D. M. Golden, and S. W. Benson, to be published. Presented at the American Chemical Society Meeting in Los Angeles, Spring, 1971.

III APPARATUS

The VLPP work reported here has been carried out in two basic apparatuses, VLPP-1 (with modifications to allow measurements of high-temperature reactions) and VLPP-II. The construction of the two systems (and modifications) and the experimental procedures are summarized in this section.

VLPP-I

The simpler of the two basic apparatuses that have been used for this work is known as VLPP-I. It was the first of the apparatuses built for these studies. The basic components were purchased with SRI funds although the gas-handling apparatus was constructed with funds provided under this contract. A schematic diagram is shown in Figure 5.

The following series of sketches and photographs of VLPP-I illustrates the basic system. Modifications have been made as needed, but the flexibility of the original design has mitigated the need for appreciable changes since its construction in 1967.

Features of VLPP-I are:

- Three separate gas-handling channels are available for simultaneous introduction of two or three gases into the mass spectrometer. The gas flows of two of these channels may be measured to 1% precision.
- The third gas-handling channel may be used to provide a standard mixture for calibrating the stability and reproducibility of the mass spectrometer.

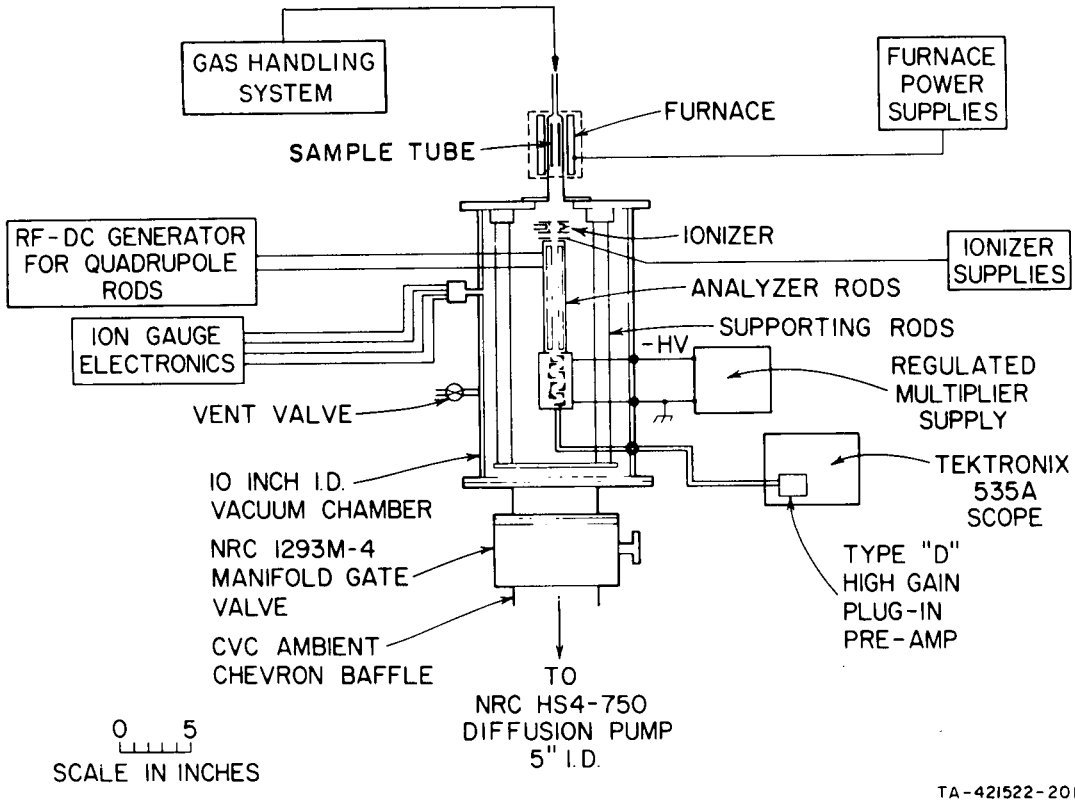

FIGURE 5 GENERAL SCHEMATIC OF LOW-PRESSURE PYROLYSIS APPARATUS

- A rapid pump out of the inlet system permits speedy measurement of the "residuals" mass spectrum--a feature important for accurate work. It also permits rapid changeover from one gas to another.
- A new design of mass spectrometer ionizer permits determination of appearance potentials.

These features have given the apparatus great versatility. Photographs and explanatory sketches of the VLPP-I and of the ionizer and quadrupole mass spectrometer and its ionizer are presented in Figures 6 and 13.

Figure 6 shows the rear of the apparatus. To the left are gas purification apparatus and high vacuum pump for the inlet system; a large gas buret is also located here. The mass spectrometer (in the 24-liter aluminum chamber) and reactor are located above the table, and associated diffusion and rotary pumps are below the table. The electronics for supplying the mass spectrometer (EAI Quad 200) is on the right of the picture. There are six glass storage bulbs located in an oil-filled box just to the left of center in the photograph. These bulbs are connected by individual stopcocks to the gas flow system at the front of the apparatus. Figure 7 is an explanatory sketch of the rear of the apparatus.

Figure 8 shows the front (gas-handling) side of the apparatus. The gas flow control system is located above the table, and the mass spectrometer protection and pressure monitoring units are below the table. Figure 9 is an explanatory sketch of Figure 8. The details of the gas flow monitoring system are given in more detail in Figure 10. Gas flows

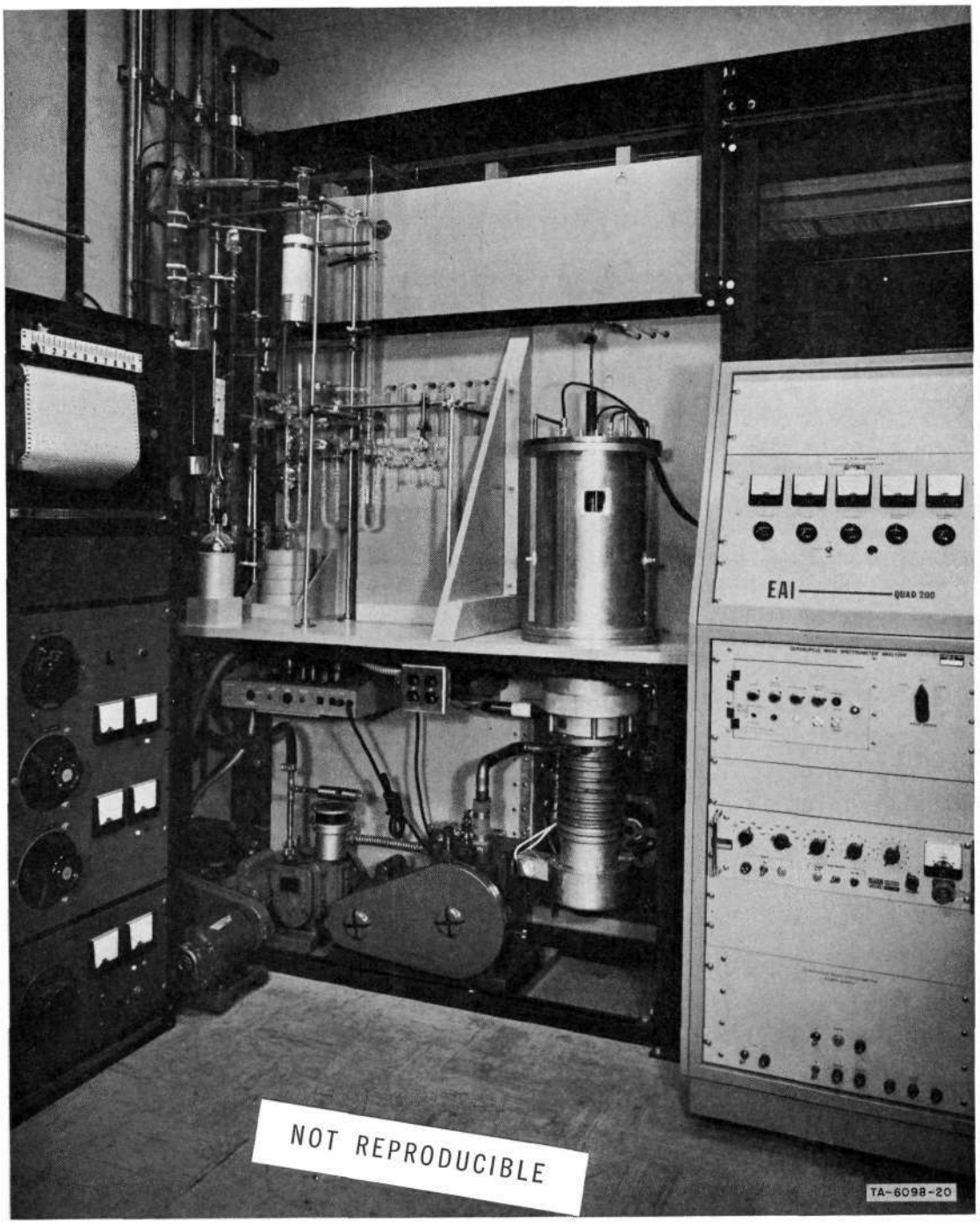

FIGURE 6 PHOTOGRAPH OF MASS SPECTROMETER SIDE OF THE APPARATUS

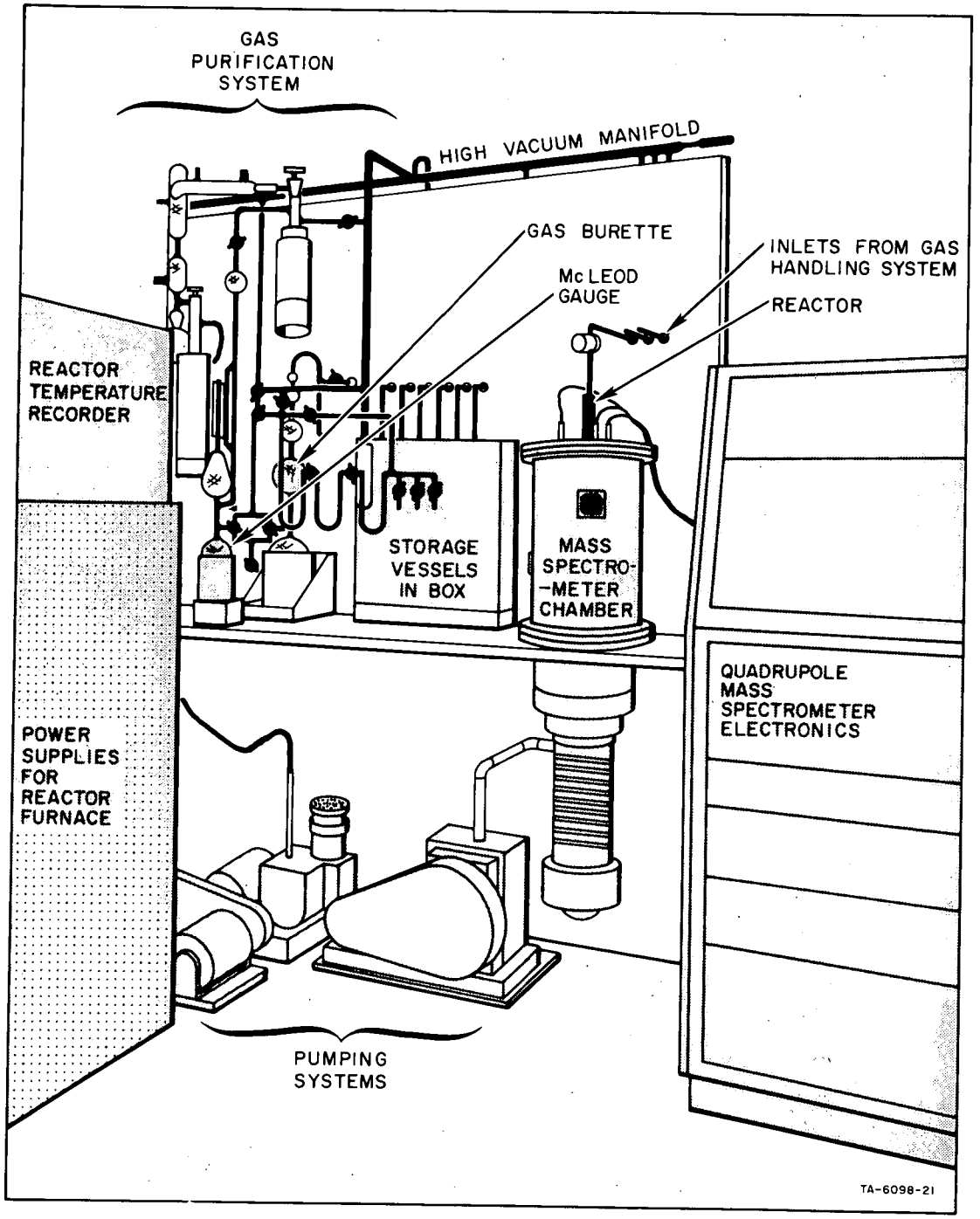

FIGURE 7 EXPLANATORY SKETCH OF FIGURE 6

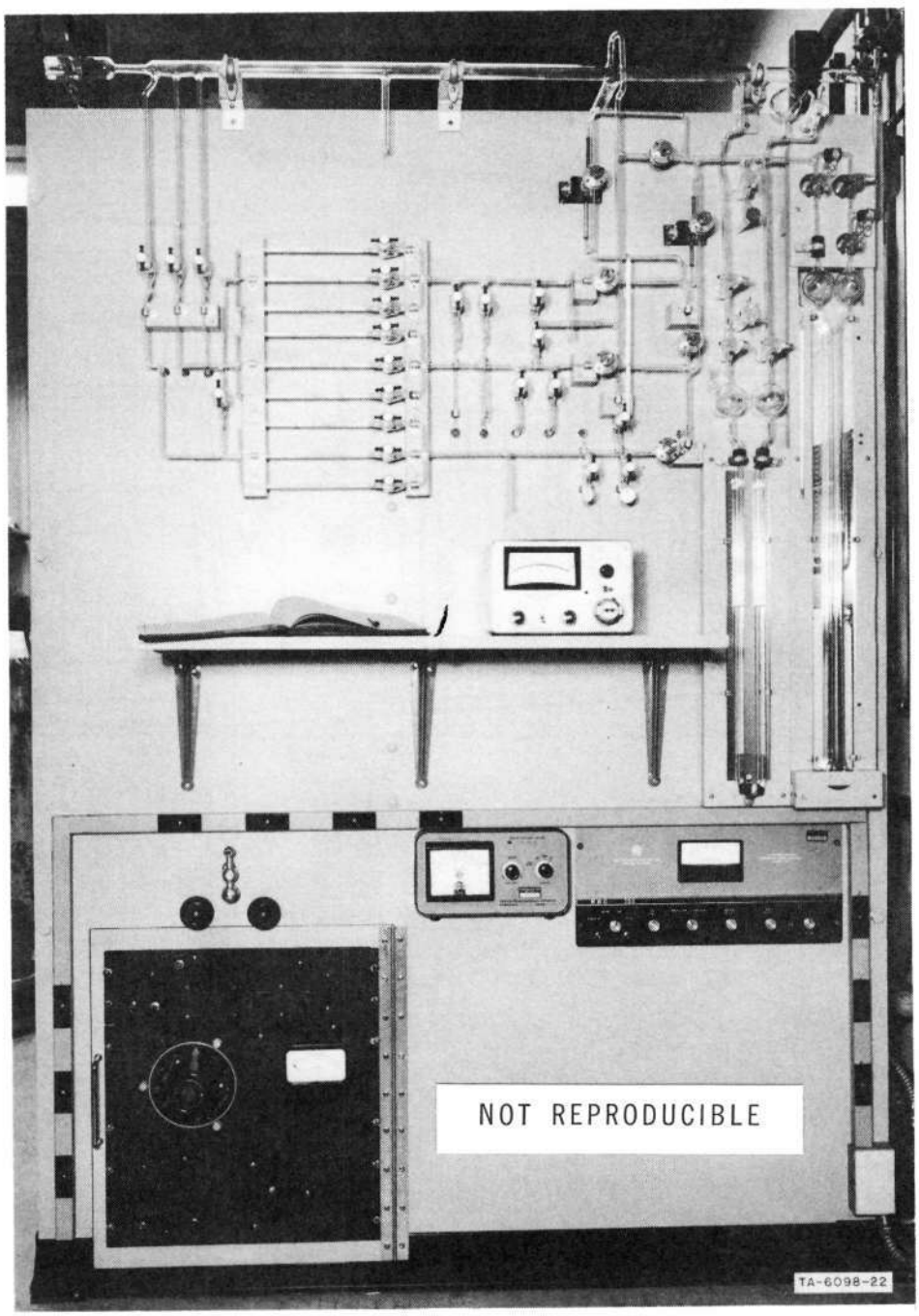

FIGURE 8 PHOTOGRAPH OF FRONT (GAS-HANDLING) SIDE OF APPARATUS

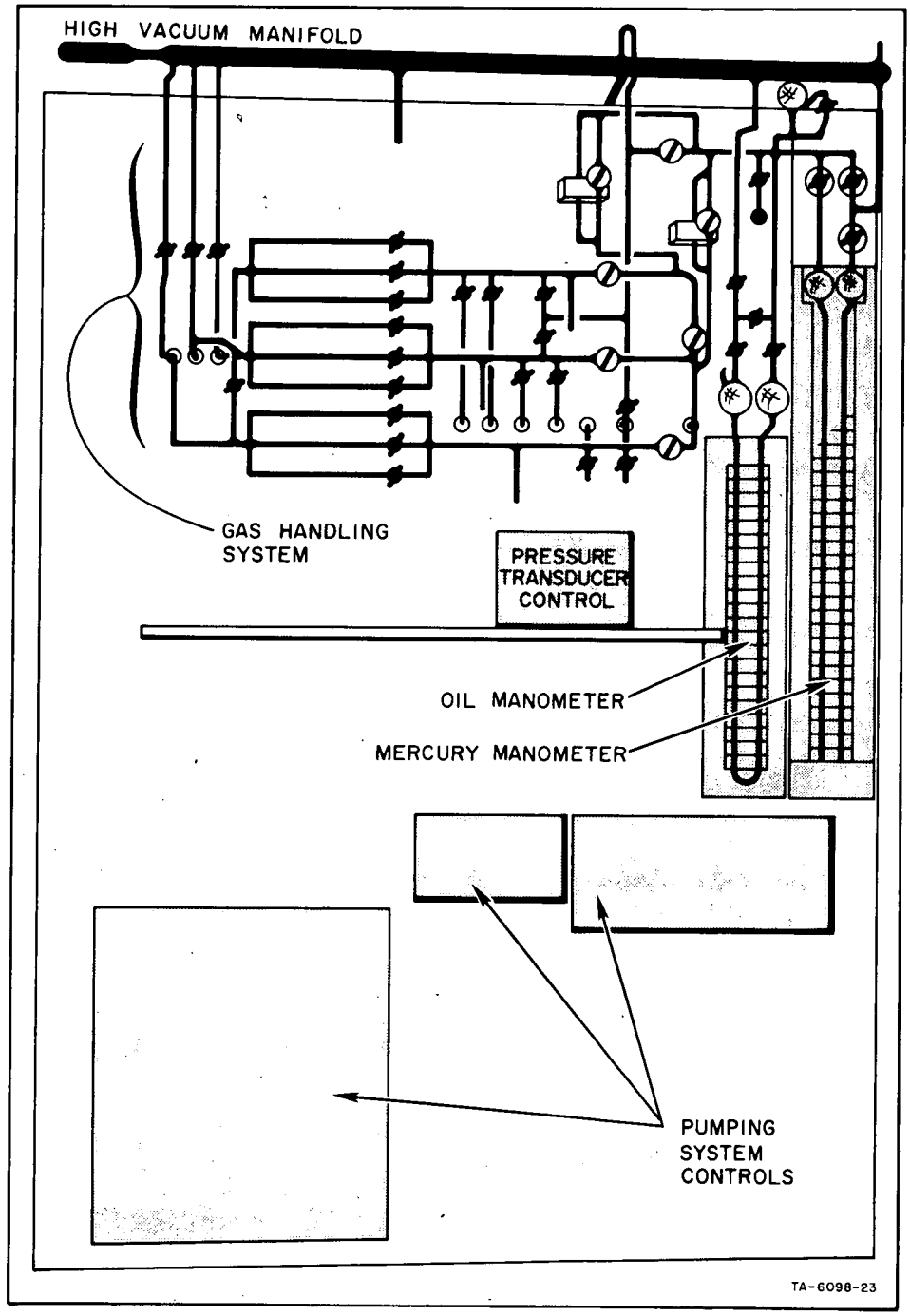

FIGURE 9 EXPLANATORY SKETCH OF FIGURE 8

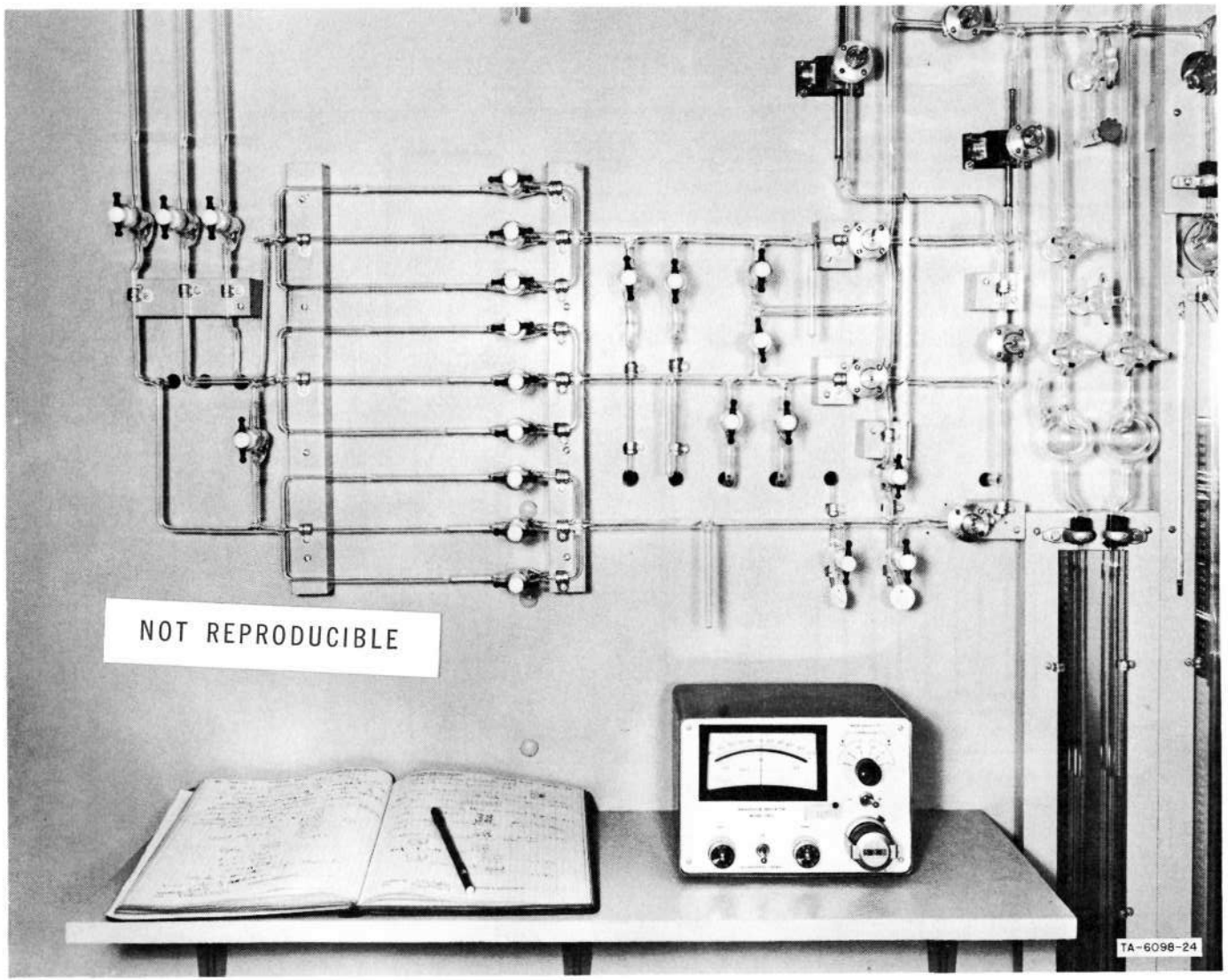

FIGURE 10 PHOTOGRAPH OF DETAILS OF GAS-FLOW MONITORING SYSTEM

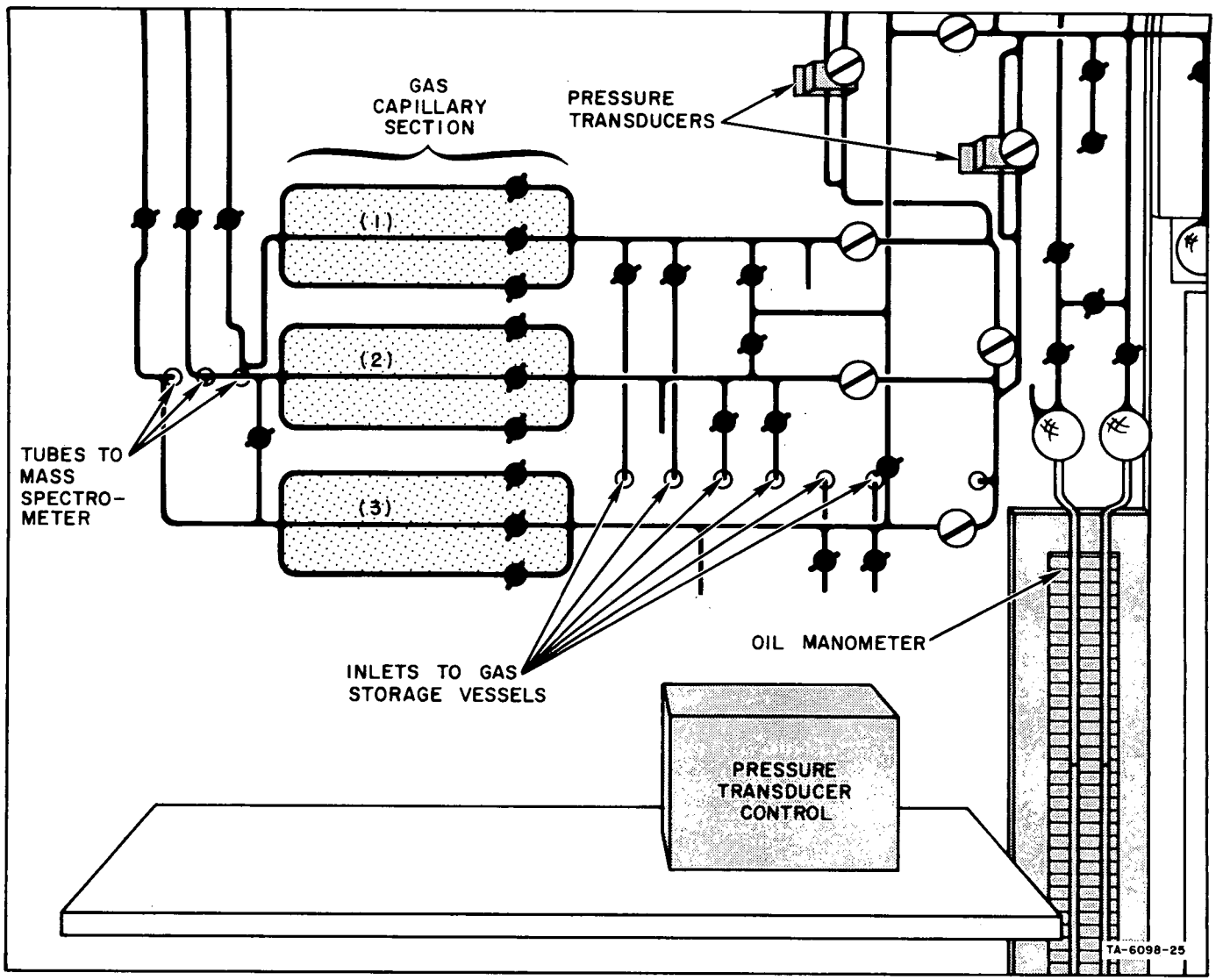

FIGURE 11 EXPLANATORY SKETCH OF FIGURE 10

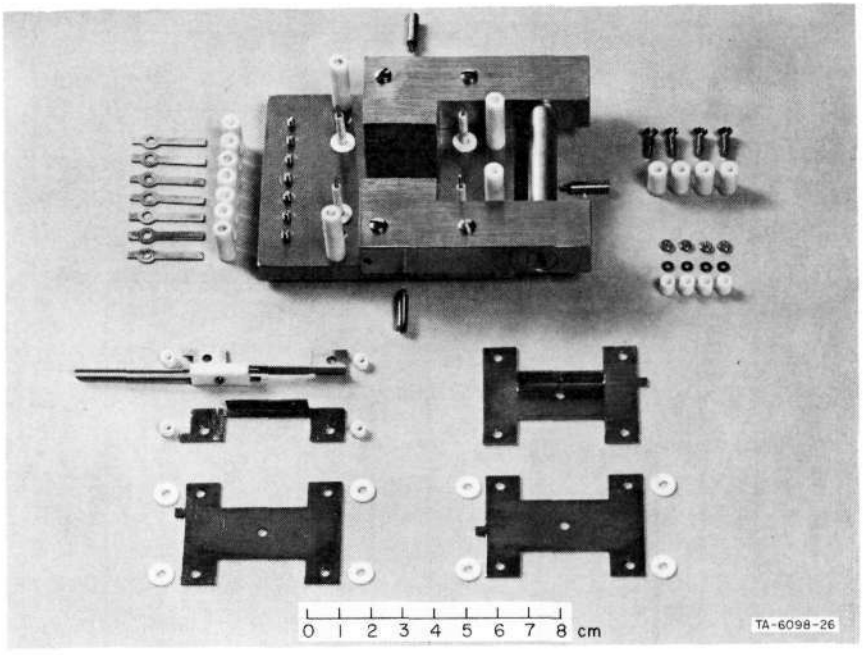

FIGURE 12 VIEW OF PARTLY DISASSEMBLED IONIZER

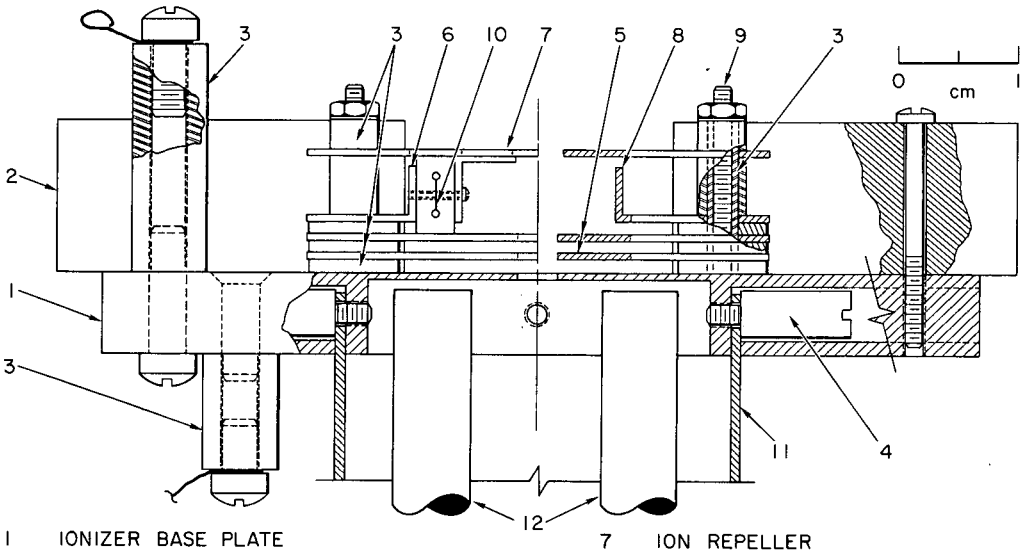

1	IONIZER BASE PLATE	7	ION REPELLER
2	SOFT IRON MAGNET POLE-PIECE	8	ELECTRON TRAP
3	ALUMINA INSULATORS	9	ELECTRODE SUPPORT ROD
4	SET SCREW	10	ELECTRON EMITTING FILAMENT
5	ION FOCUS ELECTRODES	11	QUADRUPOLE ANALYZER HOUSING
6	ELECTRON REPELLER ELECTRODE	12	QUADRUPOLE ANALYZER RODS

SECTION *A-A*

TB-6098-27

FIGURE 13 SKETCH OF CROSS SECTION OF MASS SPECTROMETER IONIZER

are monitored by determining the change of pressure in the storage volume. Pressure transducers are connected to oil and mercury manometers for reference. Gas flows are limited by fine capillaries. Figure 11 is an explanatory sketch of Figure 10.

Figure 12 shows the partly disassembled mass spectrometer ionizer. Insulators are of aluminum oxide; screws, electrodes, and baseplate are of stainless steel. (The magnet is of Alnico, and the pole pieces are chromium-plated soft iron.) The connecting wires and lugs are nickel. Tungsten is used for filaments. Threaded, 1/16-inch-diameter molybdenum rods are used for support of the electrode structure.

Figure 13 shows a cross section of the ionizer.

High-Temperature Reactor

One of the temperature limitations of our system has been the softening point of quartz. The softening point of quartz is ordinarily about 1400°C; however, during a run on the pyrolysis of tetrafluoroethylene, we ran a reactor at 1200°C for a while and it collapsed. In practice, therefore, we have confined our work to 1100°C and below. Unfortunately, many of the reactions of most interest to us proceed with negligibly slow rates (in comparison with 1 sec^{-1}) at temperatures of 1100°C (for example, the reaction $SiO_2 + C(s)$ is slow at only 1100°C).

The reactor system shown in Figure 14 was designed to overcome these limitations. The system was designed to extend our temperature capabilities to at least 1800°C. Its central element is a pure alumina muffle tube, capable (according to the manufacturer) of withstanding 1900°C. It is wound with a molydenum ribbon heater of a design similar to that

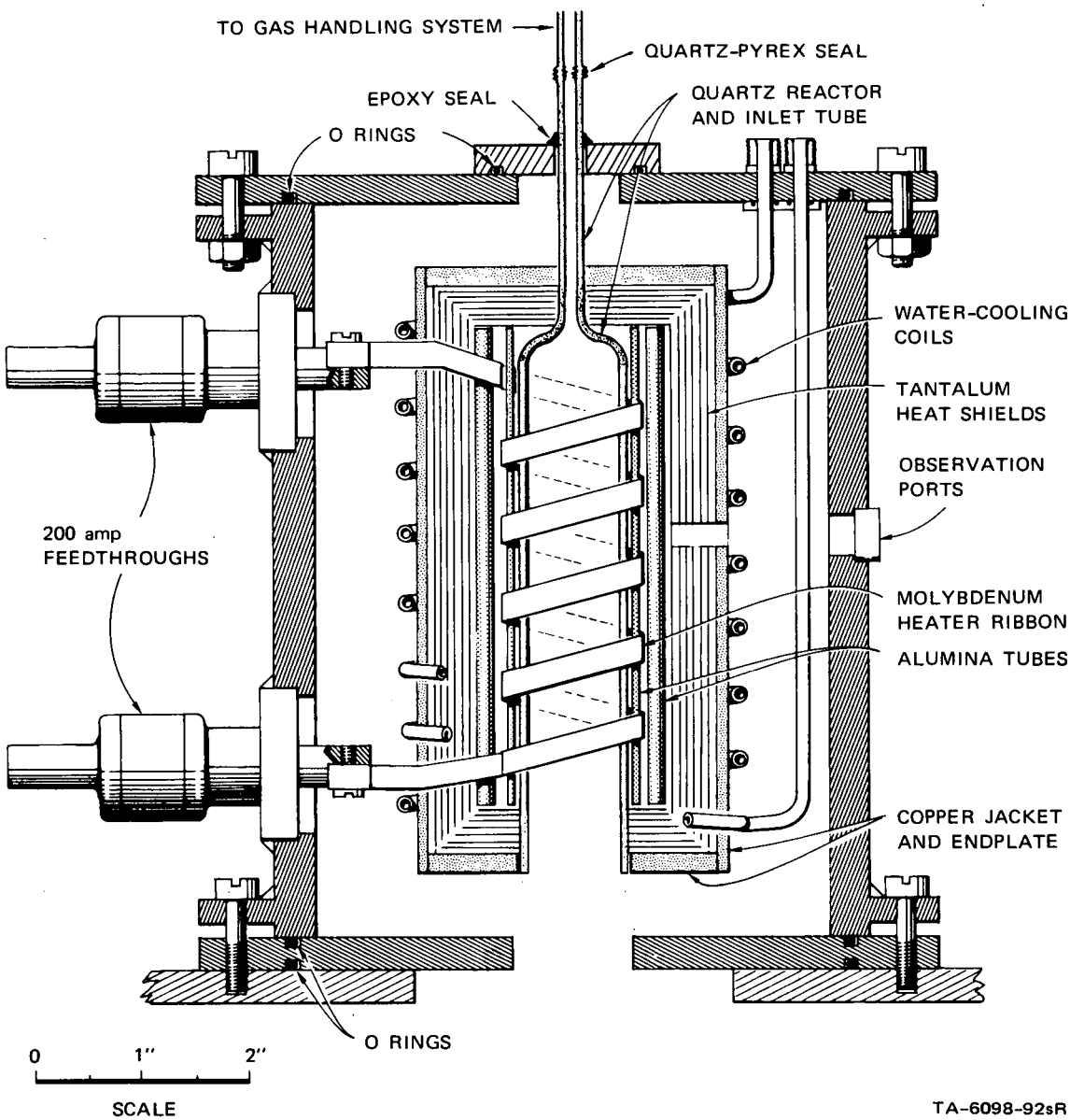

FIGURE 14 HIGH-TEMPERATURE REACTOR SYSTEM WITH QUARTZ REACTOR IN PLACE

of Hansen.[17] Heat insulation is provided by multiple tantalum heat shields. If it should prove feasible, thoria parts could at some time in the future replace alumina, and tungsten heaters could be used instead of molybdenum. The system temperature could thus be extended to 2500°C or more. The outgassing problems could be overcome, if necessary, by additional pumping on the furnace section.

By removing the quartz reactor tube shown in Figure 14 and providing an alumina gas inlet tube, we have a reactor system that we refer to as the alumina reactor. This alumina reactor is described below:

- The reactor has no "quartz reactor tube."
- The gas inlet consists of a 1/4-in. o.d. x 1/8-in. i.d. Al_2O_3 tube projecting down through 1/4-in. clearance holes in the upper tantalum heat shields.
- The inlet tube is sealed to uranium glass and Pyrex glass inlet tubing, which is connected to our inlet system.
- A bare Pt-Pt 10% Rh thermocouple is inserted into the reactor from below. The wires are 0.020-in. diameter and the thermocouple tip is at the center of the alumina muffle tube. The temperatures mentioned in the discussion of results below were those recorded by this couple, with ice as a reference. Gases make on the average only one collision with the platinum thermocouple wires.

---

[17]E. L. Hansen, Rev. Sci. Instr., 35, 242 (1964).

Gases injected into the inlet were subjected to 80 to 100 collisions with the heated Al_2O_3 tube. At their departure they may have collided 2 or 3 times with the tantalum heat shielding at the bottom of the reactor, and perhaps 10 times with the (carbonized) tantalum heat shields at the top of the reactor. [These collision numbers are deduced roughly as follows: random walk distance $\sim$ 1/2-in. per collision. Molecules travel about 4 inches from the place at which they make their first wall collision to the reactor exit hole. The average molecule will thus make about $(4 \times 2)^2$ collisions, plus an additional 30 collisions in the upper (dead space) part of the reactor, making a total of about 94 collisions. The actual number will be a bit less than this, owing to end effects.]

We have used a 0 to 40 Vdc power supply to power the furnace heater. During early work on the high-temperature furnace system, we discovered a small but significant peak at 23 amu. The peak height corresponded to a flow of neutral sodium equal to about 2×10^4 atoms sec^{-1}. As a result a white pasty solid was deposited at various places in the furnace. Debye-Scherrer x-ray pictures showed this material to be Na_2CO_3 (presumably caused by sodium reaction with atmospheric water and carbon dioxide); K_2CO_3 was negligible. These deposits were subsequently eliminated by use of a purer form of alumina muffle tube.

Carbonaceous and other black deposits were found on copper parts of the system but not on the inside of the alumina reactor tube. These black deposits were not extensive and may have resulted from secondary pyrolysis of hydrocarbons passed through the system; some oxidation of copper is possible but not probable since so little O_2 is available in the system.

Various metallic deposits were found on the Al_2O_3 core of the system but not on the center parts of the inside of the muffle tube. These deposits have not been analyzed, but they may be aluminum (unlikely, owing to the high vapor pressure of Al at $\sim 1600^{\circ}C$), molybdenum, tantalum, or even rhodium or platinum. During one of the early runs, the heater burned out. Blackened, solidified globules found on the outside of the reactor core tube were obviously caused by melting and resolidification of the Al_2O_3, since reactor core parts had melted and run down to touch the heater ribbons. Al_2O_3 had dissolved the molybdenum heater winding at such spots, and this was the cause of heater failure; this melting effect did not penetrate through to the inside of the alumina reactor core.

Mass spectra were examined for Mo, MoO, Mo_2O_3, Ta, and TaO, but these species were not found. A correlation was established between O_2 flow and some peaks at around 200 amu. The peaks turned out to be Hg^+, however, and all the various isotopes were found. This observation means that we could pick up reaction products at the level of 10^{-3} of the gas flows. The Hg came from the walls of the inlet system, which may have been contaminated with mercury from the diffusion pumps used on the system.

Another advance in VLPP techniques has been the development of the multi-aperture reactor shown in Figures 15 and 16. External manipulation of the small aperture plates shown in the figure provides a means of rapidly changing reactor collision number without changing gas flows or wall conditions or breaking vacuum.

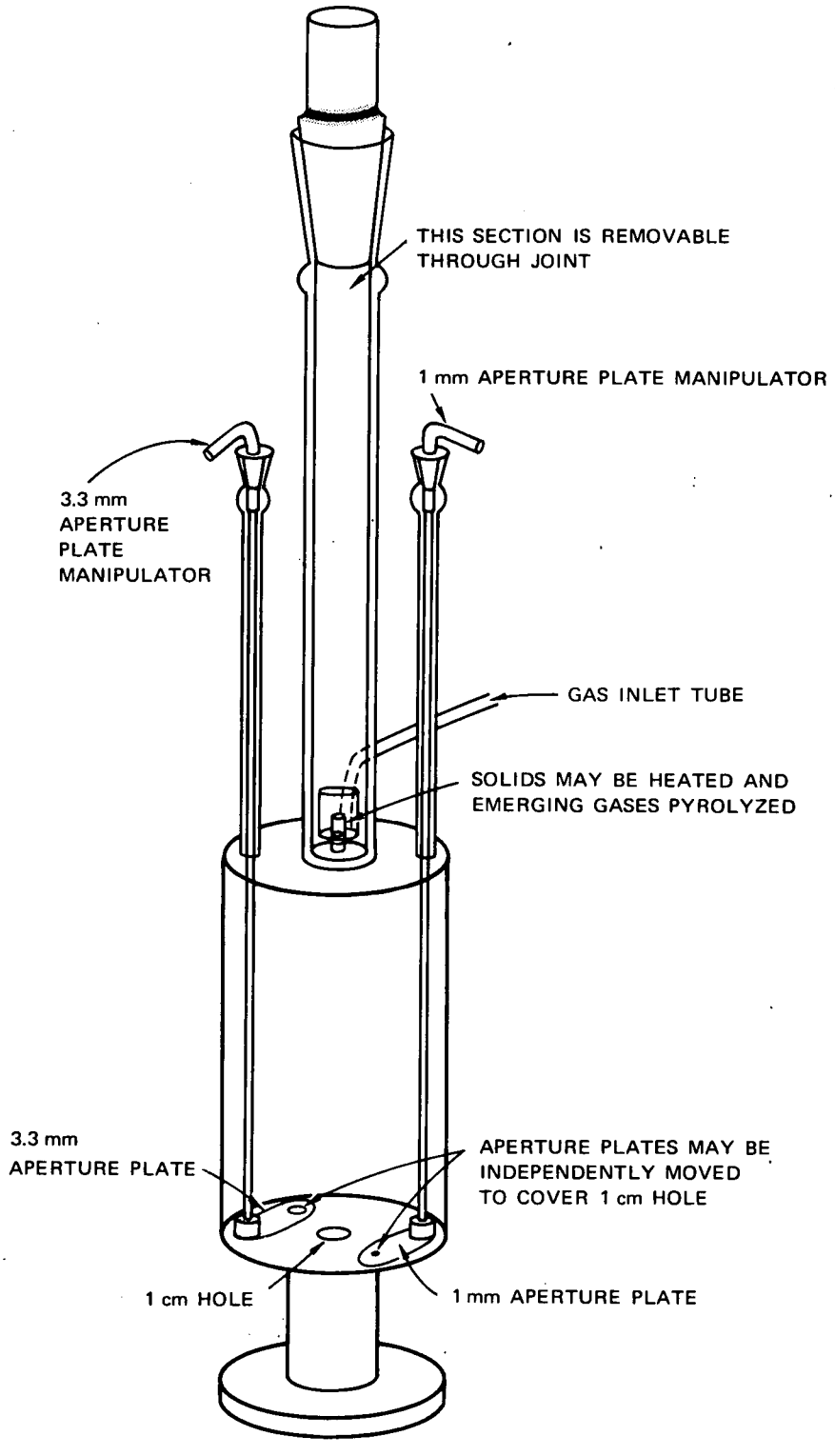

FIGURE 15 TRIPLE APERTURE QUARTZ REACTOR SYSTEM

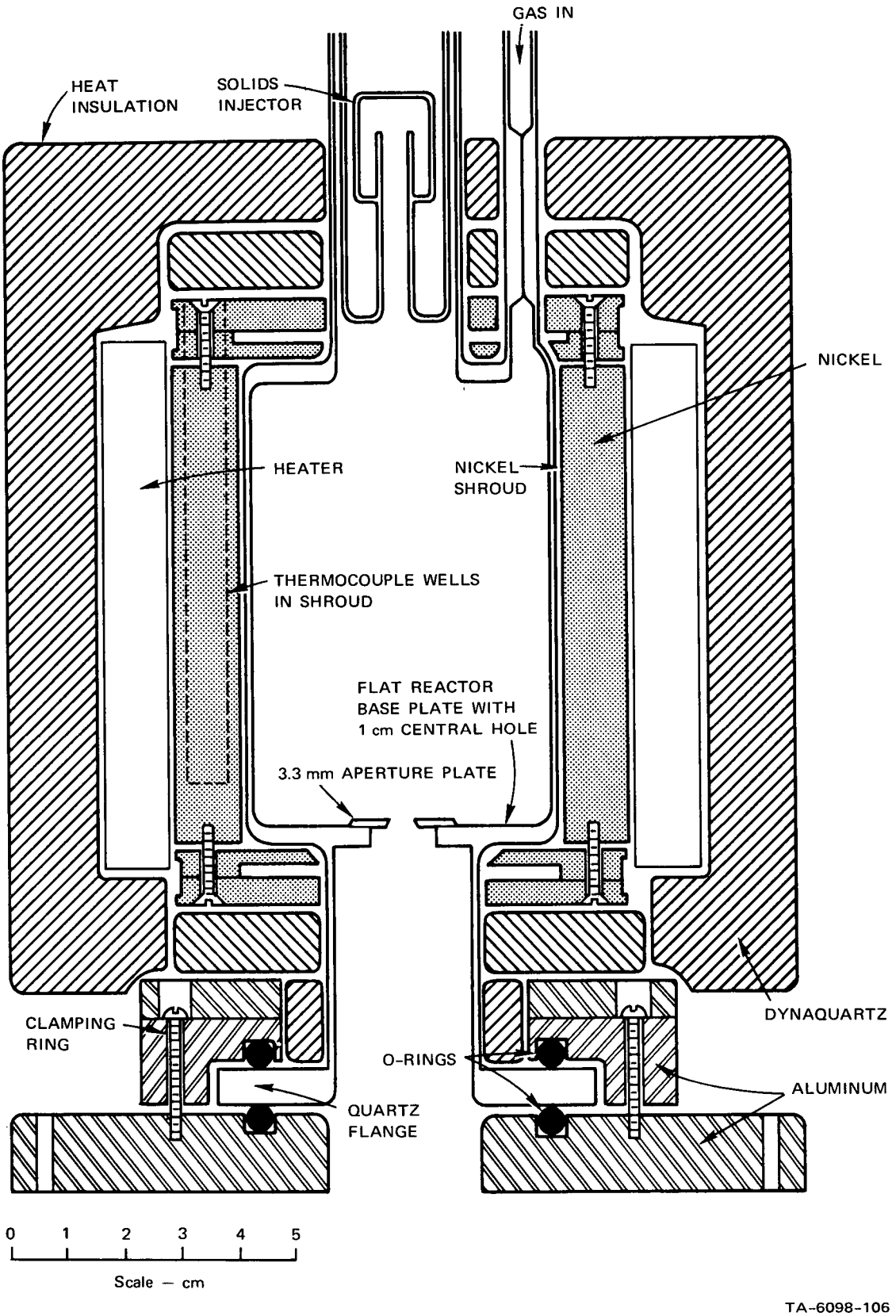

FIGURE 16 TRIPLE APERTURE CROSS SECTION

VLPP-II

This system was designed primarily to measure the rate constants of bimolecular reactions. Figure 17 shows the details of construction of this system. The chief difference between this sytem and the VLPP-I system is the provision of a differential pumping chamber between the reactor and the mass spectrometer. This system is therefore capable of operating with much higher reactor pressures than system I. Thus, it is possible to study relatively slow bimolecular reactions as well as unimolecular reactions. Figure 18 is a sketch of the VLPP-II gas-handling system. The heated inlet system permits work with low vapor pressure gases such as iodine vapor.

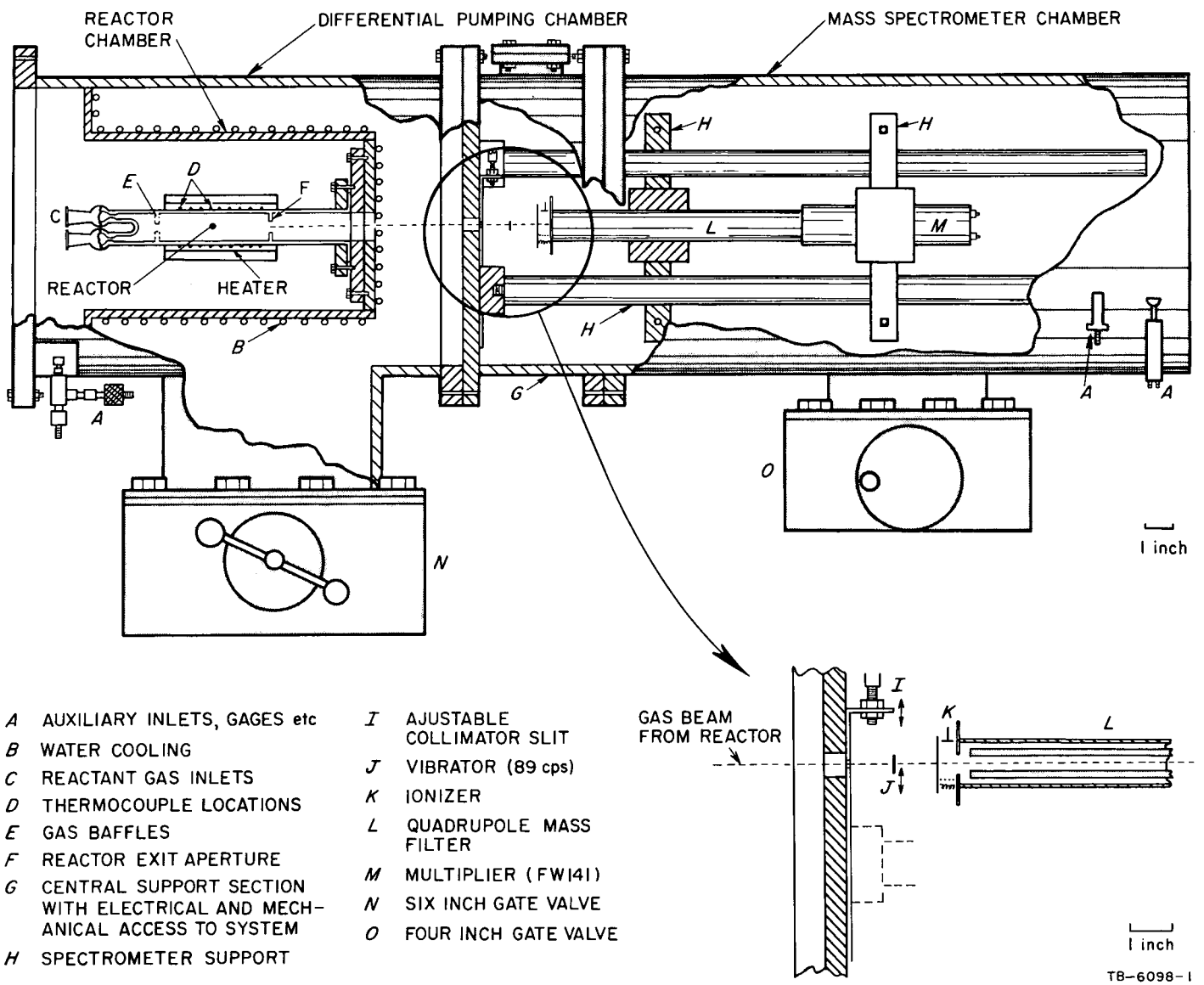

FIGURE 17 VLPP-II FOR STUDIES OF BIMOLECULAR REACTIONS

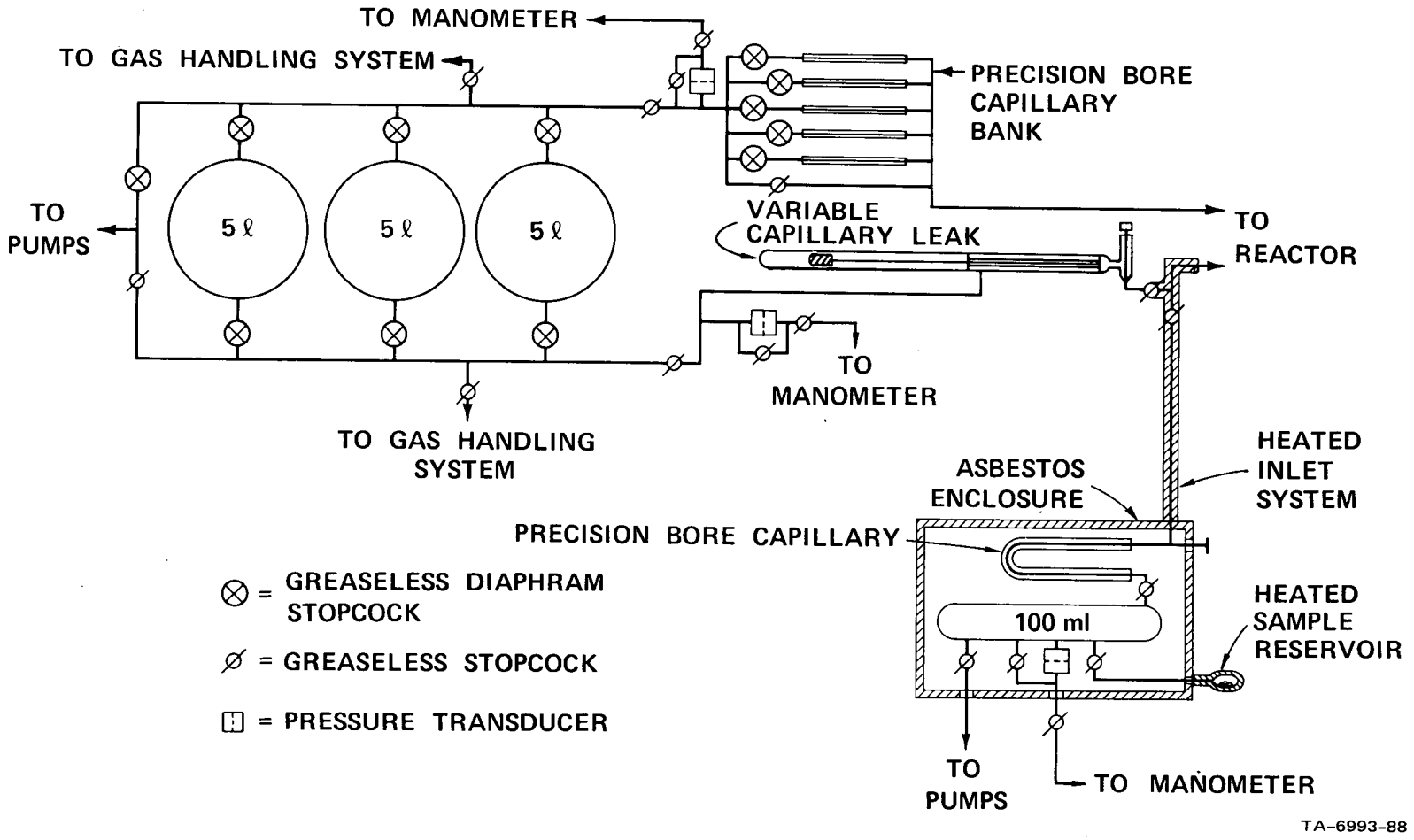

FIGURE 18 SKETCH OF VLPP-II GAS-HANDLING SYSTEM

IV THEORY OF VLPP—UNIMOLECULAR REACTIONS

Flow Kinetics

The conditions in a VLPP reactor normally correspond closely to those in a stirred-flow reactor.[12b] We can represent the mechanism by a pair of kinetic equations in which A represents a reactant molecule and P and Q are products of the unimolecular reaction of A.

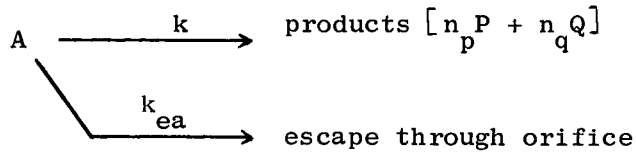

By measuring the fraction of decomposition f, we can use the relation

$$k = k_{ea} \frac{f}{(1 - f)} \tag{1}$$

to determine the unimolecular reaction rate constant k.

From kinetic theory, we have

$$k_{ea} = \frac{1/4\bar{C}_A A_h}{10^3 V} \text{ sec}^{-1} \tag{2}$$

where A_h is the hole area in cm^2, V= volume in cm^3, and $\bar{C}_A$ is the mean molecular speed of A. Hence,

$$k = \frac{3.65\ A_h T^{1/2} f}{V M_A^{1/2} (1 - f)} \tag{3}$$

Induction Kinetics

Benson and Spokes[12b] have shown that induction periods can be accounted for by using a slight variant of equation (1). The result is

$$k = \frac{k_{ea} f\beta}{(1 - f\beta)}$$

where $\beta = \exp\{k_{ea}(\tau_i - \tau_m)\}$. The induction periods τ_i and τ_m correspond respectively to the chemical induction period and the mixing induction period. Details are explained in the original paper.

RRK Theory of the Unimolecular Rate Constants

The Rice-Ramsperger-Kassel (RRK) theory of unimolecular reactions assumes that a stationary population of vibrationally excited species results as a balance of three processes. They are collisional activation, collisional deactivation, and spontaneous unimolecular decomposition.[18] The rate constant falls off from its high-pressure limit when spontaneous decomposition depletes the upper energy states responsible for reaction faster than collisional deactivation does.

For an arbitrary reactant molecule A, the RRK scheme is

$$\text{wall} + A \underset{k_d}{\overset{k_a}{\rightleftarrows}} A^* + \text{wall}$$

$$A^* \xrightarrow{k_r} \text{products}$$

Here k_a and k_d are rate constants for vibrational energy exchange at

[18] a. F. A. Lindemann, Trans. Faraday Soc., 17, 598 (1922);
b. L. S. Kassel, Kinetics of Homogeneous Gas Reactions, Reinhold, New York, 1932, Chap. 5.

the wall, and k_r is the specific decomposition rate of a critically energized molecule with internal energy $E \geq E^*$, the activation energy for reaction at 0^0K. RRK theory leads to

$$\frac{E^*}{E_m} = 1 - \left(\frac{k_w}{A}\right)^{1/(n-1)} \tag{4}$$

where k_w is the wall collision frequency assumed equal to k_d. The number of classical oscillators in the molecule is n, and A is the Arrhenius A-factor. E_m is that level of energy in a molecule that leads to its decomposition at low pressures with a rate constant equal to k_w.

Benson and Spokes[12b] gave for k

$$k = \frac{k_w}{2\sqrt{2\pi}} \left[\frac{eE_m}{(n-1)RT}\right]^{n-1} \exp - \left(\frac{E_m}{RT}\right) \tag{5}$$

which permits solution for E_m from the observed value of k and the appropriate value of n. When the high-pressure Arrhenius parameters A and E^* are known, as is often the case, n is the only unknown parameter and it can be determined accurately.

Equations (4) and (5) can be solved easily using a slide rule with a log scale. For higher accuracy we have used a computer program[19] that solves the equation.

$$I(SBD) = \frac{1}{\Gamma(S)} \int_0^\infty \frac{X^{S-1} e^{-X} dx}{1 + 10^{D[X/(B+X)]^{S-1}}} \tag{6}$$

[19]Generously provided to us by Dr. G. Emanuel of the Aerospace Corporation.

where $X = \frac{E - E^*}{kT}$, $B = \frac{E}{kT}$, $D = \log A - \log k_w$, and $s = \frac{C_{vib}}{R}$.

Molecules, such as n-PrI, that can undergo competing unimolecular reactions present a more complex case. Details of this theory, presented in a recent publication,[15] are beyond the scope of this introductory section.

V THEORY OF VLPP-RADICAL MOLECULE REACTIONS

In the past eight years the Thermochemistry and Chemical Kinetics Group at SRI has reported the rate constants for I-atom reactions of the type, $RH + I \overset{1}{\rightarrow} R + HI$ and $RI + I \overset{2}{\rightarrow} R + I_2$, as well as the ratio of the rate constants for the reverse processes. On the assumption that the Arrhenius activation energy for the reverse of process 2 is zero, we have calculated the heats of the above reactions. We then calculate the only unknown heat of formation in either case, that of the free radical, R.

The assumption of zero activation energy for all exothermic processes $R + I_2 \rightarrow RI + I$ is founded on some experimental determinations of $CH_3 + I_2 \rightarrow CH_3I + I$, relative to $CH_3 + O_2$, which is supposedly a zero activation energy process. When the C-H bond dissociation energy (BDE) is determined by assuming that $C_2H_5 + I_2 \rightarrow C_2H_5I + I$ has zero activation energy, the value obtained is 98 kcal/mole. The method of photobromination, which is scaled to the assumption that $CH_3 + I_2 \rightarrow CH_3I + I$ has zero activation energy, yields the same result. This indicates that both CH_3 and C_2H_5 radicals fit the assumption within the same precision.

Clearly, a direct measure of $R + I_2$ or $R + HI$, or both, is desirable in every case. This is especially true in those cases where R is very much different from CH_3.

VLPP lends itself well to the determination of absolute values of radical-molecule reaction rate constants. The basis for this statement is seen from the simplified scheme shown below.

Consider the reaction $R^{\bullet} + AX \xrightarrow{ka} RX + A^{\bullet}$

$$(AX)_{ss} = \frac{R_{rx}}{k_{eax} + k_a(R^{\bullet})_{ss}} \tag{7}$$

$$(R^{\bullet})_{ss} = \frac{R_{r^{\bullet}}}{k_{er} + k_a(AX)_{ss}} \tag{8a}$$

$$(R^{\bullet})_{o} = \frac{R_r}{k_{er}} \tag{8b}$$

$$(RX)_{ss} = \frac{k_a(R^{\bullet})_{ss}(AX)_{ss}}{k_{erx}} \tag{9}$$

$$\frac{(R^{\bullet})_o}{(RX)_{ss}} = \frac{R_{r^{\bullet}} k_{erx}}{k_{ec} k_a (R^{\bullet})_{ss} (AX)_{ss}} \tag{10}$$

$$\frac{(R^{\bullet})_o}{(RX)_{ss}} = \frac{k_{erx}}{k_a(AX)_{ss}} + \frac{k_{erx}}{k_{er}} \tag{11}$$

$$\frac{k_{er}(R^{\bullet})_o}{k_{erx}(RX)_{ss}} = 1 + \frac{k_{er}}{k_a(AX)_{ss}} = 1 + \frac{k_{er}k_{eax}}{k_a k_{eax}(AX)_{ss}} \tag{12}$$

R_i = flow rate of substance into the reactor

k_{ei} = escape constant for substance

$(i)_{ss}$ = steady state concentration of substance

The signal at a given mass (λ) is related to the flux of a given species as:

$$I_i^{\lambda} = \alpha_{\lambda}^{i} k_{ei} (i)_{ss}$$

$$\frac{\left(I_{R^{\bullet}}^{\lambda_1}\right)_o}{I_{R_X}^{\lambda_2}} = \frac{\alpha_{R^{\bullet}}^{\lambda_1}}{\alpha_{R_X}^{\lambda_2}} \left[1 + \frac{k_{er} k_{eax}}{k_a} \frac{\alpha_{AX}^{\lambda_s}}{I_{AX}^{\lambda_3}} \right] \tag{13}$$

A plot of the left hand side of equation (13) versus $1/I_{AX}^{\lambda_3}$ will thus yield a straight line; from its slope, k_a is readily extractable.

It is often difficult to observe a mass spectral peak because of the radical $R^{\bullet}$. The usual methods of radical generation, however, allow a way around the problem. Typically, radicals are generated from pyrolysis reactions of the type $R\text{-}Y\text{-}R \rightarrow 2R + Y$, where Y is a stable molecule. In these cases, since

$$2k_{ey}(Y)_{ss} = k_{er}(R)_o$$

equation (13) becomes

$$\frac{2I_Y^{\lambda_4}}{I_{RX}^{\lambda_2}} = \frac{\alpha_Y^{\lambda_4}}{\alpha_{RX}^{\lambda_2}} \left[1 + \frac{k_{er}k_{eax}\alpha_{AX}^{\lambda_3}}{k_a I_{AX}^{\lambda_3}} \right] \qquad (14)$$

We have measured (see Figure 19) the rate constant for the reaction $CH_3 + DB_r \rightleftarrows CH_3D + Br$ using the above technique.[13b] We have also used this method to determine some preliminary values of the rate constants for $CH_3 + HI \rightarrow CH_4 + I$ and $C_3H_5 + DI \rightarrow C_3H_5D + I$.

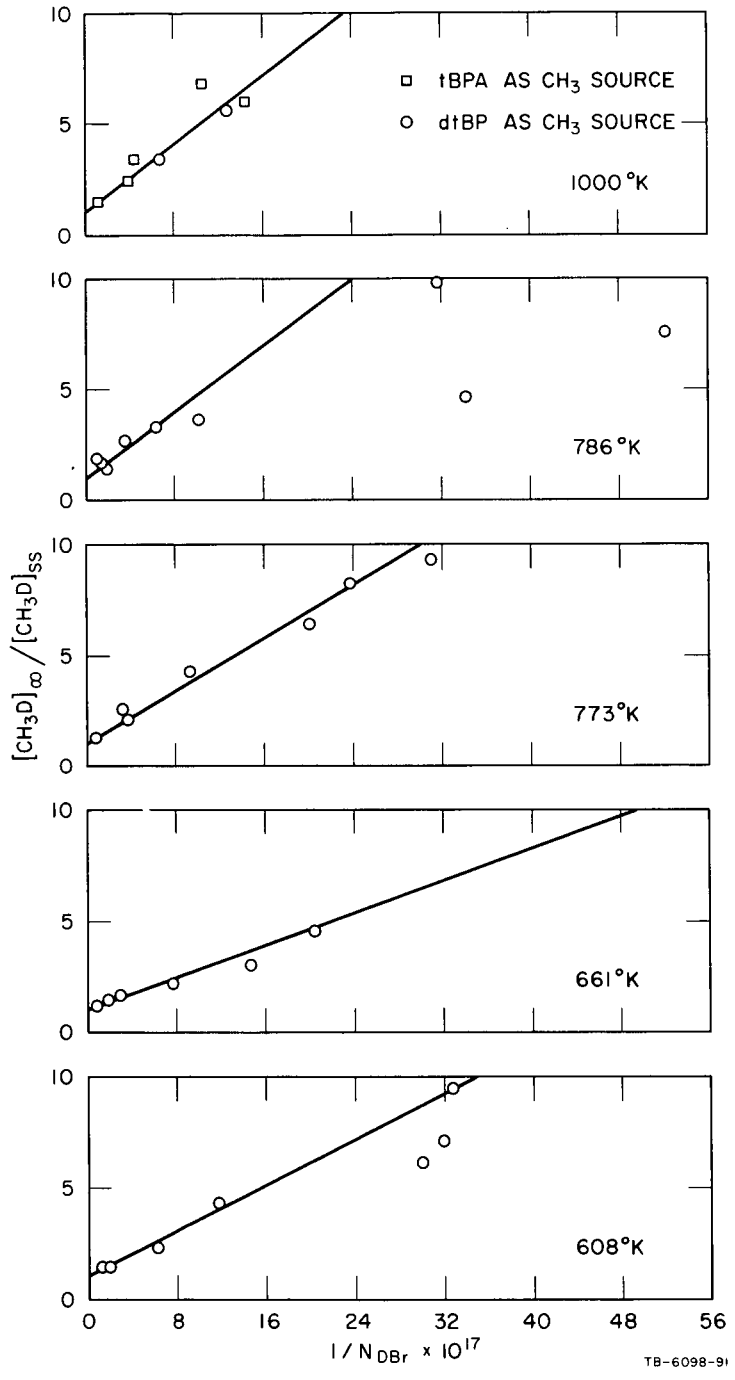

FIGURE 19 TITRATION OF CH_3 WITH DBr

VI PUBLISHED WORK AND RELATED UNREPORTED DATA

The following publications on VLPP have been generated by SRI staff since inception of the technique. Publications 1 through 7 have resulted as a direct consequence of our research efforts under NASA Contract NAS7-472. Publications 8 and 9 have resulted through partial sponsorship under this contract, and publications 10 through 12 were produced under other sponsorship.

1. Oxidation of a Thin Film of a Carbonaceous Char at Pressures Below 10^{-4} Torr, G. N. Spokes and S. W. Benson, Fuandamentals of Gas-Surface Interactions (edited by H. Saltsburg, J. N. Smith, Jr., and M. Rogers), Academic Press, New York, 1967, p. 318.

2. Equilibrium Constant for Allyl Radical Recombination. Direct Measurement of "Allyl Resonance Energy," David M. Golden, Norman A. Gac, and Sidney W. Benson, J. Amer. Chem. Soc., 91, 2136 (1969).

3. Absolute Rate Constants for Radical-Molecule Reactions Over a Wide Temperature Range: $CH_3 + DBr \rightleftarrows CH_3D + Br$. The Heat of Formation and Entropy of the Methyl Radical, Norman A. Gac, David M. Golden, and Sidney W. Benson, J. Amer. Chem. Soc., 91, 3091 (1969).

4. Thermal Degradation of Nadic Methyl Anhydride-cured Epoxy Novolac, Norman A. Gac, G. Neil Spokes, and Sidney W. Benson, J. Polym. Sci., Part A-1, 8, 593 (1970).

5. Pyrolysis of Hydrocarbons in Knudsen Cells, G. N. Spokes, and S. W. Benson, Recent Developments in Mass Spectroscopy (edited by K. Ogata and T. Hayakawa), University of Tokyo Press, 1970, p. 1146.

6. A Comparison of RRK and RRKM Theories for Thermal Unimolecular Processes, David M. Golden, Richard K. Solly, and Sidney W. Benson, J. Phys. Chem., 75, 1333 (1971).

7. Very Low-Pressure Pyrolysis. IV. The Decomposition of i-Propyl Iodide and n-Propyl Iodide, Keith D. King, David M. Golden, G. Neil Spokes, and Sidney W. Benson, Int. J. Chem. Kinetics, 3, 0000 (1971).

8. Very Low-Pressure Pyrolysis. II. Decomposition of Nitropropanes, G. N. Spokes and S. W. Benson, J. Amer. Chem. Soc., 89, 6030 (1967).

9. Very Low-Pressure Pyrolysis. V. Benzylamine, N-Methylbenzylamine, and N-N-Dimethylbenzylamine and the Heat of Formation of the Amino, Methylamino, and Dimethylamino Radicals, D. M. Golden, R. K. Solly, N. A. Gac, and S. W. Benson, submitted to J. Amer. Chem. Soc.

10. Very Low-Pressure Pyrolysis. I. Kinetic Studies of Homogeneous Reactions at the Molecular Level, S. W. Benson and G. N. Spokes, J. Amer. Chem. Soc., 89, 2525 (1967).

11. Application of Very Low-Pressure Pyrolysis to Combustion Kinetics, S. W. Benson and G. N. Spokes, Eleventh Symposium (International) on Combustion, Combustion Institute, 1967, p. 95.

12. Very Low-Pressure Pyrolysis. III. t-Butyl Hydroperoxide in Fused Silica and Stainless Steel Reactors, S. W. Benson and G. N. Spokes, J. Phys. Chem., 72, 1182 (1968).

We see that NASA sponsorship has been instrumental in the support of this program during a significant growth period of VLPP. The results of VLPP work have been presented at several professional society meetings.

We will not repeat here details of all the published work done under this contract. The objective of this section is to select highlights from the published work and add relevant unpublished results that have been obtained in the course of work done under this contract. Recent work that has been accepted for publication will likewise not be treated in depth.

Ten copies of this report have been furnished to NASA with a complete set of reprints and preprints of our published work. The authors will be pleased to send copies of these reprints to requestors as long as the supply lasts.

1. Oxidation of a Thin Film of a Carbonaceous Char at Pressures Below 10^{-4} Torr, by G. N. Spokes and S. W. Benson, Fundamentals of Gas-Surface Interactions (edited by H. Saltsburg, J. N. Smith, Jr., and M. Rogers), Academic Press, New York, 1967, p. 318.

Abstract

A study was made of the heterogeneous reactions of molecular oxygen with a thin film of carbonaceous char. The reactions were carried out in a stirred-flow reactor in which temperature was maintained at values up to 920°C. The production of CO and CO_2 was first order in oxygen over this temperature range, and activation energies for CO and CO_2 production were 26 and 22 kcal per mole, respectively. A simple mechanism was proposed to fit the observed experimental facts. The mechanism involved formation of a peroxy radical site that can decompose to give back molecular oxygen or an O atom and, subsequently, CO gas or a surface oxide that may yield CO_2.

Figure 20 shows the experimental arrangement used for the research, and Figure 21 shows the Arrhenius plot of the rate constant data obtained from Table I.

Table I

REACTION OF OXYGEN WITH DEN438 CHAR

	Temperatures, °C				
	510	610	720	810	920
$(CO/O_2)_{av}$	0.073	0.034	0.13	0.48	0.94
$(CO_2/O_2)_{av}$	0.003	0.045	0.12	0.22	0.23
$(CO_2/CO)_{av}$	0.045	1.55	1.3	0.53	0.25

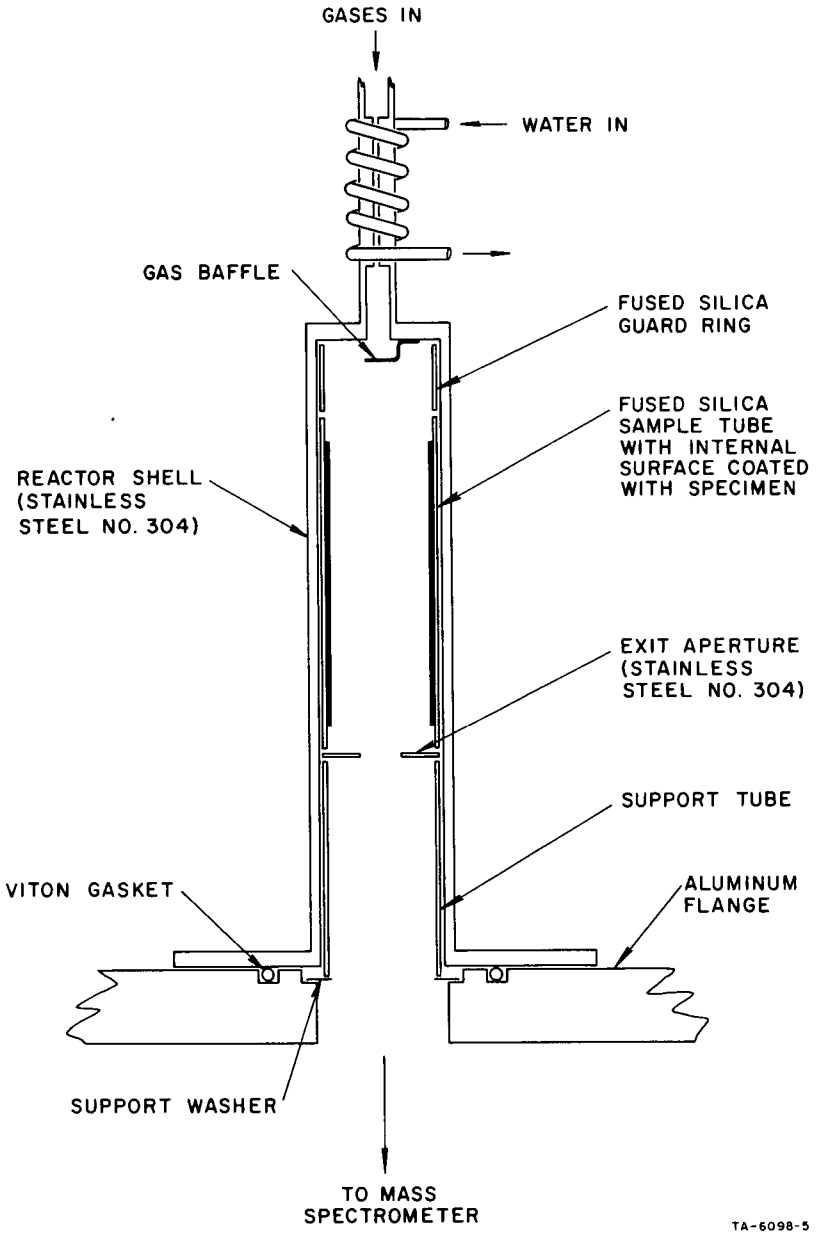

FIGURE 20 REACTOR FOR EXAMINATION OF HETEROGENEOUS REACTIONS OF OXYGEN WITH CARBON FILMS

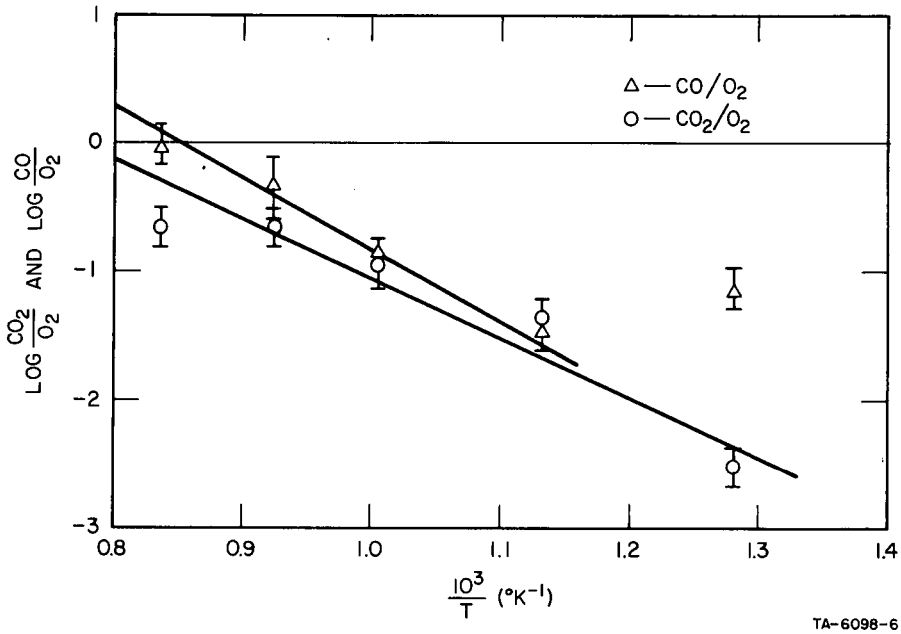

FIGURE 21 ARRHENIUS PLOTS OF RELATIVE RATE CONSTANTS FOR CO AND CO_2 PRODUCTION. Slopes correspond to activation energies of 26 ± 5 kcal mole for CO production and 22 ± 5 kcal mole CO_2.

C.2.

The proposed mechanism for the reaction was

$$\geq\dot{C} + O_2(g) \rightleftarrows \geq C\text{–}O\text{–}O^{\bullet} \quad \text{fast} \tag{15}$$

$$\geq C\text{–}O\text{–}O^{\bullet} \rightarrow \geq C\text{–}O + O(g) \tag{16a}$$

$$O(g) + \geq C^{\bullet} \rightarrow \geq C\text{–}O^{\bullet} \tag{16b}$$

$$\rightarrow >C\begin{matrix}O\\ \diagup\\ \diagdown\\ O\end{matrix} \rightarrow CO_2(g) \tag{17}$$

$$\geq C\text{–}O \rightarrow CO(g) + \text{site} \tag{18}$$

After the publication of the above research results, our work on oxidation of chars continued; our results are summarized below.

Oxygen was flowed into a reactor arranged as shown in Figure 20, except that there was no coating of carbon on the inside surface of the sample tube. Considerable reaction occurred above 600°C. It was concluded that as much as 50% of the previously observed reaction was occurring on exposed metal parts in the reaction chamber. This was believed to be caused by deposits of carbonaceous material on the few square centimeters of metal exposed to the oxygen. To avoid this problem, we replaced the metal-shelled reactor shown in Figure 20 with a quartz-shelled reactor of very similar design. The new reactor was designed to receive sample tube inserts, and the exit aperture system was now made of quartz instead of metal.

Sample tubes were coated internally with a thin layer of epoxy novolac. This was accomplished by permitting slow drainage of an epoxy solution in acetone from the sample tube as shown in Figure 22. The

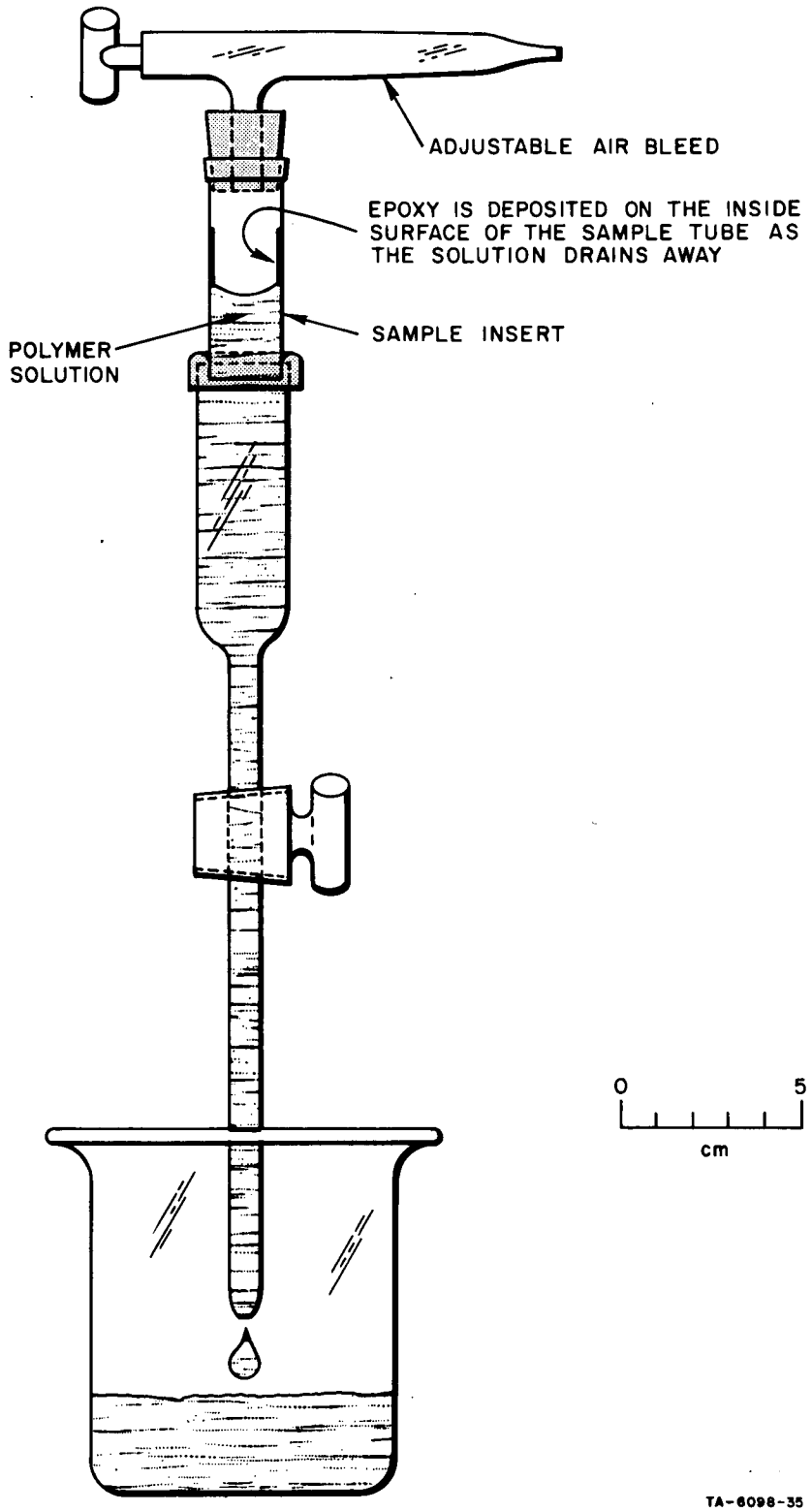

FIGURE 22 EPOXY COATING PROCEDURE

thickness of sample depended on the concentration of the epoxy solution.

Using 1-mm and 1-cm exit apertures, we studied the reaction of oxygen and various other gases with several char samples. Results for one sample are presented in Tables II through VI, and in Figures 23 through 25. The tables include data on reactions of oxides of nitrogen with chars.

At first we had considerable difficulty in understanding the irreproducible nature of the results. See, for example, how different the initial results are for the 5.45-mg char layer and the 5.285-mg char layer (Table II and Figure 23 versus Tables III and IV and Figure 24, and then again, Tables V and VI and Figure 25). As the work proceeded, however, a pattern became clear as the importance of the chemical history of the sample was exposed.

The arrows on the Arrhenius plot in Figure 25 refer to the chronology of the experimental runs. We see that with this one sample several roughly parallel Arrhenius lines are described. The apparent activation energy ranges from 35 to 45 kcal/mole in the temperature range 1100 to 1250°K. Over the range 1200 to 1400°K, values are lower and go from about 20 to 30 kcal/mole. We note that, as the char sample disappears by reaction with oxygen, so eventually, the rate constant falls away to low values and finally to zero.

The reduced rate constants obtained at higher oxygen flows implies that there is competition among the oxygen molecules for the available reactive sites. The fact that CO_2 is typically only 10% of the CO production tells us that the bulk of the oxygen that reacts does so through a reaction complex that easily permits one of the oxygen atoms

Table II

FIRST RESULTS OF OXIDATION OF A THIN 5.45-mg FILM OF CARBON CHAR IN AN ALL-QUARTZ SYSTEM [a]

Run No.	Number of Data	Temp, °C	CO/O_2 [b]	Hole Diameter, mm
1	9	1000	0.16	10
2	1	935	0.07	10
3	1	940	0.05	10
4	1	950	0.08	10
5	2	980	0.15	10
6	7	1000	0.25	10
7	4	940	0.075	10
8	4	996	0.21	10
9	6	1040	0.47	10
10	3	1006	0.33	10
11	1	1017	0.33	10
12	4	1022	0.32	10
13	3	963	0.17	10
14	5	908	0.04	10
15	3	1022	0.32	10
16	3	758	0.05	1
17	5	856	0.20	1
18	4	854	0.22	1
19	7	951	5.3	1
20	2	751	0.08	1
21	4	766	0.04	1
22	4	837	0.34	1
23	3	953	9.7	1

[a] Runs are in chronological order. Exit aperture size governs collision number. This is allowed for in the Arrhenius plot, Fig. 23, by multiplying the CO/O_2 ratios by 10^2 for runs 1-15.

[b] These data are actually ratios of mass spectrometer signals at 28 and 32 amu. They may be reduced to relative fluxes of CO and O_2 by dividing by 1.1.

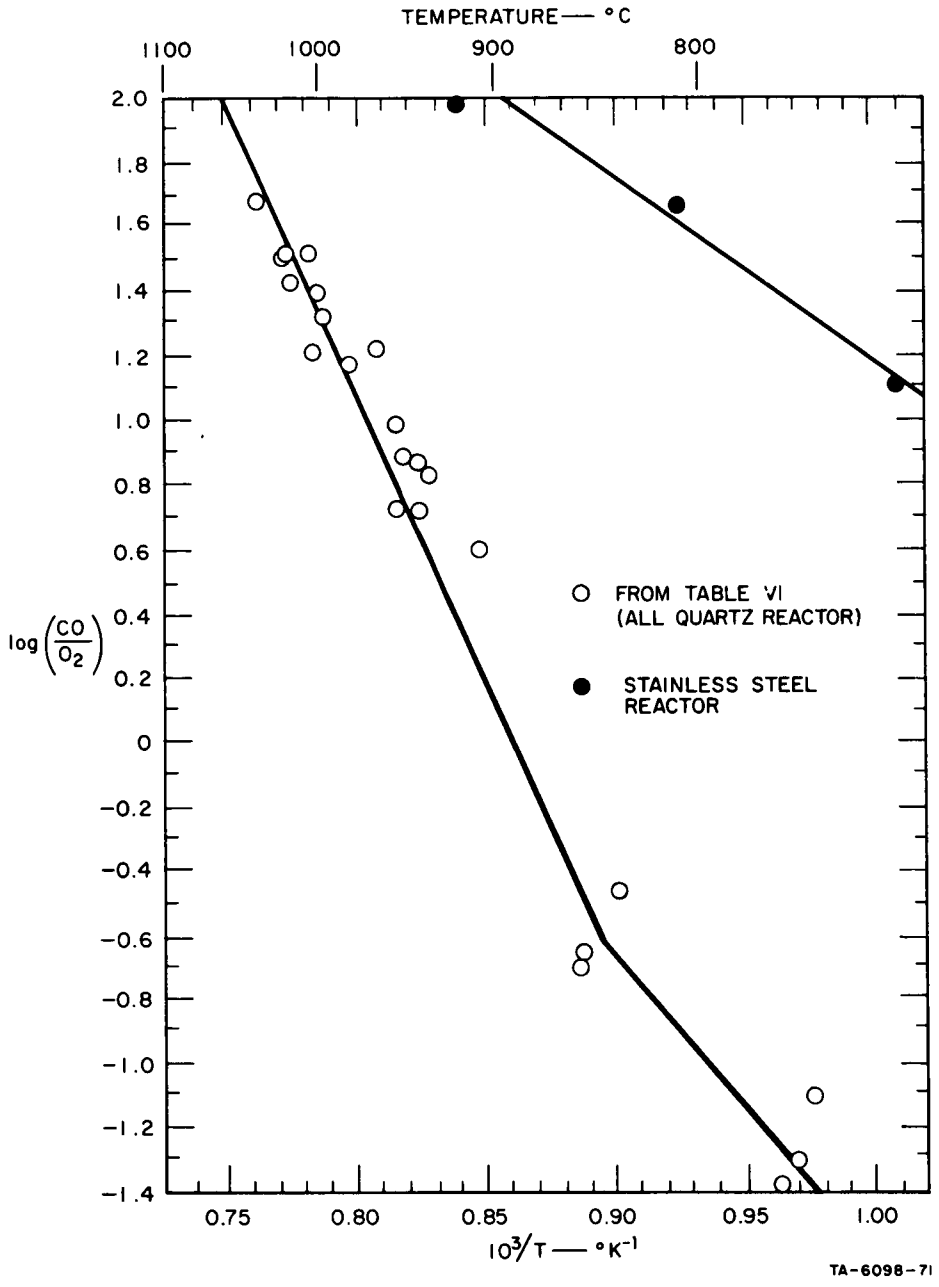

FIGURE 23 OXIDATION OF A THIN FILM OF CARBONACEOUS CHAR. Plot of data of Table II.

Table III

OXIDATION OF A 5.285-mg CHAR SAMPLE IN A REACTOR WITH A 1-cm-DIAMETER EXIT APERTURE

	I^{28}/I^{32}	I^{28}/I^{32} Blank	I^{28}/I^{32} Corrected	Chronological Order
1. 1080°C	0.068	0.025	0.043	
	0.063		0.038	
	0.056		0.031	
	0.056		0.031	8
2. 1066°C	0.065	0.05	0.015	
	0.072		0.02	
	0.105		0.05	
	0.085		0.035	
	0.089		0.04	
	0.098		0.05	1
3. 1040°C	0.049	0.02	0.03	
	0.044		0.02	
	0.042		0.02	
	0.039		0.02	
	0.042		0.02	7
4. 1005°C	0.028	0.017	0.011	
	0.029		0.012	
	0.031		0.014	
	0.032		0.015	
	0.030		0.013	5
		Estimated		
5. 989°C	0.046	0.04	0.01	
	0.04	0.04	0.00	
	0.02	0.02	0.00	
	0.04	0.04	0.00	
	0.02	0.02	0.00	2
6. 986°C	0.037	0.02	0.017	
	0.021		0.001	
	0.025		0.005	
	0.027		0.007	
	0.025		0.005	6
7. 940°C	0.046	0.048	0.00	
	0.028	0.028	0.00	
	0.038		0.01	
	0.032		0.00	
	0.018	0.017	0.00	
	0.016			
	0.019			4
8. 930°C	0.037	0.038	0.00	
	0.036		0.00	
	0.05		0.01	
	0.06		0.02	
	0.04		0.00	
	0.037		0.00	
	0.04		0.00	3

Table IV

OXIDATION OF A 5.285-mg CHAR SAMPLE IN A REACTOR WITH A 1-mm-DIAMETER EXIT APERTURE

Run	1	2	3	4	5	6	7	8	9	10
Temp., ^{o}C	1070	1070	1062	1055	1028	960	960	960	940	875
I^{28}/I^{32}	0.58 0.61 0.44 0.57	0.74 0.65 1.10	7.2 8.7 8.3 8.3 5.6	3.12 3.6 4.6 5.5	5.5 6.0 5.0	0.75 0.55 0.68 0.70	0.53 0.63 0.59 0.66 0.70 0.78	2.5 3.2 3.0	0.75 0.79 0.83	0.86 0.84
Chronological Order	1	2	7	6	8	3	4	9	5	10

Runs 1 and 3 were made with O_2 flows of about 6×10^{14} molecules/sec, and the other runs with an O_2 flow of about 5×10^{15} molecules/sec. Runs 3 through 10 were made on the day following runs 1 and 2.

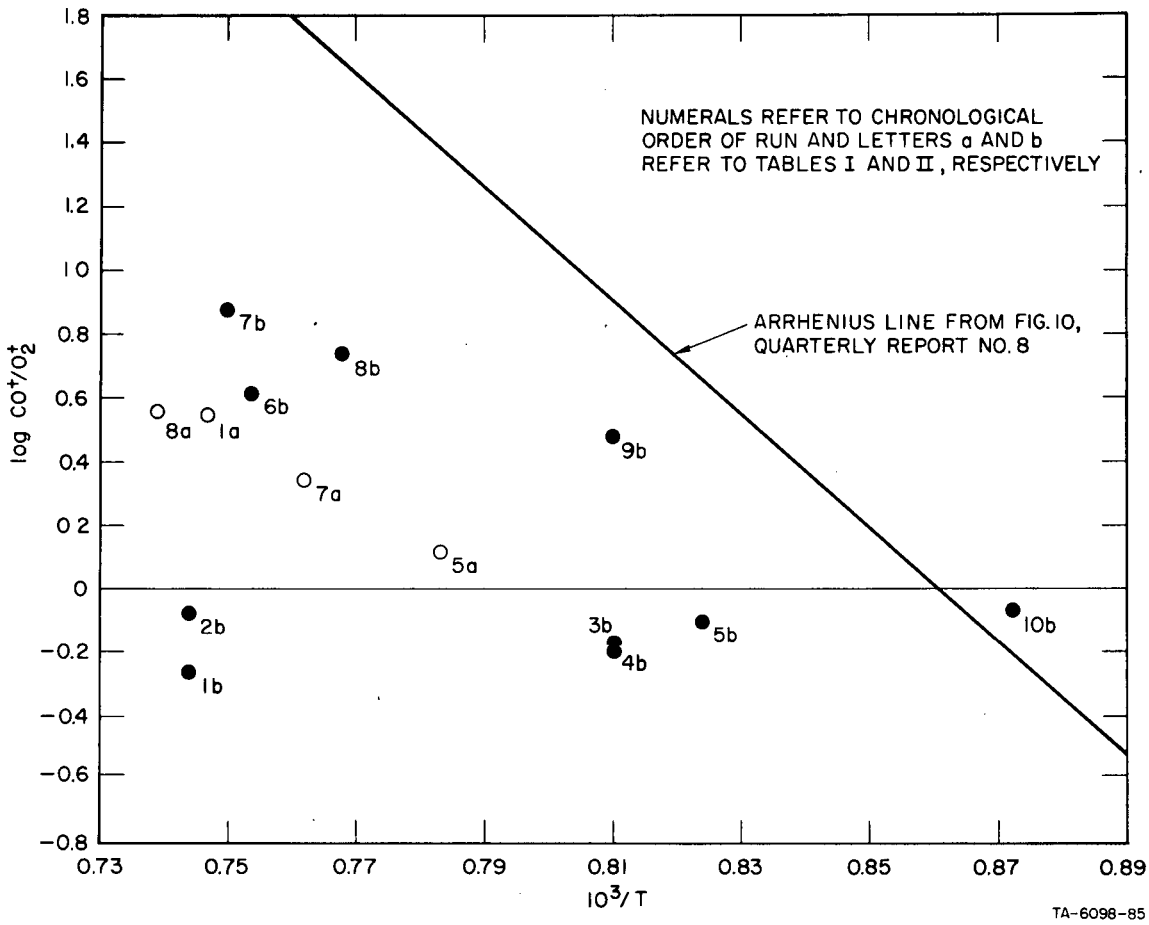

FIGURE 24 OXIDATION OF A 5.28-mg CARBONACEOUS CHAR FILM. Plot of data from Tables III and IV. (Note: CO^+/O_2^+ ratios from Table IV were multiplied by 100 to make them comparable with those from Table III.)

Table V

CO PRODUCTION DURING OXIDATION OF A CARBONACEOUS CHAR SAMPLE

DATE	RUN NO.	TEMP., °C	O_2 GAS FLOW, MOLECULES/SEC	$I(CO/O_2)$
8/13/68	23	1012	6×10^{15}	17
	24	1012	6×10^{15}	16.3
	29	1080	6×10^{15}	25
	31	1078	5×10^{16}	17.0
8/14/68	10	830	6×10^{15}	0.97
	11	830	6×10^{15}	1.36
	12	830	6×10^{15}	1.95
	13	830	6×10^{15}	2.10
	14	833	6×10^{15}	2.11
	17	840	5×10^{16}	0.4
	18	840	5×10^{16}	0.53
	19	840	5×10^{16}	0.73
	20	840	5×10^{16}	0.88
	21	840	5×10^{16}	0.91
	22	840	5×10^{16}	0.91
	23a	840	6×10^{15}	2.9
	23b	840	6×10^{15}	3.2
	24a	840	6×10^{15}	2.6
	24b	840	6×10^{15}	2.6
	25	840	6×10^{15}	2.5
	26a	840	6×10^{15}	2.4
	27	840	6×10^{15}	2.6
	29	963	6×10^{15}	-
	30	963	6×10^{15}	-
	31	963	6×10^{15}	12.5
	32a	963	6×10^{15}	13
	32b	963	6×10^{15}	12.5
	33a	963	5×10^{16}	7.4
	33b	963	5×10^{16}	7.1
	34	963	5×10^{16}	5.8

Table VI

CO AND CO_2 PRODUCTION DURING OXIDATION OF A CARBONACEOUS CHAR

DATE	GAS	RUN NO.	TEMP., °C	I^{28}_{CO}/I^{30}_{NO}	$I^{28}_{CO}/I^{32}_{O_2}$	I^{30}_{NO}/I^{40}_{Ar}	$I^{32}_{O_2}/I^{40}_{Ar}$	$I^{44}_{CO_2}/I^{30}_{NO}$	$I^{44}_{CO}/I^{32}_{O_2}$	I^{30}_{NO}	$I^{32}_{O_2}$
8/21/68	NO	9	945	0.05				0.002			
		10	952	0.10				0.006			
		12	963	0.10				0.005			
		14[a]	964	0.034				0.003			
		15[a]	965	0.034				0.004			
		20	965	0.08				0.002			
		21	965	0.10				0.007			
	N_2O	34	970	0.112				--			
		35	970	0.098				--			
	O_2	38	973		3.85				0.27		
		39	973		4.00				0.31		
8/22/68	N_2O	7u	1037	0.27					--		
		8	1037	0.53					--		
		9	1037	0.45					--		
		10	1037	0.23					--		
		11	1037	0.25					--		
		13-15	1028	0.30					--		
		19-21	1030	0.21					--		
	NO	24	1034	0.32				0.006			
		25	1034	0.32				0.000			
		26	1034	0.28				0.000			
		28[a]	1035	0.12				0.001			
		29[a]	1035	0.13				0.000			
		30[a]	1035	0.14				0.000			
	O_2	32d	1038		10.2		0.14		0.15		
		32e	1038		9.7		0.14		0.17		
		32f	1038		9.0		0.15		0.16		
	NO + O_2	33l	1038		7.7	2.2	0.25		0.3	79	9
		33u	1040		--	--	0.26		0.36	790	10
		34	1040		11	3.4	0.25		0.40	129	9.3
		35	1040		8.8	3.6	0.31		0.33	135	11.5
		36[b]	1040		5.7	0.25	0.22		0.27	89	62.5
		37[b]	1040		4.35	0.31	0.29		0.19	110	100
		38	1039		4.00	1.35	0.35		0.12	135	35
		39	1039		8.5	7.9	0.34		0.31	110	4.5
8/23/68	O_2	3	1035		6.3		0.21		0.11		
		4	1035		5.5		0.22		0.11		
		5	1035		5.5		0.21		0.10		
		10	1092		8.1		0.17		0.12		
		11	1092		8.1		0.17		0.13		
	N_2O	13	1092	0.16							
		15	1097	0.15							
		16[a]	1098	0.14							
		17[a]	1098	0.105							
		19[a]	1098	0.096							
	NO	21	1099	0.36				0.002			
		22	1099	0.38				0.003			
		23[a]	1099	0.114				0.000			
		24[a]	1099	0.128				0.001			

[a] Gas flow is 15 times higher for these runs.

[b] Oxygen flow is 7 - 10 times higher for these two runs

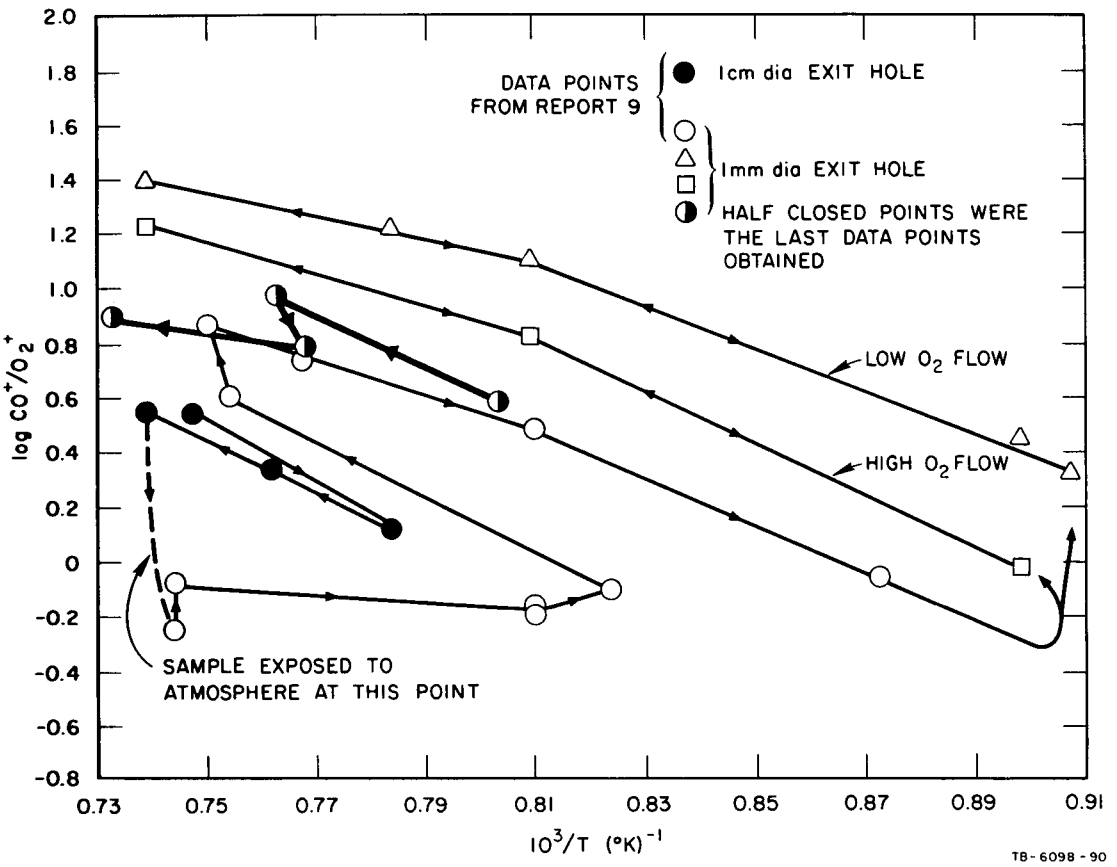

FIGURE 25 ARRHENIUS PLOT OF CARBON MONOXIDE PRODUCTION DURING REACTION OF OXYGEN WITH CHAR. Composite plot of data from Tables III, IV, V, and VI.

to migrate away from the initial settling point. The difference between the high and low oxygen flow rate constants is higher at the lower temperatures. This gives further support to the idea that at higher oxygen pressures reduced numbers of active sites are available for reaction, if we assume that the rate limiting factor is, for example, the reverse of reaction (15).

Further work will be required to establish the details of the mechanism more firmly.

2. Equilibrium Constant for Allyl Recombination. Direct Measurement of "Allyl Resonance Energy,"[20] by D. M. Golden, N. A. Gac, and S. W. Benson, J. Amer. Chem. Soc., 91, 2136 (1969).

Abstract

Pyrolysis of organic compounds usually proceeds through initiation steps involving bond-breaking. Better understanding of bond strengths will thus permit prediction of the rates of pyrolysis reactions through understanding of mechanism and reaction rate parameters. The reaction rate parameters depend strongly on the basic thermochemical parameters of reactant and product species.

The paper describes the use of VLPP to measure directly the properties of an important chemical species--the allyl radical. From our measurements we have derived a value for the allyl resonance energy (ARE). Our value of 9.6 kcal/mole is in satisfactory agreement with the value of 10 ± 1.5 kcal/mole[21] determined through study of the reaction of iodine atoms with propylene.

---

[20]Allyl resonance energy (ARE) is defined by the expression

$$ARE = DH^0_{298}(nC_3H_7\text{-}H) - DH^0_{298}(allyl\text{-}H)$$

Where $DH^0_{298}(A\text{-}B) = \Delta H^0_{f298}(A) + \Delta H^0_{f298}(B) - \Delta H^0_{f298}(AB)$.

Note: There is a sign error in footnote (1) of the published note.

[21]D. M. Golden and S. W. Benson, Chem. Rev., 69, 125 (1969).

Our VLPP studies disprove any idea that the allyl resonance energy exceeds 12 kcal/mole.

The experimental technique used entailed measurement of the rates of both the forward and reverse reactions

$$2 \text{ allyl} + M \underset{k_d}{\overset{k_r}{\rightleftharpoons}} \text{1,5-hexadiene} + M$$

Values of the equilibrium constant K_{rd} were measured at two temperatures through pyrolysis of 1,5-hexadiene (gives k_d) and pyrolysis of diallyl oxalate (generates allyl radicals and hence yields k_r). The third body M was the wall of the VLPP reactor.

The work was done in the VLPP-II system.

3. Absolute Rate Constants for Radical-Molecule Reactions Over a Wide Temperature Range: $CH_3 + DBr \rightleftarrows CH_3D + Br$. The Heat of Formation and Entropy of the Methyl Radical, by N. A. Gac, D. M. Golden, and S. W. Benson, J. Amer. Chem. Soc., 91, 3091 (1969).

This publication presents the results obtained using a reliable new method of measuring in a direct way the reaction rate constants of free radicals. Methyl radicals were generated in our VLPP-II reactor by pyrolysis of either di-tertiary butyl peroxylate or di-tertiary butyl peroxide (dtBP). DBr was added and the products monitored. The derived rate constants over the wide temperature range, 335 to 728°C, were consistent with an Arrhenius representation, $\log k_a = 8.8 - 1.5/2.303\ RT$ liter mole^{-1} sec^{-1}.

From these values, it can be shown that $S^0_{300}(CH_3) = 45.3 \pm 0.8$ gibbs/mole and $\Delta H^0_{f300}(CH_3) = 33.9 \pm 0.7$ kcal/mole. Assumptions include the supposition that the ratio $k_H/k_D = 1.5 \pm 0.5$, where k_H/k_D refer to

the reaction rates of methyl radicals with HBr and DBr, respectively. Tabulated for reference are the raw and partially treated data from which Figure 1 in the paper was derived.

Di-tertiary butyl peroxide was found unsuitable for use at 990°C as DBr was found to react with acetone at these temperatures. Data are presented in Table VII.

Attempts were therefore made to extend the rate constant measurements to higher temperatures using azomethane as a source of CH_3. The results are presented in Table VIII. The rate constant derived from these data at 1010°C is $10^{9.2}$ liter $mole^{-1}$ sec, compared with a predicted value of $10^{8.5}$ liter $mole^{-1}$ sec. The measured value is a factor of 5 higher than the value expected from the published lower temperature data. This could be because the methyl radicals generated by azomethane pyrolysis are "hot" or excited. At this time we have not resolved the reason for the high value of the apparent rate constant.

4. Thermal Degradation of Nadic Methyl Anhydride-cured Epoxy Novolac, by N. A. Gac, G. N. Spokes, and S. W. Benson, J. Polym. Sci., Part A-1, 8, 593 (1970).

Abstract

A DEN438 epoxy novolac-Nadic methyl anhydride-cured polymer was pyrolyzed in vacuum at temperatures to 800°C. Detailed analyses of the products yielded information on the mechanism of decomposition. Two-thirds of the weight loss of the polymer results in formation of relatively involatile high-molecular-weight gases. Carbon dioxide evolution indicates that at least 50% of the initial anhydride forms diester groups. The degradation of diester sites yields methylcyclopentadiene (MCPD) that is almost entirely decomposed to carbonaceous char.

The vacuum pyrolysis experiments that we did on the NMA-cured Dow epoxy novolac showed the importance of previously neglected high-boiling

TABLE VII

TITRATION EXPERIMENTS

dtBP + DBr at 991°C

Series	Run	T,°C	N_{dtBP} x 10^{-16}	N^0_{DBr} x10^{-16}	I'_{43} [a] (2000 mv)	N_{AC} [b] x10^{-16}	ΔN_{AC} x10^{-16}	I'_{16} [a] 500mv	I''_{16} [c] 500mv	I_{16} [c] 500mv	N_{CH_4} [b] x10^{-16}	%CH_4	I_{17} [a] 500mv	N_{CH_3D} [b] x10^{-16}	f	I_{96} [a]	N_{CH_3Br} x10^{-16}	I_{83} [a] 20mv	N^{83}_{DBr} [b] x10^{-16}	N^{flow}_{DBr} x10^{-16}
dtBP-1	7	992	1.95	0	110.8	3.68	0	137.6	135.9	135.9	1.60	41.0	2.2	0.026	--	0	0	0	0	0
T - 1	8	988	1.94	1.19	104.6	3.47	0.21	--	--	--	--	--	46.7	0.551	0.144	6.10	0.104	13.0	0.26	0.64
T - 2	9,10	1002	1.94	2.32	82.6	2.74	0.94	--	--	--	--	--	84.6	1.00	0.261	13.8	0.236	43.0	0.89	1.32
T - 3	11,12	992	1.94	0.556	101.6	3.45	0.23	236	215	100	1.17	30.2	26.1	0.310	0.081	6.72	0.115	1.2	0.025	0.25
dtBP-2	13,14	992	1.95	0	110.6	3.67	0	126.4	125.0	125.0	1.47	37.7	1.8	0.021	--	0	0	0	0	0
dtDP-3	19	992	1.89	0	95.4	3.16	0	124.6	123.3	123.3	1.45	38.4	1.6	0.019	--	0	0	0	0	0
T - 4	20	990	1.93	2.70	101.6	2.67	0.55	314	253	167	1.97	51.1	100.2	1.18	0.309	13.7	0.234	61.5	0.73	1.52
T - 5	21	995	1.91	0.886	80.4	3.08	0.13	263.6	229.3	120.3	1.42	37.2	42.6	0.501	0.132	3.75	0.064	10.8	0.22	0.386
T - 6	22	985	1.90	1.21	92.8	2.97	0.24	265.6	221.6	116.6	1.37	36.0	54.6	0.645	0.168	6.25	0.107	17.5	0.36	0.560
dtBP-4	24	985	1.87	0	98.4	3.26	0	119.8	118.7	118.7	1.39	37.0	1.4	0.017	--	0	0	0	0	0

[a] Primed intensity values indicate correction for background only.

[b] $N_X = I'_y/\alpha^x_y$

$\alpha^{AC}_{43} = 3.01 \pm 0.16 \times 10^{-15}$

$\alpha^{CH_4}_{16}$ 8.48 x 10^{-15}

$\alpha^{CH_3D}_{17}$ 8.48 $\pm$ 0.18 x 10^{-15}

$\alpha^{CH_3Br}_{96} = 5.65 \times 10^{-15}$

$\alpha^{DBr}_{83} = 4.83 \pm 0.80 \times 10^{-15}$

[c] $I''_{16} = I'_{16} - \frac{I^{16}}{I_{17}}_{CH_3D} \times I'_{17}$

$I'''_{16} = I''_{16} - f(I'_{16})_{DBr=0}$

TABLE VIII

TITRATION EXPERIMENTS

AM + DBr at 1010°C

Series	Run	T, °C	N^0_{AM} x10^{-16}	N^0_{DBr} x10^{-16}	I'_{16} (1000 mv) [a]	I''_{16} [a]	I'''_{16} [b]	% CH_4	I_{17} (1000 mv) [b]	I_{28} (1000 mv.) [b]	f	I_{43} (100 mv) [b]	I_{96} (500 mv) [b]	N_{CH_3Br} x10^{-16}	I_{83} (500 mv) [b]	$\left(N_{DBr}\right)_{I_{83}}$ x10^{-16}	$\left(N_{DBr}\right)_{flow}$ x10^{-16}	$\frac{1}{f}$	$\left(\frac{1}{f}\right)'_{corr}$ [c]	$^1N_{DBr}$ x10^{+17}
AM-3	5	1000	0.373	0	23.0	23.0	23.0	16	0	96	0	29	0	0	0	0	0	- -	- -	- -
T - 1	6	1010	0.361	3.88	110	43	38	27	83	80	0.746	21	- -	- -	60.3	3.22	3.34	1.34	0.88	2.99
T - 2	7	1000	1.13	3.70	313	174	148	38	173	230	0.540	51	0.48	0.23	38.8	2.08	2.48	1.85	1.00	4.03
AM-4	8	1000	1.13	0	98	98	98	23	0	350	0	139	0	0	0	0	0	- -	- -	- -
AM-5	13	1008	0.473	0	39	39	39	21	8.0	169	0	53	0	0	00	0	0	- -	- -	- -
T - 3	14	1008	0.470	3.60	161	64	52	29	120	119	0.726	32	0.24	0.11	54.3	2.90	2.92	1.38	0.95	3.42
T - 4	15	1010	0.460	7.75	143	45	42	24	122	99	0.885	38	0.24	0.11	137.3	7.34	6.94	1.13	1.02	1.44
AM-6	16	1020	0.455	0	45	45	45	25	6.0	147	0	47	0	0	0	0	0	- -	- -	- -
T - 5	17	1010	0.465	2.58	135	53	45	25	102	107	0.685	32	0.12	0.06	38.3	2.05	1.94	1.46	1.02	5.14
T - 6	18	1005	0.456	1.05	115	63	49	28	64	101	0.452	37	0.04	0.002	12.1	0.65	0.64	2.21	1.44	15.6
T - 7	19	1000	0.455	0.666	105	71	51	29	42	109	0.276	37	0	0	5.70	0.305	0.415	3.62	2.64	24.1
T - 8	20	1010	0.461	0.386	105	76	52	29	36	123	0.218	50	0	0	2.90	0.155	0.185	4.76	3.31	54.1

[a] $\alpha^{43}_{CH_2CHCH_2D} \cong \alpha^{42}_{CH_2CHCH_3} = 8.27 \pm 0.41 \times 10^{-15}$

[b] $\alpha^{CH_4}_{16} \sim 19.4 \times 10^{-15}$ $\quad \alpha^{AM}_{43} = 144 \pm 7 \times 10^{-15}$

$\alpha^{CH_3D}_{17} = 19.4 \pm 1.0 \times 10^{-15}$ $\quad \alpha^{DBr}_{83} = 1.87 \pm 0.15 \times 10^{-15}$

$\alpha^{N_2}_{28} = 27.9 \pm 0.5 \times 10^{-15}$ $\quad \alpha^{CH_3Br}_{96} \sim 2.1 \times 10^{-15}$

[c] $\left(\frac{1}{f}\right)_{corr} = \frac{1}{f} - \frac{I'''_{16}}{I_{17}}$

polymeric materials among the product materials. The pie chart in Figure 26 showing products illustrates our results.

Our data are the basis for our model of the mode of action of a char portrayed in Figure 2 of this report. In an ablating epoxy novolac polymer, high-boiling tarry substances will be ejected from the polymer reaction zone into the slightly porous zone closer to the ablative surface. Here the temperature is higher and the material will undergo further degradation through pyrolysis reactions. Breakdown of the molecular structure of these substances will yield progressively more stable, lower molecular weight substances, including benzene, hydrogen, carbon monoxide, and ethylene. Solid carbonaceous material will also form. Evidence for this kind of action has been reported in the literature.[2,3]

The compounds referred to are:

DEN438

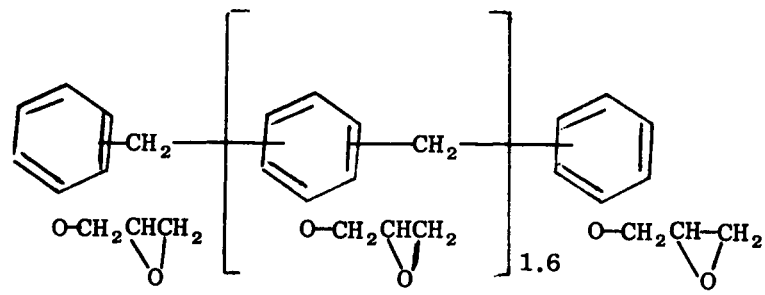

Polyglycidyl ether of phenol-formaldehyde novolac (DEN 438)

and nadic methyl anhydride

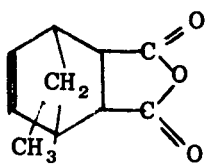

Methylbicyclo[2.2.1]hept-5-ene-2,3-dicarboxylic anhydride (NMA)

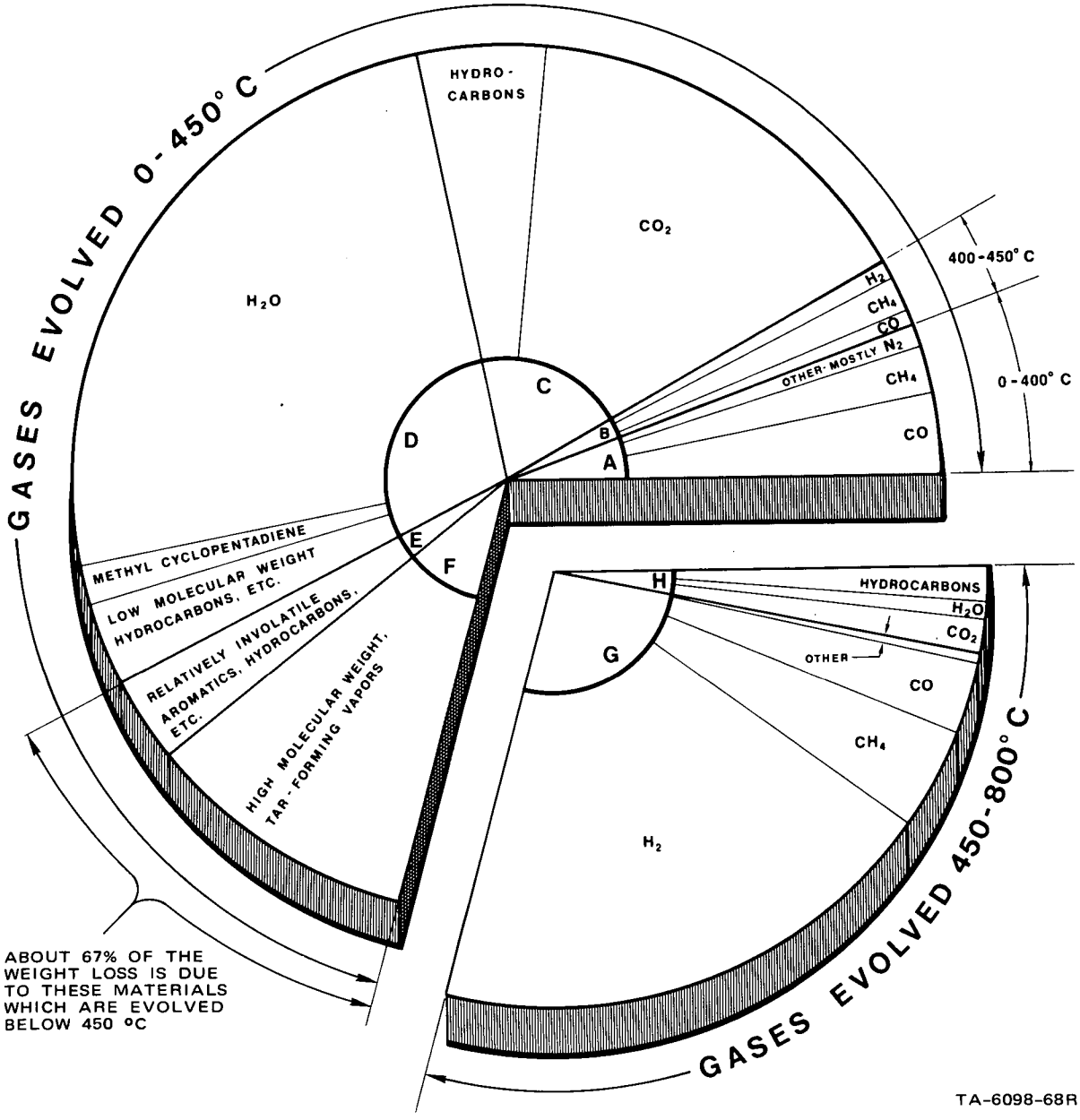

FIGURE 26 GASES EVOLVED DURING PYROLYSIS OF A SAMPLE OF DEN438-NMA CURED POLYMER

The char yield of this combination under vacuum pyrolysis is 20 ± 2% by weight. We conclude that decomposition proceeds in three stages. The first stage is the elimination of NMA from monoacid-monoester sites at temperatures to 350°C. These sites apparently react to form additional ether links not present in the original cured polymer. The second stage is a reverse Diels-Alder elimination of MCPD at about 350 to 400°C. The MCPD does not escape from the polymer but reacts and thereby enhances carbon formation. About one-third of the char comes from the degradation of MCPD. The remaining two-thirds comes from a breakdown of the maleic diester groups that are left when MCPD is eliminated. The aromatic backbone is apparently stable at temperatures of 350 to 400°C. The third stage of decomposition commences at 450°C; the resin backbone structure begins to crack and give phenol-like, high-boiling materials. A significant result of this work is that these high-boiling materials that are evolved as gases constitute two-thirds of the weight loss of polymers. The char is almost completely formed at 450°C. Pyrolysis at 800°C led to a further weight loss of only 4%.

5. Pyrolysis of Hydrocarbons in Knudsen Cells, by G. N. Spokes and S. W. Benson, Recent Developments in Mass Spectroscopy (Edited by K. Ogata and T. Hayakawa), University of Tokyo Press, 1970, p. 1146.

Abstract

Hydrocarbon gases have been pyrolyzed in reactors at very low pressures, and the products of pyrolysis have been monitored using mass spectroscopy. Gases, such as ethane, ethylene, and benzene, have been found to react with high probability (> 0.005 per collision) at temperatures above 1600°K. Reactor walls participate in the chemical reaction. For example, carbon monoxide is copiously evolved when benzene or toluene react in an alumina reactor; carbon monoxide is also a significant product when pyrolysis is carried out in a quartz reactor. Ethane is significantly less reactive than the unsaturated compounds in quartz, alumina, and carbon reactors.

An additional breakthrough registered during the course of the research program was in the area of high-temperature chemical kinetics in static systems.

The only previous systematic wide-ranging work on gas-phase reactions above 1000°C has been done in shockwaves. The current work has opened up the 1300 to 1900°K range of temperature for systematic exploration in static systems.

Figure 14 is a sketch of one modification of the apparatus used for this work. A quartz reactor was used in the configuration shown. The quartz reactor insert may simply be removed, thereby exposing the aluminum oxide muffle tube (alumina reactor). An ATJ carbon tube and end cap may be inserted to form the carbon reactor configuration. One further simple configuration is referred to as alumina and quartz plate. A quartz plate 5 cm x 1.2 cm x 1 mm was located in the alumina reactor system. The plate was held by thin platinum wires.

Tabulation of Data on the Reactions of Hydrocarbons at High Temperatures

We present in Table IX all the data that have been obtained to date on the pyrolysis of hydrocarbons at high temperatures. The data are presented in condensed form from about 1000 photographs of mass spectra, each of which has from 5 to 10 important mass peaks. The reduction methods used are as follows.

1. Ethane-Argon. The ethane-argon mixture consisted of 30.5 parts ethane and 24.3 parts argon. The argon mass peak at 40 amu, therefore, served as a reference to determine the level of decomposition of the ethane. Contributions to mass 29 and 30 came from ethane and isotopic

Table IX

RESULTS OF PYROLYTIC REACTIONS AT HIGH TEMPERATURES

C_2H_6

Date	Run	Temperature (C°)	$\frac{(I/I_{40})_{through}}{(I/I_{40})_{bypassed}}$ 26*	27	28	29	30	$\frac{(I_{40})_{through}}{(I_{40})_{bypassed}}$ 40	
3-27	2	Amb			0.99			1.25	
3-28	2-3	Amb	1.06		1.06		0.82	1.37	
	4-5	Amb	0.95		1.05		1.00	1.15	
	6-7	Amb	0.92		—		0.97	1.37	
	9-10	690	0.80		0.79		0.96	1.34	
	12-13	897	0.91		0.83		0.94	1.30	
	16-17	1060	0.97		0.96		1.00	1.15	QUARTZ REACTOR
	18-19	1060	0.94		1.5		0.93	1.30	
3-31	3-4	1184	1.02		0.96		1.0	1.31	
	7-8	1250	1.22		1.27		1.13	1.17	
	10-11	1320	0.90		0.93		0.93	1.33	
4-1	2-3	Amb	0.98		1.0		0.97	1.28	
	11-12	1527	0.83		—		0.86	1.30	
	15-16	1512	0.87		—		0.84	1.19	
4-15	2-3	1034	1.01				0.98	1.26	
	5-6	1240	0.97				0.91	1.26	
4-18	20-21	1383	1.04				0.92	1.19	
4-19	15-17	1416	0.91	0.89		0.84	0.83	1.26	
	24-26	1415	0.94	0.91		0.84	0.87	—	
6-30	6-9	1180	1.01	0.97	1.06	0.94	0.91	1.29	GRAPHITE REACTOR
	12-15	1439	0.98	0.92	1.17	0.66	0.94	0.93	
	23-25	1570	0.74	0.76	0.97	0.38	0.62	1.17	
	26-29	1575	0.85	0.77		0.80	0.77	1.61	
7-1	19-20	1592	0.7	0.64		0.42	0.62	—	
	23-24	1592	0.98	0.97	1.23	0.94	1.04	0.92	

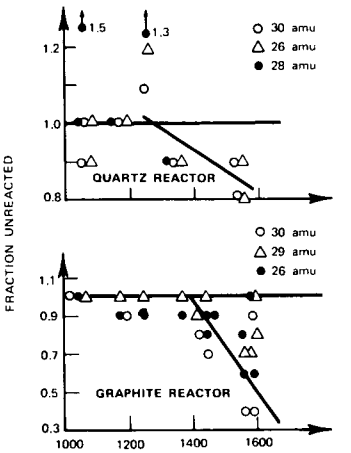

C_2H_4

Date	Run	Temperature	$I_{through}/I_{bypassed}$ 26	27	28	
12-23	4-5	1460°C	1.19	1.24		
	9-10	1600	1.02	1.08		ALUMINA
	9-11	1600	1.04	1.07		
12-24		25	1.38	1.45	1.42	
2-4	6-9	25	1.32	1.30	1.35	
	13-16	1160	1.29	1.27		
	"	"	1.25	1.27	1.25	
	22-25	1358	1.11	1.11		
	28-29	1463	0.94	0.93		ALUMINA + QUARTZ PLATE
	31-32	1462	0.97	0.96		
2-5	4-7	1162	0.94	0.94	0.94	
	11-13	1500	0.97	0.95	1.8	
	18-20	1500	0.97	0.97	1.57	
3-26	2-3	25	1.5	1.54	1.43	
	5	25	1.34	1.29	1.22	
	5	25	1.34	1.29	1.25	
3-27	1	25	1.33	1.31	1.34	QUARTZ
3-31	12-13	1320	1.36	1.34	1.33	
4-1	4-5	25	1.29	1.29	1.28	
	9-10	1528	0.77	0.80	1.0	
	17	1507	0.81	0.79	(0.8)	
4-15	7-8	1237	1.04	1.08	(1.29)	
4-18	6-10	1158	1.2	1.18	1.2	
	14	1385	0.77	0.83	—	GRAPHITE
	16	1385	0.74	0.83	—	
4-19	30-33	1415	1.04	1.02		

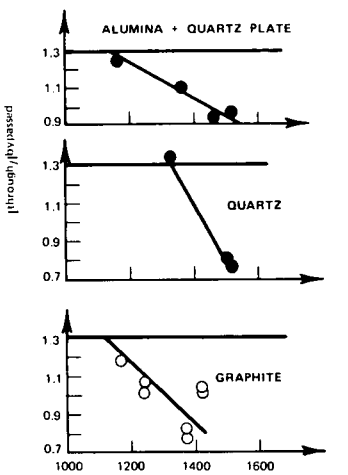

C_6H_6

Date	Run	Temperature	$I_{through}/I_{bypassed}$ 26	28	39	50	52	78	I_{28}/I_{78}	I_{28}/I_{50}	
12-19	32	1575°C	.58	6.4	.93	.73	.69	.73	5.3		
	33	1575	—	6.2	—	—	—	.73	5.1		
	34	1575	.75	6.0	.82	.73	.74	.70	5.1		ALUMINA REACTOR
	37		.75	6.0	.82	.73	.77	.74	5.0		
	38	1575	.58	5.9	.75	.69	.74	.73	5.0		
12-23	13	1604			0.74	0.75				13	
	16	1604			0.74	0.75				13	
3-26	4	25			1.32	1.25			1.35		
3-27	3	25			1.1	1.25			1.29		
3-31	14-15	1316			1.28						QUARTZ REACTOR
	16-17	1318	1.2		1.37	1.37	1.35	1.30			
4-1	6-7	25	1.2		1.25		1.29	1.22			
	13-14	1515	0.83		0.75		0.8	0.67			
4-15	9-10	1234	1.2		1.05	1.10	1.08	1.11			
4-18	25-26	1381	1.0	1.58	0.96	0.95	0.98	0.97			
	27-30	1381	0.95	2	1.00	0.98	1.00	1.00			
4-19	8-9	1416	1.0	—	1.0	0.97	0.96	0.95			
	12	1416	1.0	—	0.97	1.03	1.00	1.0			GRAPHITE REACTOR
	10-11	1416	—	—	0.97	0.98	1.00	0.98			
7-1	3-4	1200	1.15	3.2	1.12	1.10	1.08	—			
	7-8	1198	1.00	2.4	1.03	1.00	1.15	1.10			
	9-10	1484	0.92	—	0.82	0.84	0.87	0.85			
	13-16	1594	0.85	—	0.77	0.79	0.75	0.73			

*Column headings are atomic mass units.

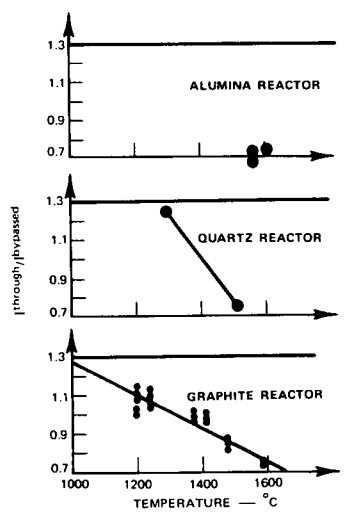

TB-6098-101

$C^{12}O^{17}$, $C^{12}O^{18}$, and $C^{13}O^{16}$ plus small miscellaneous (but constant) contributions from impurities in the system. All of these interference peaks were subtracted out when preparing data for the table. The signals at 26, 27, and 28 amu were contributed to by ethane, ethylene, acetylene, and carbon monoxide plus, of course, background signals. As far as possible, these background signals were subtracted out to ascertain information about products. Products should be recognized by comparison of signals with those at 29 and 30 amu, which presumably came only from ethane. The tabulations for ethane give the fraction unreacted, f, as estimated from the relation

$$f = \frac{[I^{amu}_{thru}]}{[I^{40}_{thru}]} \times \frac{[I^{40}_{bypass}]}{[I^{amu}_{bypass}]}$$

where I^{x}_{thru} and I^{x}_{bypass} are the measured signal changes at mass peak x amu for the reactants when passed through the reactor and when bypassed directly into the mass spectrometer. The value of $I^{40}_{thru}/I^{40}_{bypass}$ is included for completeness. This ratio has been found to be close to 13 under almost all conditions.

2. Ethylene. The important ethylene peaks are 26, 27, and 28 amu. Loss of ethylene is determined chiefly through reduction of the 26 and 27 amu signals. Acetylene production would be expected to increase the signal of 26 amu relative to 27 amu, although propylene production would be expected to yield an increase at 27 amu, which might compensate for the change at 26 amu. One thing is certain: a decrease at 27 amu implies a loss mechanism for ethylene. We tabulate $[I^{amu}_{thru}/I^{amu}_{bypass}]$,

and we see that cold gases commonly give a value for this ratio of about 1.3. We infer that deviations from this ratio imply that the fraction undecomposed has an upper limit of $\left\{\left[I^{amu}_{thru}/I^{amu}_{bypass}\right]/1.3\right\}$.

3. Benzene. The situation for benzene is more clear-cut than for ethylene because there is no interference from products at 39, 50, 51, 52, 77, and 78 amu. The fraction unreacted is again given by $\left\{\left[I^{amu}_{thru}/I^{amu}_{bypass}\right]/1.3\right\}$.

The Reaction Between Alumina and Carbon

We pointed out earlier that certain hydrocarbons reacted with alumina at temperatures above 1400°C to yield carbon monoxide and other products. We surmised that the alumina was reduced to carbon monoxide and a lower oxide of aluminum--perhaps aluminum metal. It is known that intimate mixtures of alumina and carbon will react to yield carbon monoxide and aluminum at 1800 to 2300°C. However, high yields of CO were obtained at only 1450°C when a carbon liner was used in the reactor furnace. This is surprising, since the carbon and alumina were not touching except at support points at the top and bottom ends of the liner. Further, the vapor pressure of pure carbon at 1470°C is less than 10^{-9} torr and that of pure alumina is below 10^{-6} torr.

Copious CO evolution took place at an indicated temperature of 1470°C. The pressure indicated in the mass spectrometer was 3×10^{-4} torr. The gas pressure at the carbon-alumina interface must have been orders of magnitude higher. Figure 27 is an Arrhenius plot of the ionization gauge pressure reading as a function of temperature. (Mass spectra

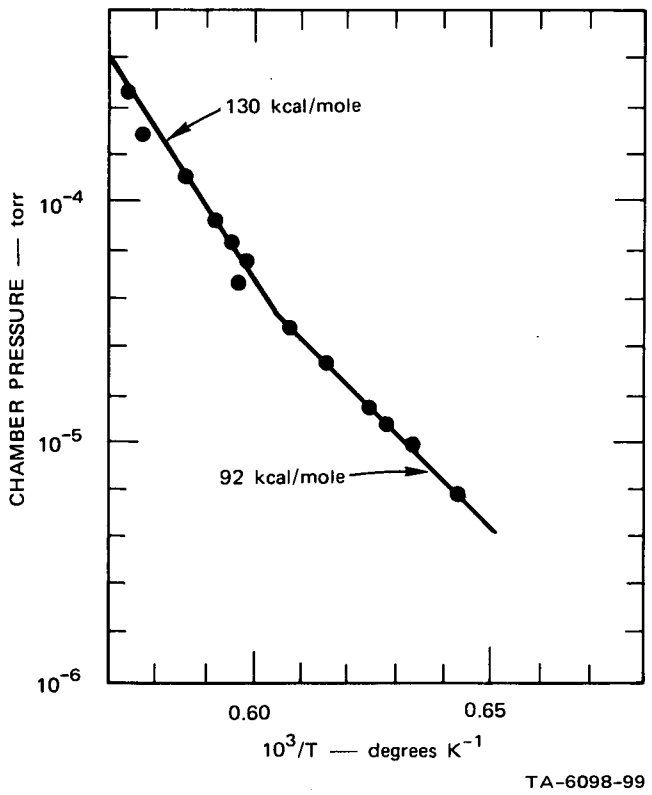

FIGURE 27 GAS EVOLUTION FROM CARBON-ALUMINA REACTION.
Arrhenius plot of mass spectrometer chamber pressure.

showed CO to be the only gaseous product.) The meaning of the high activation energies obtained is not clear, but such high values are typical of volatilization energies of fragments of molecules from refractory materials.

Inspection of the system after disassembly showed that extensive deposits of a grey metal had occurred in all cool parts of the system that were exposed to vapors emerging from the reactor. Heavy deposits on the heat shields at the exit hole of the reactor were weighted. About 1/2 gram of material had collected there after three hours at 1470°C. The deposits were basically aluminum metal.

Figure 28 shows the appearance of an unused carbon liner and the carbon liner after reaction; Figure 29 shows the inside of the alumina muffle tube--sectioned into halves; and finally, in Figure 30 we see that etch pits in the alumina match up exactly with etch pits in the carbon. A mirror was placed between the Al_2O_3 and the carbon liner to show the one-to-one relation between carbon etch pits and alumina etch pits.

In addition to deep pitting, there was noticeable general erosion of the carbon. The alumina was less heavily pitted on one side, probably because the carbon was not a perfect fit and was not so closely juxtaposed on that side.

At the time of writing this report, the details of the chemistry have not been evaluated. We know from the literature, however, that in a reducing atmosphere of aluminum metal in the absence of oxygen, the rate of decomposition of the alumina is much enhanced. The close interaction between the carbon and the decomposing oxide is expected to yield large amounts of CO and aluminum, and the latter is then able to

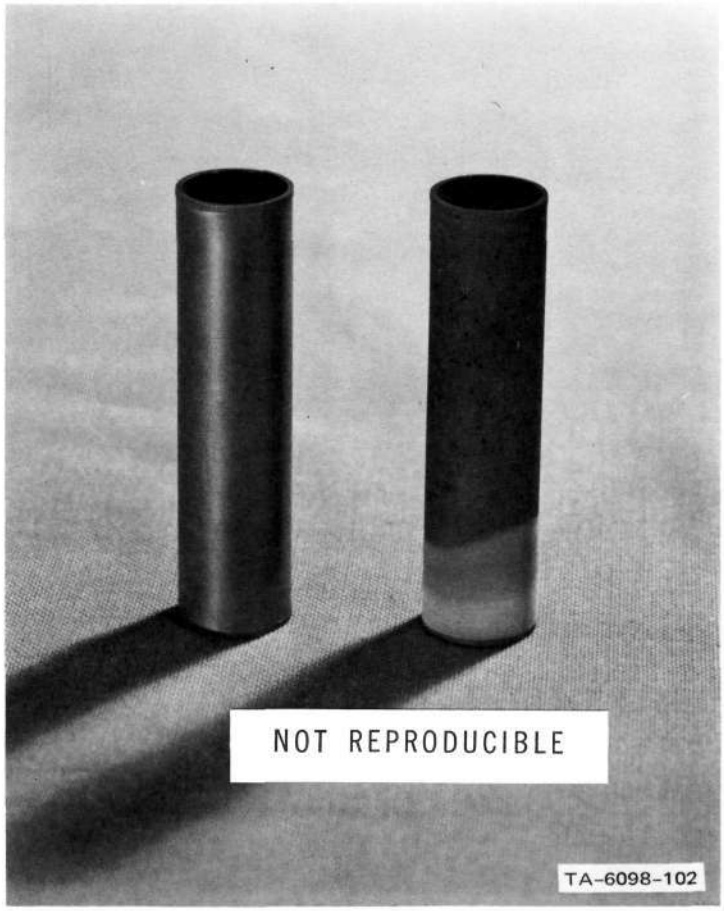

FIGURE 28 CARBON LINER BEFORE (LEFT) AND AFTER (RIGHT) REACTION WITH A PURE ALUMINA TUBE AT 1470°C

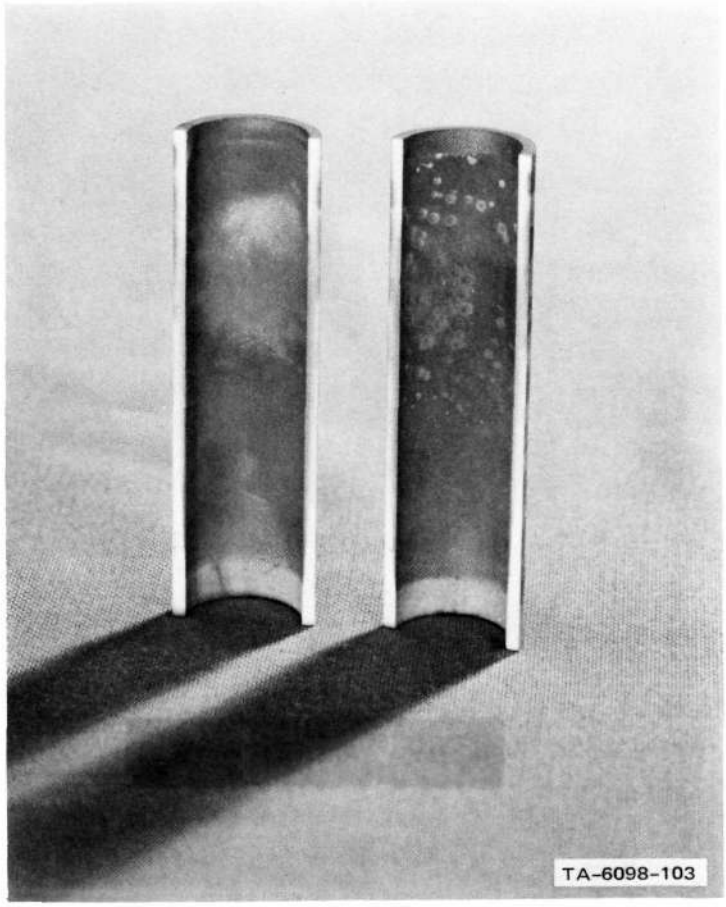

FIGURE 29 SECTIONED ALUMINA TUBE REACTED WITH CARBON

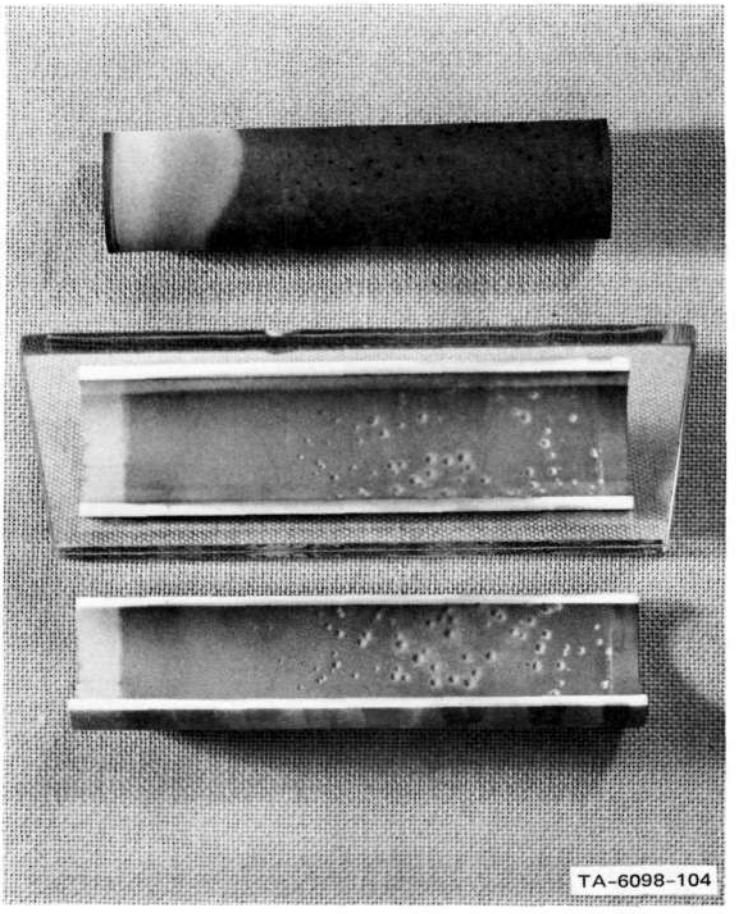

FIGURE 30 A MIRROR PLACED BETWEEN THE CARBON LINER AND THE ALUMINA TUBE SHOWS THAT ETCH PITS IN CARBON CORRESPOND WITH THOSE IN ALUMINA

catalyze decomposition of further amounts of alumina.

The proposed mechanism is:

$$Al_{(g)} + Al_2O_{3(s)} \rightarrow Al_2O_{(g)} + AlO_{2(s)}$$

$$Al_2O_{(g)} + C_{(s)} \rightarrow 2Al_{(g)} + CO_{(g)}$$

$$3Al_{(g)} + AlO_{2(s)} \rightarrow 2Al_2O_{(g)}$$

$AlO_{2(s)}$ refers to an aluminum deficient surface site on the $Al_2O_{3(s)}$. The stoichiometry is

$$Al_2O_{3(s)} + 3C_{(s)} \rightarrow 2Al_{(g)} + 3CO$$

since, with the configuration of the system, we can expect $Al_2O_{(g)}$ to react with carbon rather than escape. Evidently, the gas pressure is limited only by the rate at which aluminum vapor is evolved and pumped away along with the other (mass spectrometrically) observed product--CO.

Conclusions

Heterogeneous reactions may lead to very fast reactions of hydrocarbons with both refractory materials and with carbon at temperatures in excess of 1300°C. Refractory oxides such as aluminum oxide have been reduced by hydrocarbons including ethane, benzene, ethylene, and toluene. Detectable gaseous products have included carbon monoxide.

In a char-forming ablative material, the reducing gases that flow through the char to high-temperature zones will react with refractory oxide substrate material if the temperatures exceed 1300°C. At appreciably higher temperatures, the oxide refractory material may react endothermically with the carbon of the char layer.

6. A Comparison of RRK and RRKM Theories for Thermal Unimolecular Processes, by D. M. Golden, R. K. Solly, and S. W. Benson, J. Phys. Chem., 75, 1333 (1971).

Abstract

It is shown that in prescribed temperature regions the Kassel integral of RRK theory gives values of k/k_∞ in good agreement with values computed from RRKM theory for a number of widely different thermal unimolecular processes. The parameter s is uniquely defined as $C_{vib}(T)/R$.

The results are presented in Tables X and XI. In this paper we have shown that the relatively simple RRK theory can give valid predictions of falloff data for pyrolysis of various molecules at low pressure. Validity is checked against RRKM theoretical values using parameters given in Table XII. The importance of this paper is that it gives further validation to our simple interpretation of our low-pressure pyrolysis rate constants. It shows in essence that estimation of the frequencies of the transition state, for use with the Marcus formulation of the RRK theory, corresponds to estimation of the reaction A-factor. O'Neal and Benson have shown how the reaction A-factor may be predicted for most molecules from a study of the structure of the ground and transition states. Such values of A-factor coupled with a knowledge of heat capacity and a rough idea of the activation energy permit the use of the RRK theory for prediction of low-pressure falloff data.

These data could be of importance in predicting homogeneous phase pyrolysis rates of low-molecular-weight hydrocarbons at high temperatures where their rate constants fall into the second order region. Such conditions could pertain in an ablative environment. Table XI shows calculations of two such examples.

Table X

CALCULATED FALLOFF DATA [$k/k_\infty(T)$] FOR MODELS 1-8

1. HHH $\quad \underline{n}C_4H_{10} \rightarrow 2C_2H_5$

$\log k_\infty = 18.2 - 81.7/\theta$ [a]

P [b]	k/k_∞(300)		k/k_∞(600)		k/k_∞(900)		k/k_∞(1200)	
	M [c]	K(s=7) [d]	M	K(s=16)	M	K(s=23)	M	K(s=27)
10^3	1.0	.55	1.0 (-1)	.97	9.9 (-1)	9.4	8.7 (-1)	8.1
10^1	1.0	.078	9.9 (-1)	7.0	7.9 (-1)	5.5	3.5 (-1)	2.9
10^{-1}	1.0	.0033	8.1 (-1)	2.3	2.6 (-1)	1.3	4.0 (-2)	3.9
10^{-3}	9.3 (-1)[e]	.0067	2.8 (-1)	.30	2.6 (-2)	1.4	1.8 (-3)	2.3
k_∞	3.4×10^{-42}		2.4×10^{-12}		2.1×10^{-2}		1.9×10^{3}	

2. HHL $\quad C_2H_6 \rightarrow 2CH_3$

$\log k_\infty = 18.3 - 90.6/\theta$

P	k/k_∞ (300)		k/k_∞ (600)		k/k_∞ (900)		k/k_∞(1200)	
	M	K(s=2)	M	K(s=7)	M	K(s=10)	M	K(s=13)
10^3	1.0	8.7×10^{-6}	9.1 (-1)	1.1	6.0 (-1)	1.9	2.9 (-1)	1.4
10^1	.84	8.7×10^{-8}	3.3 (-1)	.051	9.0 (-2)	1.5	2.2 (-2)	1.0
10^{-1}	.20	8.7×10^{-10}	2.1 (-2)	.011	3.0 (-3)	5.2	5.2 (-4)	3.4
10^{-3}	8.5×10^{-3}	8.7×10^{-12}	4.3 (-4)	.016	4.7 (-5)	1.1	7.0 (-6)	7.3
k_∞	6.78×10^{-48}		2.36×10^{-15}		2.19×10^{-4}		6.95×10^{1}	

a At $\langle T \rangle = 900^0K$, units sec^{-1}, $\theta = 2.3\ RT$ kcal/mole

b Torr

c $k/k_\infty(T)$ as computed from RRKM theory.

d $k/k_\infty(T)$ as computed from RRK theory ($s \equiv C_{vib}(T)/R$)

e (-1) signifies multiplication by 10^{-1} for entries in both columns M and K.

continued...

Table X (continued)

3. LHH $\phi\dot{C}O \rightarrow \phi^{\bullet} + CO$

$\log k_{\infty} = 14.6 - 28.6/\theta$

P	k/k_{∞} (300)			k/k_{∞} (600)			k/k_{∞} (900)			k/k_{∞} (1200)		
	M		K(s=10)	M		K(s=19)	M		K(s=24)	M		K(s=27)
10^{3}	1.0		.96	9.7	(-1)	9.4	6.9	(-1)	6.6	2.9	(-1)	2.9
10^{1}	9.9	(-1)	5.4	5.4	(-1)	4.4	9.5	(-2)	9.7	1.2	(-2)	1.3
10^{-1}	6.9	(-1)	.89	6.5	(-2)	5.8	3.0	(-3)	3.7	1.9	(-4)	2.1
10^{-3}	9.6	(-2)	.39	2.0	(-3)	2.9	4.5	(-5)	7.1	2.1	(-6)	2.4
k_{∞}	5.6×10^{-7}			1.4×10^{6}			4.3×10^{7}			2.3×10^{9}		

4. LHL $CH_3NHNH_2 \rightarrow NH_3 + CH_2{=}NH$

$\log k_{\infty} = 13.2 - 53.9/\theta$

P	k/k_{∞} (300)			k/k_{∞} (600)			k/k_{∞} (900)			k/k_{∞} (1200)		
	M		K(s=4)	M		K(s=9)	M		K(s=13)	M		K(s=15)
10^{3}	1.0		.87	1.0		.99	1.0		.99	9.8	(-1)	9.7
10^{1}	1.0		.18	9.9	(-1)	8.0	9.0	(-1)	7.6	6.4	(-1)	5.5
10^{-1}	9.8	(-1)	.056	7.3	(-1)	2.2	3.2	(-1)	2.0	9.9	(-2)	8.2
10^{-3}	4.2	(-2)	.0076	1.1	(-1)	.16	2.0	(-2)	1.6	3.4	(-3)	4.1
k_{∞}	8.7×10^{-27}			3.5×10^{-7}			1.2			2.3×10^{3}		

5. HLH $t\text{-}BuO \rightarrow (CH_3)_2CO + CH_3$

$\log k_{\infty} = 15.5 - 16.9/\theta$

P	k/k_{∞} (300)			k/k_{∞} (600)			k/k_{∞} (900)			k/k_{∞} (1200)		
	M		K(s=9)	M		K(s=18)	M		K(s=23)	M		K(s=27)
10^{3}	8.0	(-1)	4.6	1.5	(-1)	1.5	1.5	(-2)	1.6	2.2	(-3)	2.1
10^{1}	1.5	(-1)	.49	4.4	(-3)	6.2	2.0	(-4)	2.3	2.3	(-5)	2.1
10^{-1}	3.3	(-3)	1.8	5.5	(-5)	12	2.1	(-6)	2.5	2.4	(-7)	2.2
10^{-3}	3.4	(-5)	3.5	5.6	(-7)	17	2.1	(-8)	2.6	2.4	(-9)	2.2
k_{∞}	2.2×10^{3}			2.1×10^{9}			2.3×10^{11}			2.5×10^{12}		

continued...

Table X (concluded)

6. HLL $CH_3CO \rightarrow CH_3 + CO$

$\log k_\infty = 14.5 - 21.5/\theta$

P	k/k_∞ (300) M	K(s=2)	k/k_∞ (600) M	K(s=6)	k/k_∞ (900) M	K(s=8)	k/k_∞ (1200) M	K(s=9)
10^3	4.6 (-1)	.031	1.5 (-1)	1.1	5.1 (-2)	6.1	1.9 (-2)	2.5
10^1	1.2 (-2)	.0031	2.5 (-3)	3.2	6.8 (-4)	16	2.3 (-4)	4.7
10^{-1}	1.3 (-4)	.0031	2.5 (-5)	5.0	6.8 (-6)	24	2.3 (-6)	6.1
10^{-3}	1.3 (-6)	.0031	2.5 (-7)	5.9	6.8 (-8)	29	2.3 (-8)	6.9
k_∞	8.3×10^{-2}		4.2×10^6		1.7×10^9		3.5×10^{10}	

7. LLH n-hexyl → s-hexyl

$\log k_\infty = 10.0 - 13.5/\theta$

P	k/k_∞ (300) M	K(s=12)	k/k_∞ (600) M	K(s=25)	k/k_∞ (900) M	K(s=33)	k/k_∞ (1200) M	K(s=39)
10^3	1.0	1.0	1.0	1.0	1.0	1.0	9.9 (-1)	9.9
10^1	1.0	1.0	9.8 (-1)	9.7	8.3 (-1)	8.2	5.4 (-1)	5.4
10^{-1}	9.7 (-1)	8.4	4.9 (-1)	4.7	9.1 (-2)	9.2	1.7 (-2)	1.7
10^{-3}	4.1 (-1)	2.5	2.6 (-2)	3.1	1.3 (-3)	1.4	1.9 (-4)	1.8
k_∞	1.3		1.3×10^5		5.8×10^6		3.8×10^7	

8. LLL Cyclobutene → Butadiene

$\log k_\infty = 12.8 - 32.1/\theta$

P	k/k_∞ (300) M	K(s=4)	k/k_∞ (600) M	K(s=11)	k/k_∞ (900) M	K(s=15)	k/k_∞ (1200) M	K(s=18)
10^3	1.0	.72	1.0	.98	9.8 (-1)	9.5	9.0 (-1)	8.5
10^1	9.9 (-1)	.83	8.6 (-1)	6.3	5.3 (-1)	4.2	2.4 (-1)	2.0
10^{-1}	61 (-2)	.19	2.0 (-1)	1.1	4.2 (-2)	4.1	8.6 (-3)	9.2
10^{-3}	180 (-4)	.23	3.9 (-3)	5.8	6.2 (-4)	14	1.1 (-4)	1.8
k_∞	1.5×10^{-11}		1.2×10^1		9.7×10^4		8.4×10^6	

Table XI [a]

CALCULATED FALLOFF DATA [$k/k_\infty(T)$]

1. $CH_4 \rightarrow CH_3 + H$ [Model 2]

$\log k_\infty(2500) = 15.5 - 107.2/\theta$

P/Torr	k/k_∞(1000) M	K(s=5)	k/k_∞(1500) M	K(s=6)	k/k_∞(2500) M	K(s=8)	k/k_∞(4000) M	K(s=9)
10^8	1	1	1	.99	1	1	9.9 (-1)	9.8
10^6	1	.96	9.8 (-1)	9.2	8.6 (-1)	8.3	5.6 (-1)	5.3
10^4	8.8 (-1)	4.2	6.3 (-1)	3.2	2.2 (-1)	2.0	4.7 (-2)	4.9
10^2	2.2 (-1)	.29	7.4 (-2)	2.0	1.0 (-2)	1.0	1.1 (-3)	1.3
1	4.6 (-3)	.60	1.2 (-3)	.44	1.3 (-4)	2.3	1.2 (-5)	2.1
k_∞	1.7×10^{-8}		8.7×10^{-1}		1.4×10^{6}		4.8×10^{9}	

2. $CF_3H \rightarrow CF_2 + HF$ [Model 2]

$\log k_\infty(1400) = 14.66 - 71.99/\theta$

P Torr	k/k_∞ (600) M	K(s=5)	k/k_∞(1000) M	K(s=7)	k/k_∞(1400) M	K(s=8)	k/k_∞(1800) M	K(s=8)	k/k_∞(2200) M	K(s=8)
10^8	1	1	1	1	1	1	1	1	1	1
10^6	1	1	1	1	9.9 (-1)	9.8	9.5 (-1)	9.4	8.9 (-1)	8.6
10^4	9.9 (-1)	8.0	8.7 (-1)	7.6	6.3 (-1)	5.9	4.1 (-1)	3.5	2.5 (-1)	2.0
10^2	6.7 (-1)	1.5	2.6 (-1)	1.5	8.9 (-2)	7.7	3.2 (-2)	2.5	1.3 (-2)	.96
1	6.9 (-2)	.52	1.2 (-2)	.72	2.6 (-3)	2.9	7.0 (-4)	6.6	2.3 (-4)	2.0
k_∞	4.1×10^{-12}		8.9×10^{-2}		2.6×10^{3}		8.4×10^{5}		3.4×10^{7}	

a Nomenclature identical with Table X.

Table XII

MOLECULAR PARAMETERS USED

	1. n-C_4H_{10}		2. C_2H_6		3. ØCO		4. CH_3NHNH_2		5. t-BuO		6. CH_3CO		7. n-hexyl		8. cyclobutene	
	Molecule	Complex	Molecule	Complex	Molecule	Complex	Molecule	Complex	Molecule	Complex	Molecule	Complex	Molecule	Complex	Molecule	Complex
	2950 (6)	2950 (6)	2974 (2)	2960 (6)	3060 (5)	3060 (5)			2980 (6)	2980 (6)	2900 (3)	2900 (3)	2940 (7)	2920(12)	3080 (2)	3300 (6)
	2870 (4)	2870 (4)	2950 (2)	1436 (6)	1700 (1)	1950 (1)	3300 (2)	3293 (3)	2900 (3)	2900 (3)	1714 (1)	1900 (1)	2870 (6)	2200 (1)	2950 (4)	1320(12)
	1460 (6)	1460 (6)	2915 (2)	95 (2)	1600 (3)	1600 (3)	3000 (2)	2890 (2)	1465 (6)	1465 (6)	1400 (3)	1400 (3)	1460 (7)	1462 (7)	1566 (1)	660 (5)
	1370 (3)	1370 (3)	1469 (2)	66 (2)	1483 (1)	1483 (1)	2800 (2)	2250 (2)	1350 (4)	1350 (4)	1109 (1)	450 (2)	1360 (4)	1376 (2)	1430 (2)	
	1280 (3)	1280 (3)	1460 (2)		1260 (3)	1290 (2)	1500 (4)	1600 (1)	1220 (2)	1220 (2)	900 (2)	256 (1)	1303 (3)	1270 (8)	1250 (4)	
Frequencies (cm^{-1})	1170 (2)	1180 (1)	1388 (1)		1160 (2)	1160 (2)	1250 (3)	1350 (2)	1106 (2)	1106 (1)	512 (1)		1250 (3)	1040 (3)	1090 (3)	
and	1030 (2)	1030 (2)	1370 (1)		1035 (3)	1035 (3)	1050 (3)	1140 (5)	1013 (3)	1013 (2)	150 (1)		1160 (2)	940 (5)	986 (1)	
Degeneracies	960 (2)	952 (1)	1190 (2)		940 (3)	940 (3)	850 (2)	821 (2)	919 (1)	919 (1)			1040 (4)	890 (2)	840 (4)	
	820 (2)	803 (1)	995 (1)		785 (3)	785 (3)	447 (1)	700 (2)	748 (1)	530 (2)			890 (3)	800 (3)	640 (2)	
	730 (1)	730 (1)	822 (2)		655 (2)	655 (1)	315 (1)	300 (1)	450 (3)	450 (1)			760 (3)	575 (2)	325 (1)	
	431 (1)	109 (2)	260 (1)		440 (3)	440 (3)	257 (1)		350 (2)	350 (2)			474 (1)	420 (2)		
	271 (1)	32 (2)			350 (2)	310 (1)			250 (3)	225 (2)			336 (2)	300 (2)		
	210 (2)				154 (1)	175 (2)				200 (2)			212 (2)	212 (1)		
	102 (1)				80 (1)	80 (1)							132 (2)			
													94 (1)			
													61 (1)			
$I_AI_BI_C$ $(gmcm^2)^3$ x 10^{120}	$2.01x10^6$	$1.56x10^7$	$1.85x10^4$	$3.28x10^5$	$5.83x10^7$	$1.17x10^8$	$1.97x10^5$	$7.06x10^5$	$5.60x10^6$	$1.20x10^7$	$7.99x10^4$	$3.25x10^5$	$2.95x10^7$	$2.42x10^7$	$5.68x10^5$	$5.68x10^5$
[a] $\pi I_{ri}(gmcm^2)x10^{40}$	---	$9.16x10^2$	---	2.92	---	$3.00x10^1$	---	---	---	5.15	---	3.34	---	---	---	---
[b] $\pi\ \sigma_{ir}$	---	27	---	3	---	3	---	---	---	3	---	3	---	---	---	---
[c] Sigma	2	2	6	6	1	1	0.5	0.5	3	1	1	1	1	1	2	2
Collision Diameter (Å)	6.0		5.0		6.0		4.0		5.0		5.0		6.0		4.0	

[a] Product of reduced moments of inertia for internal rotors (Internal symmetry is equal to "foldness" of the rotor).

[b] Product of internal rotation symmetry numbers.

[c] Sigma = σ/n, where σ is the symmetry number for external rotation and n is the number of optical isomers.

7. Very Low-Pressure Pyrolysis. IV. The Decomposition of i-Propyl Iodide and n-Propyl Iodide, by K. D. King, D. M. Golden, G. N. Spokes, and S. W. Benson, Int. J. Chem. Kinetics, 3, 0000 (1971).

Abstract

The decomposition rate constant of i-PrI under conditions of VLPP is completely consistent with the well known high-pressure Arrhenius parameters and the RRK(M) theory. The decomposition of n-PrI under the same conditions proceeds via two pathways: the anti-Markovnikov dehydroiodination, and C-I bond scission. The data, analyzed by taking into account the mutual interaction of the two pathways, are completely consistent with the known Arrhenius parameters for the bond scission step and, when combined with a reasonable A-factor, yield an activation energy for HI elimination that is as predicted for these semi-ion pair transition states.

This paper describes the first use of the triple-aperture VLPP reactor (see Figures 15 and 16) to determine the rate constants of some basic chemical reactions. The data are consistent with a simple reaction for isopropyl iodide

$$i\text{-}C_3H_7I \rightarrow C_3H_6 + HI$$

and with a mechanism involving both radical and nonradical pathways for n-propyl iodide

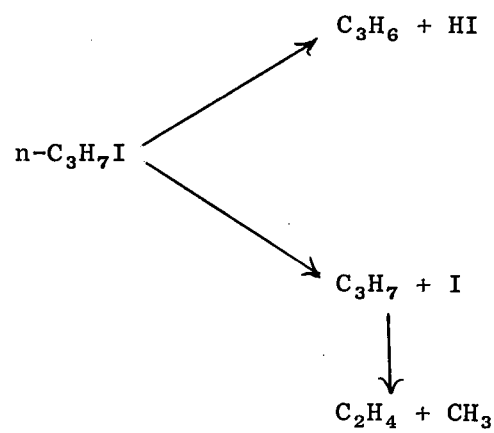

Isopropyl iodide decomposition is monitored by measuring the disappearance of parent compound and the production of propylene. Normal propyl iodide decomposition also yields ethylene through the I-atom elimination pathway.

RRK and RRKM theories are shown to give similar falloff predictions for the i-PrI decompositions; an exact fit is found to the data using an Arrhenius rate law, $\log k = 13.69 - 45.5/\theta$ Results are shown in Figure 31.

RRK theory was fitted to the n-propyl iodide data using $\log k = 12.9 - 48.4/\theta$ for the rate constant law for dehydrohalogenation. Results are shown in Figure 32. The alternate pathway for reaction--C-I bond breaking--leads to drop off in rate constant from the simple RRK theory value. A special modification of this theory known as RRK/2 was developed to account for this drop off. Agreement with the new theory is seen to be excellent.

In Figure 33 we show the results of the n-PrI decomposition reaction that yields ethylene. We find that the rate law is expressed by the relation $\log k = 15.5 - 54.9/\theta$ (for C-I bond scission reaction). Agreement with both simple RRK and the new RRK/2 theory is excellent.

The use of the triple-aperture reactor marks a significant step forward in VLPP technology because the experimenter can change the escape rate constants of his reactor very rapidly without changing reactor temperature and without letting the reactor come to atmospheric pressure.

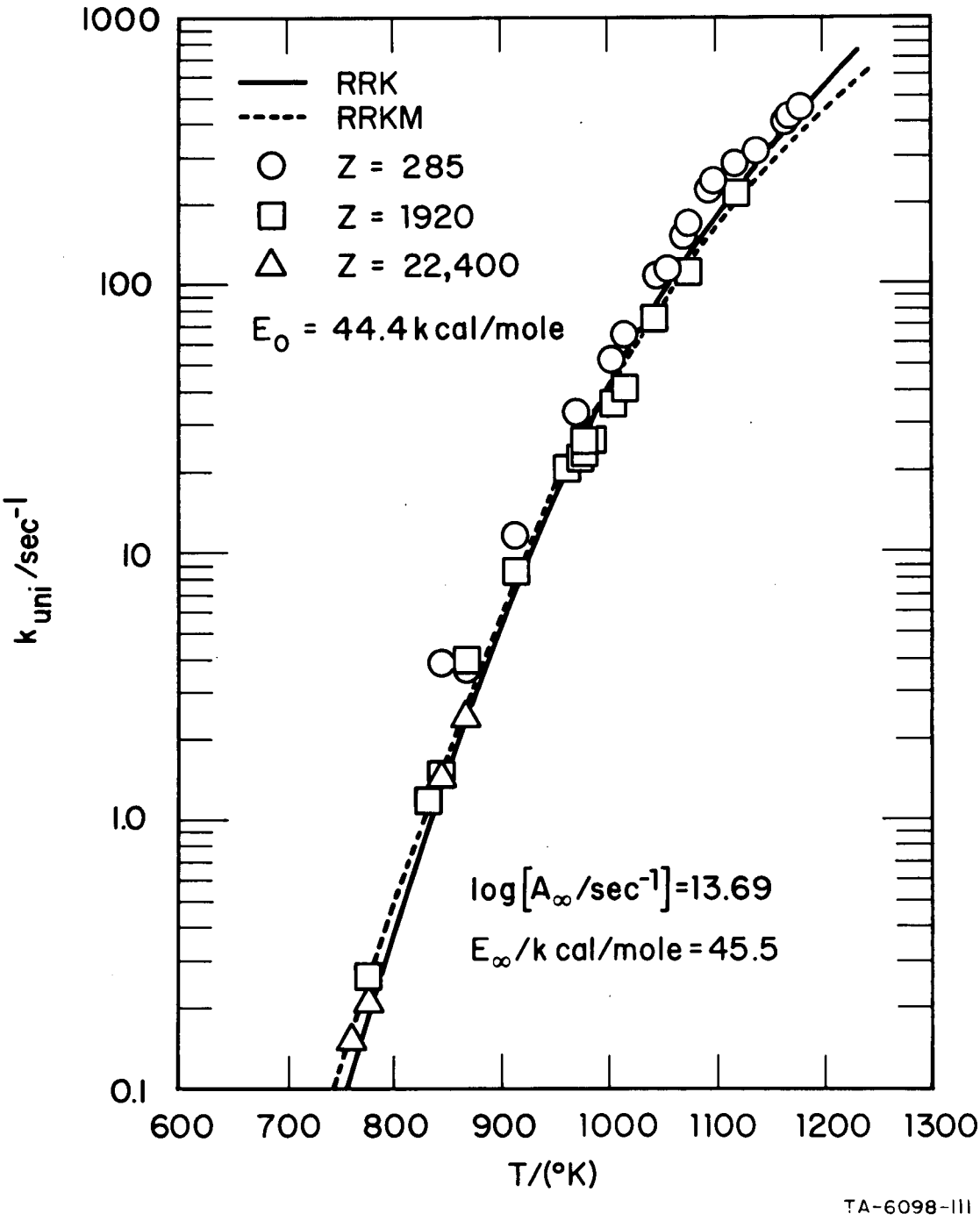

FIGURE 31 PLOT OF k_{uni} VERSUS T FOR HI ELIMINATION FROM iPrI

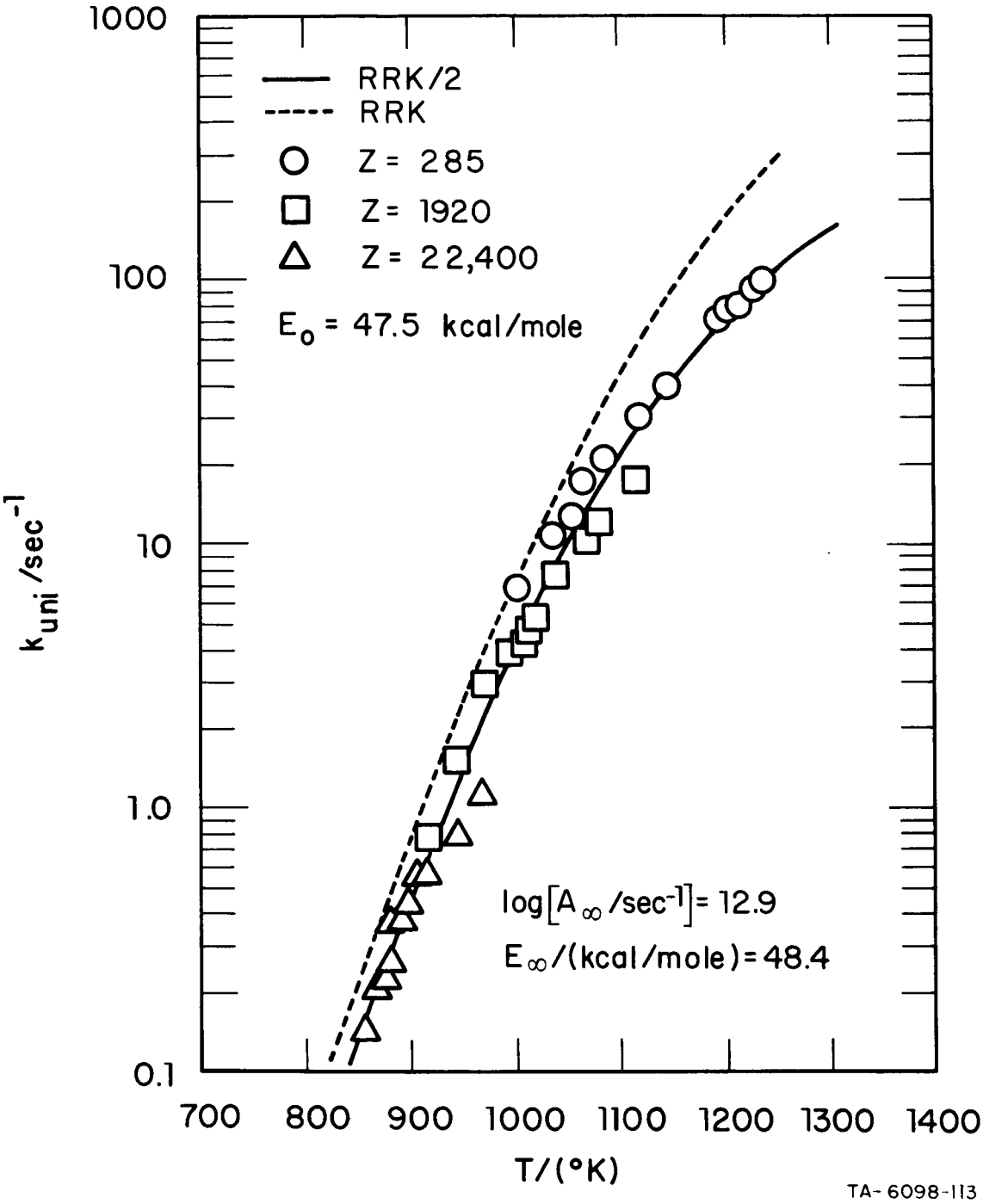

FIGURE 32 PLOT OF k_{uni} VERSUS T FOR HI ELIMINATION FROM nPrI

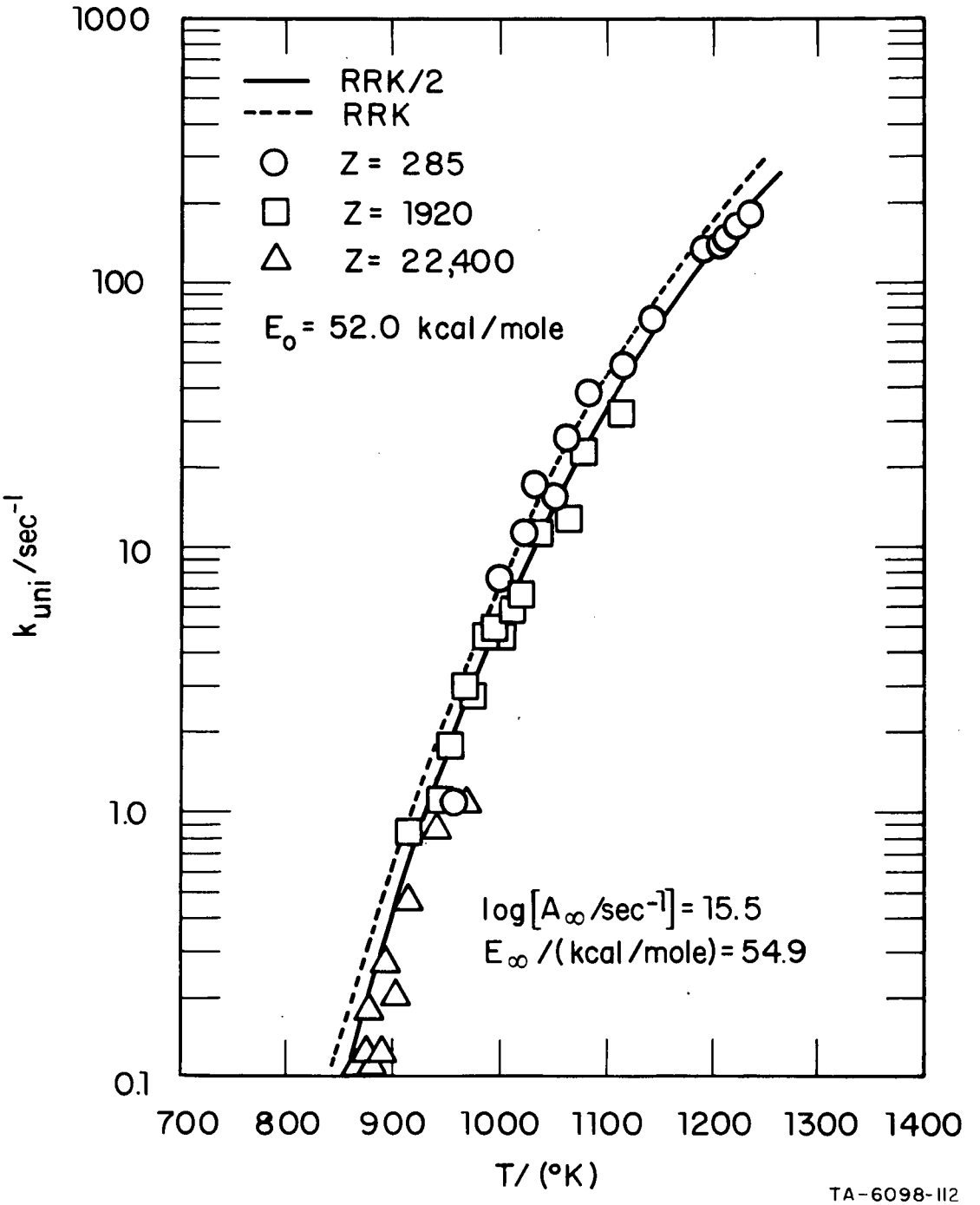

FIGURE 33 PLOT OF k_{uni} VERSUS T FOR C-I BOND SCISSION IN nPrI

8. Very Low-Pressure Pyrolysis. II. Decomposition of Nitropropanes, by G. N. Spokes and S. W. Benson, J. Amer. Chem. Soc., 89, 6030 (1967).

Abstract

The technique of VLPP has been applied to 1- and 2-nitropropane. Pyrolysis was carried out at pressures from about 2 to 10 μ and at temperatures ranging from 650 to 1100°K, in a quartz vessel with residence time of about 0.4 sec. Both isomers gave the same primary reaction products, $HNO_2 + C_3H_6$, with HNO_2 decomposing further at the reaction conditions. The first-order rate parameters agreed well with those estimated from low-temperature studies. The activation energies and thermochemistry show that the reverse reaction, the exothermic addition of HNO_2 to an olefin, follows the Markovnikov rule. Addition of the NO_2 group to the CH_3-bearing C atom is favored by 7.2 kcal/mole of activation energy.

The production of propylene through a five-center elimination of HNO_2 from nitropropane was unexpected, both from the viewpoint of energy and entropy. The A-factors for the elimination are $10^{11.3}$ sec^{-1} and $10^{11.5}$ sec^{-1} for the 2-nitropropane and 1-nitropropane, respectively. Such low A-factors correspond to the loss of a great deal of entropy in the transition state. The ring strain of about 5 kcal/mole would be expected to make a seemingly unlikely elimination even more unlikely.

The VLPP results appear to confirm, however, the conclusion of Smith and Calvert[22] that HNO_2 elimination is favored for 2-nitropropane.

Figure 34 is an Arrhenius plot of both literature and our own rate constants for pyrolysis of ethyl and nitropropanes. We see that for 2-nitropropane there is excellent consistency between our results and the literature data over eight orders of magnitude variation in rate constant. The VLPP data show slight falloff at the highest temperatures; this fall-off is predicted by RRK theory.

---

[22]T. E. Smith and J. G. Calvert, J. Phys. Chem., 63, 1305 (1959).

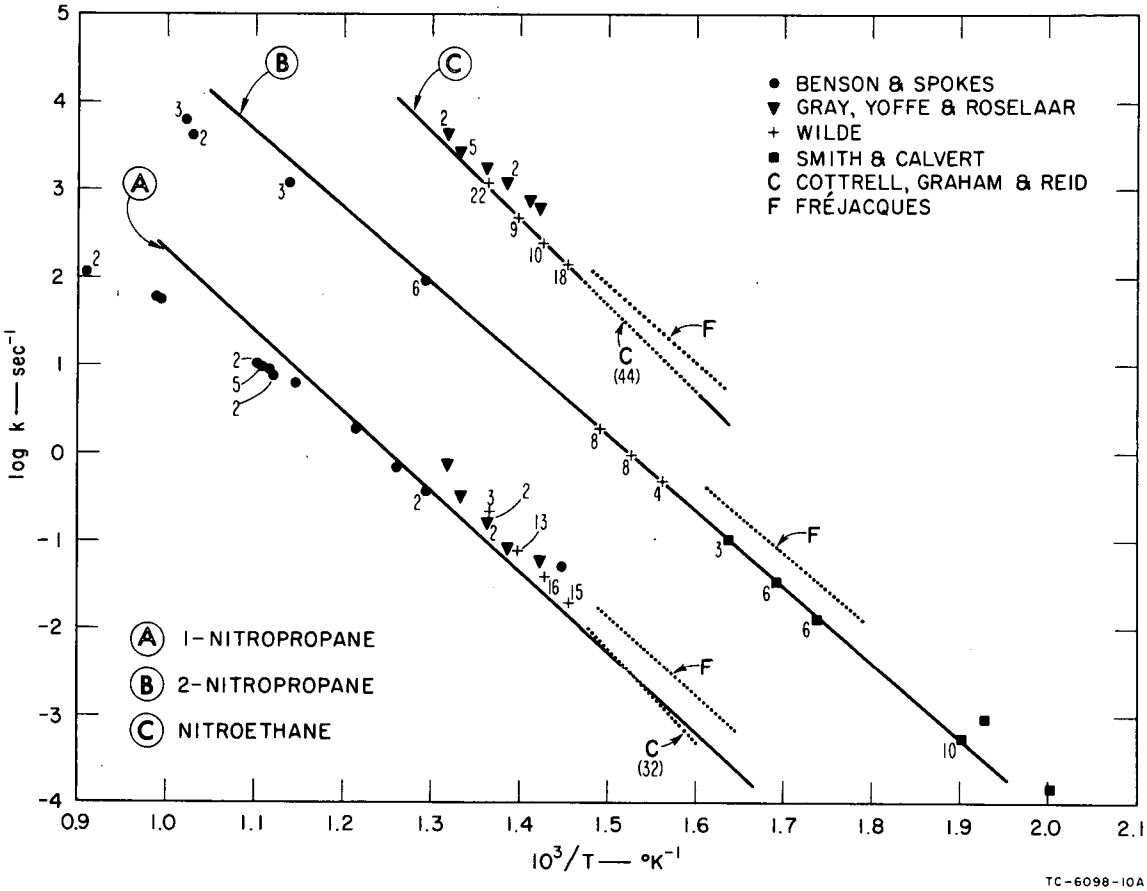

FIGURE 34 ARRHENIUS PLOTS OF AVAILABLE DATA ON THE PYROLYSIS OF NITROETHANE AND NITROPROPANES. Small numerals adjacent to data points or lines refer to experimental weight where this is different from unity.

IMPORTANT NOTE: The rate constants for 2-nitropropane and nitroethane have been increased by 10^2 and 10^4, respectively, to present the data more clearly.

9. Very Low-Pressure Pyrolysis. V. Benzylamine, N-Methylbenzylamine, and N-N-Dimethylbenzylamine, and the Heat of Formation of the Amino, Methylamino, and Dimethylamino Radicals, by D. M. Golden, R. K. Solly, N. A. Gac, and S. W. Benson, J. Amer. Chem. Soc., submitted.

Abstract

VLPP studies of the benzylamino bond homolysis in benzylamine, N-methylbenzylamine, and N-N-dimethylbenzylamine yield heats of formation of the amino, methylamino, and dimethylamino radicals, respectively, if RRKM or RRK theory is used to relate the low-pressure rate constants measured to the high-pressure Arrhenius parameters. Values of the high-pressure A-factors were obtained by analogy with the relevant alkyl benzenes. Heats of formation for the three radicals are 47.2, 45.2, and 38.2 kcal/mole, respectively. These lead to $DH^0(NH_2-H)$ = 110, $DH^0(CH_3NH-H)$ = 103, and $DH^0((CH_3)_2N-H)$ = 95 kcal/mole, all considerably higher than previously reported.

Extensive studies on the pyrolyses of the benzylamino compounds under VLPP conditions have led us to conclude that the nitrogen-hydrogen bond strength is considerably higher than previously reported. The N-H bond in ammonia, as inferred from our VLPP work, is 110 kcal/mole at 298°K, compared with the previously accepted value of 103 to 105 kcal/mole.

The VLPP data rely on a calculation of A-factor for the C-N bond scission. The paper discusses these assumptions in detail.

The values of the heats of formation of the amino radicals measured in this work lead to values of the bond dissociation energies $DH^0(NH_2-H)$, $DH^0(CH_3NH-H)$, and $DH^0(CH_3)_2N-H$, which, when considered from the viewpoint of the Periodic Table as shown below, are inherently more satisfying than the older values shown in parentheses.

CH_3–H	NH_2–H	HO–H	F–H
104	110 (103)	119	134
CH_3CH_2–H	CH_3NH–H	CH_3O–H	---
98	103 (92)	104	
$(CH_3)_2CH$–H	$(CH_3)_2N$–H	---	---
95	95 (86)		
$(CH_3)_3C$–H	---	---	---
92			

VII VLPP WORK THAT HAS NOT YET BEEN PUBLISHED

We present here unpublished results of work carried out under the sponsorship of this contract. We plan to publish much of the work at a later date. In some cases there is a need for confirmatory studies, and in some other cases further experiments are needed to make more clear the detailed mechanisms involved.

Pyrolysis of C_2F_4

A qualitative study has been made of the pyrolysis of C_2F_4 gas. Tetrafluoroethylene obtained from pyrolysis of pure polymeric tetrafluoroethylene was pyrolyzed in a fused silica VLPP reactor. The volume of the reactor was 34.7 cm^3, and its exit aperture was a circular hole of 1-mm diameter. Flow rates approximated 10^{15} molecules per second. Oxygen was added to test for reaction with CF_2.

The 70-eV mass spectrum data are presented in Table XIII. The absolute values of signals are affected by changes in ionizer electron emission current brought about by chemical changes in the system.[23] Attention should thus be focused on relative values of signals rather than absolute values. The mass spectrum of the effluent gases showed no significant changes as the reactor temperature was increased from 50 to 900°C. The prominent peaks were 31 (CF), 43 (C_2F), 50 (CF_2), 69 (CF_3), 81 (C_2F_3), and 100 (C_2F_4). There was a very small peak at 131 amu (C_3F_5?) ascribable to a small amount of impurity, perhaps a higher fluoro-olefin.

[23]This work was done before acquisiton of the EAI Quad 200 mass spectrometer that has emission control built into its ionizer supply.

Table XIII

MASS SPECTRAL ANALYSIS OF GASES RESULTING FROM PYROLYSIS OF C_2F_4 IN A FUSED SILICA REACTOR

	RUN						
	10	12	16	17	E	I	L
Flow Rate, molecules sec $\frac{C_2F_4}{O_2}$	10^{15}	10^{15}	10^{15}	trace	$5\ 10^{15}$	$5\ 10^{15}$	$2\ 10^{15}$
	--	--	10^{15}	10^{15}	---	$\sim 5\ 10^{15}$	---
Temperature, °C	~ 800	~900	~900	~900	~1130	~1130	~800
Pressure x 10^6, torr	1.9	2	4	3.5	4	6.8	2.8
Relative Signal Intensity at Various amu							
100 (C_2F_4)	8	5	9	1.2	5	2	2.1
85 (SiF_3)	--	--	1.3	0.2	18.5	4.5	0.2
81 (C_2F_3)	18	10	18	2.7	9	3	4.5
69 (CF_3)	5	2.7	5	0.8	2.2	1	0.7
66 (COF_2)	--	--	--	--	--	0.8	--
50 (CF_2)	15	7.8	2 5	2.2	23	10	27
43 (C_2F)	4	2.2	5	0.8	13.5	10	5
39 (K)	2	0.8	0.5	0.2	18.5	12	0.5
32 (O_2)	2	1.3	off scale	off scale	1.4	60	1.3
31 (CF)	>40	22	35	6	16	10	6.5
28 (N_2,CO)	10	6	41	9	39	19	2.5
18 (H_2O)	34	22	29	5	18.5	14	9
16 (O)	--	--	18	26	--	5	--

In addition to these peaks, there were small contributions at 17 and 18 amu (due to H_2O) and at several other points in the mass spectrum.

In run 16, O_2 was added to the reactor through a second port at a flow rate of $\sim 10^{15}$ molecules/sec: the C_2F_4 flow was maintained at 10^{15} molecules/sec. This brought about a large increase in the peaks at 28 and 85 amu, in addition to the expected peaks at 32 and 16 amu; the relative heights of peaks associated with C_2F_4 remained constant. Shutting off the C_2F_4 eliminated the peaks at 85 and 28 amu. We therefore concluded that these peaks are the result of actions of O_2 with C_2F_4 or with its products, or with both.

With the reactor temperature at $\sim 1130^{\circ}C$ (somewhat cooler at the ends), C_2F_4 at a flow rate of $\sim 5 \times 10^{15}$ molecules/sec was admitted to the reactor, resulting in a substantial peak at 85 amu and a relatively large increase in the signal at 50 and 28 amu. Also apparent were relative increases in the signals at 43 and 31 amu, compared with the $900^{\circ}C$ spectrum.

Oxygen addition while the reactor was at $\sim 1130^{\circ}C$ had little effect until the O_2 flow reached $\sim 5 \times 10^{15}$ molecules/sec, when a small peak appeared at 66 amu (COF_2).

In addition, while working at the highest temperatures, particularly in runs E and I, we noted a prominent peak at 39 amu, which was probably due to potassium from the reactor itself. On cooling back down to $800^{\circ}C$ in the absence of O_2, the peaks at 28, 50, and 85 amu reverted to their normal values in relation to other C_2F_4 peaks.

Discussion

The peaks at 85 and 28 amu are ascribed to SiF_3 (indicative of the presence of SiF_4) and CO, respectively. These substances could come from the reaction $2CF_2 + SiO_2 \rightarrow SiF_4 + 2CO$. They might, however, also come from $C_2F_4 + SiO_2 \rightarrow SiF_4 + 2CO$ at the surface. The latter is considered unlikely since these products are not seen at $\sim 900^oC$, which means that the activation energy of the process being observed is quite high, whereas a surface reaction with a tight transition state (and consequently, a low A-factor) would have to have a low activation energy to account for the observed decomposition at 1130^oC.

Although the experiments performed so far are preliminary, and necessary caution should be exercised in drawing conclusions based on them, four cogent qualitative points can be ascertained from the data summarized in Table XIII:

(1) The mass spectrum of C_2F_4 seems to be fairly well characterized by peaks at 31, 43, 50, 69, 81, and 100 amu, even though there seems to have been some fluctuation in the intensities of the 31 and 43 amu peaks. The others seem relatively constant.

(2) The addition of O_2 at $\sim 900^oC$ is accompanied by the appearance of a small peak at 85 amu and a large increase in the peak at 28 amu, which in light of (3) may mean that O_2 somehow catalyzes the decomposition of TFE.

(3) At $\sim 1130^{\circ}C$, the TFE mass spectrum changes to include a contribution at 85 amu and a large increase at 28 and 50 amu.

(4) The addition of large amounts of O_2 at $1130^{\circ}C$ is marked by the appearance of a peak at 66 amu, which probably corresponds to CF_2O and indicates that VLPP might be an excellent tool for studying this and other reactions of CF_2, especially when we get a vessel that can be heated to $\sim 1700^{\circ}C$. Note: Benson and Spokes[12c] reported an analogous reaction of $:CCl_2$ with O_2 to make CCl_2O.

Hexamethyl Ethane Pyrolysis Under VLPP Conditions

Pyrolysis of hexamethyl ethane (HME or 2,2,3,3-tetramethyl butane) yields two tertiary butyl radicals. Analysis of the rate parameters of the decomposition process should yield the heat of formation of the t-butyl radical, which is currently the subject of some controversy.

W. Tsang[24] has studied the pyrolysis of HME and reported the rate law as $k = 10^{16.3-68.5/\theta}$. The current work was undertaken to check Tsang's data by an independent technique. The triple-aperture reactor was used for this work, and we present here the theory of a novel experimental use of the reactor that permits determination of rate constants

[24] W. Tsang, J. Chem. Phys., 43, 352 (1966).

in a very simple way. The method is sensitive if the level of decomposition changes markedly as one switches apertures. The technique gives a useful additional check to the usual method of using the VLPP technique in which an inert internal standard gas is admixed with the reactant.

The new technique is especially useful for systems in which no calibrant gas can be used or in which the supply of reactant is not readily controllable or is changing in some unpredictable way (for example, a relatively involatile solid may behave in this way).

Results

Hexamethyl ethane has been pyrolyzed in the triple-aperture reactor. The ratios of the signals at 57 and 99 amu are given in Tables XIV and XVI; the derived rate constants are given in Tables XV and XVII. Reaction rate constants were derived from the signal ratios using reactor escape rate constants listed in Table XVIII. Only parent compound contributes significantly to the mass spectrum fragmentation peak at 99 amu (the parent mass peak at 114 amu is largely buried in noise). Only butanes and parent contribute at 57 amu. Since there is almost zero contribution at 58 amu, butanes are not formed in the system, and we can take ratios of mass peak heights as representative of the level of decomposition.

Falloff Calculations

We have calculated values of k/k_∞ for our VLPP system, using Emanuel's tables (see Report No. 14, page 14). The results are tabulated in Table XIX. Two models were used. Model A assumed a pyrolysis rate constant given by

$$k = 10^{16.3-68.5/\theta} \qquad \text{(W. Tsang's data}^{24}\text{)}$$

Table XIV

SIGNAL RATIO DURING PYROLYSIS OF HME

Temp., °K	897°				983°			1040°	1078°	1086°
Runs	10-15	18-21	22-25	26-31	39-43	44	45	17A-19A	20A-23A	24A-25A
$(I_{10-1})_{99}$	1.14	1.15	(1.09)	1.35	4.46	4.45	——	(20)	——	——
$(I_{10-1})_{57}$	1.21	1.23	1.19	1.28	(6)	4.7	4.42	(10)	——	——
$(I_{10-3})_{99}$				1.032	1.49	1.35	1.37	2.67	(4.4)	(4.2)
$(I_{10-3})_{57}$				1.021	1.41	1.36	1.44	2.04	(3.2)	2.75
$(I_{3-1})_{99}$				1.31	3	3.2	——	(7)	——	——
$(I_{3-1})_{57}$				1.25	(4.25)	3.4	3.1	(5)	——	——

Table XV

RATE CONSTANTS FOR PYROLYSIS OF HME DERIVED FROM DATA OF Table XIV

Temp., °K	897°				983°			1040°	1078°	1086°
Runs	10-15	18-21	22-25	26-31	39-43	44	45	17A-19A	20A-23A	24A-25A
$(I_{10-1})_{99}$	.073	.077	(.046)	.182	1.97	1.96	——	(14.1)	——	——
$(I_{10-1})_{57}$	.109	.119	.099	.145	(2.9)	2.1	1.95	(5.7)	——	——
$(I_{10-3})_{99}$	——	——	——	(.228)	3.95	2.75	2.91	18	(64.0)	(56)
$(I_{10-3})_{57}$	——	——	——	(.148)	3.25	2.83	3.52	9.6	(28)	20
$(I_{3-1})_{99}$	——	——	——	.18	1.45	1.64	——	(8.7)	——	——
$(I_{3-1})_{57}$	——	——	——	.15	(2.7)	1.85	1.54	(4)	——	——

Table XVI

SIGNAL RATIOS DURING PYROLYSIS OF HME

Temperature, Kelvins / Aperture Pairs	875°	922°		923°		1023°	1024°	
I $(10\text{-}1)_{99}$[a]	1.16	1.67	1.98	1.58	2.38	5	6.00	
I $(10\text{-}1)_{57}$	1.28	1.98	2.08	1.90	2.00	4.8	9.84	
I $(10\text{-}3)_{99}$		1.04		1.15	1.13	1.25	1.54	1.46
I $(10\text{-}3)_{57}$		1.11		(1.02)[b]	(1.02)	1.4	1.82	1.92
I $(3\text{-}1)_{99}$		1.64	1.93	1.38	2.00	4	3.7	4.3
I $(3\text{-}1)_{57}$		1.77	1.88	2.25	1.87	3.5	5.2	5.2

[a] $I(10\text{-}1)_{99}$ refers to the ratio of the signals at 99 amu with the 10-mm and 1-mm apertures.

[b] Figures in parentheses indicate weak data not used in Figure 35.

Table XVII

RATE CONSTANTS DERIVED FROM DATA OF TABLE XVI
(sec^{-1})

Temperature, Kelvins / Aperture Pairs	875°	922°		923°		1023°	1024°	
I $(10\text{-}1)_{99}$	0.08	0.36	0.52	0.30	0.72	2.3	3.0	
I $(10\text{-}1)_{57}$	0.14	0.52	0.59	0.47	0.52	2.2	5.0	
I $(10\text{-}3)_{99}$		0.28		1.07	0.93	2.0	4.5	3.8
I $(10\text{-}3)_{57}$		0.79		(0.12)	(0.12)	3.2	7.2	8.2
I $(3\text{-}1)_{99}$		0.38	0.56	0.20	0.52	2.5	2.2	2.9
I $(3\text{-}1)_{57}$		0.46	0.53	0.65	0.46	2.0	4.3	4.3

Table XVIII

REACTOR ESCAPE RATE CONSTANTS USED TO DERIVE REACTION RATE CONSTANTS (sec^{-1})

Temperature, Kelvins / Hole Diameter	875°	893°	922°	983°	1023°	1040°	1080°
0.97 mm	0.507	0.512	0.520	0.537	0.548	0.552	0.563
3.31 mm	5.94	6.00	6.08	6.30	6.41	6.46	6.59
10.00 mm	39.9	40.4	40.9	42.3	43.2	43.5	44.3

Model B assumed

$$k = 10^{15.6-34/\theta}$$ (A possible value, given by O'Neal and Benson[25]).

Unfortunately, Emanuel's tables do not extend to 48 oscillators, the value that we estimate for HME. However, the expected increase in rate constant will scarcely be much more than about 15%.

Table XIX

k/k_∞ DERIVED FROM KASSEL INTEGRAL TABLES

Temperature, Kelvins	42 Oscillators[a]		45 Oscillators	
	A	B	A	B
1078	0.082	0.100	0.100	0.113
1040	0.120	0.132	0.140	0.152
984	0.190	0.205	0.220	0.235
897	0.350	0.365	0.400	0.400

[a] The number of classical oscillators in the molecule.

Discussion of Experimental and Theoretical Results

Figure 35 is a composite of the available experimental and theoretical data on the pyrolysis of HME. The sources of data are: (1) W. Tsang,[24] and (2) this work, which comprises: experimental data (VLPP), predicted data from thermochemistry, and falloff curve based on RRK theory. Small numbers against experimental points refer to the number of experiments giving almost coincident rate constants.

[25] H. E. O'Neal and S. W. Benson, Int. J. Chem. Kinetics, 1, 221 (1969).

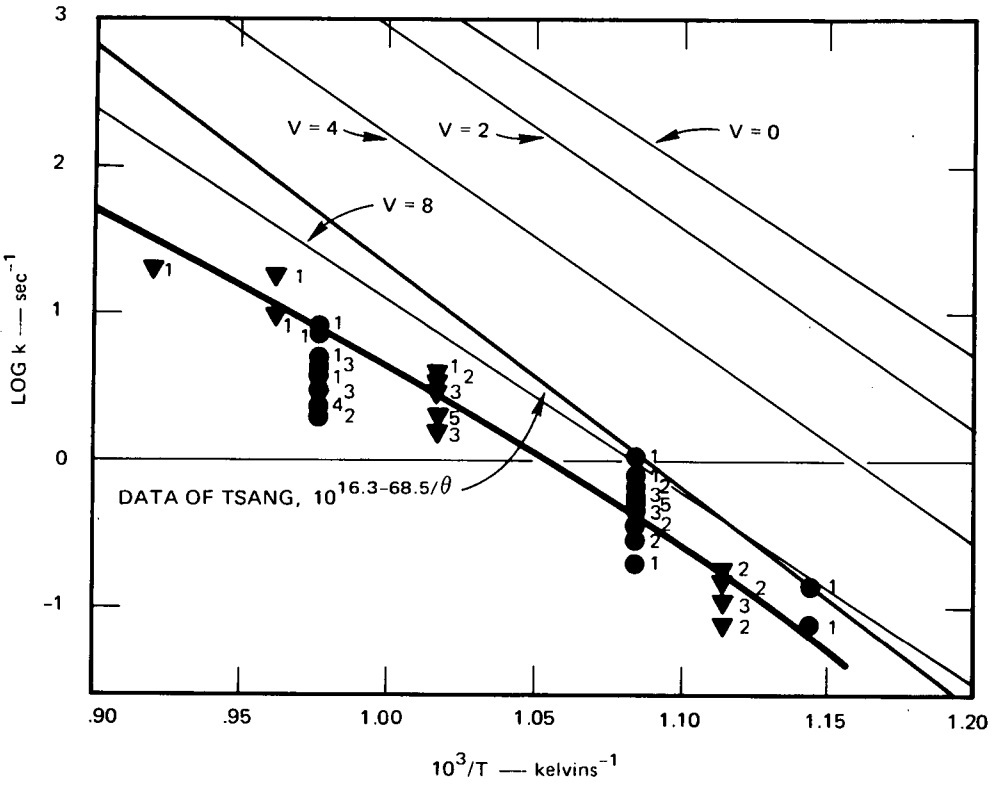

▼ Very low pressure pyrolysis of HME—data from Table XV

● VLPP of HME—data from Table XVII

——— Shock tube pyrolysis of HME—TSANG

▬▬ Predicted VLPP rate constants using TSANG's parameters

——— Theoretically predicted rate constants from thermochemistry using recombination rate constant $10^{9.5}$ liter mole^{-1} sec^{-1}. "V" values correspond to different rotational barriers in t-butyl (kcal/mole).

Note: The V = 4 and V = 8 curves are unrealistic and are presented here only for interest and completeness.

TA-6098-108R

FIGURE 35 PYROLYSIS OF HEXAMETHYL ETHANE (HME)

First, let us consider the data that we have generated using our VLPP systems. These data are scattered above and below the predicted falloff curve. Much of the data are within a factor of two of this line. The six lowest points at $10^3/T = 0.976$ were obtained after about 48 hours at temperature, and there is thus some suspicion that a surface conditioning may have been established during that time. Such a conditioning effect would lead to a low rate constant. The remarkable fact is that the rate is already two powers of ten slower than the predicted rate (assuming the thermochemical value predicted for $V = 0$). Another factor of four would be even more difficult to explain.

We have examined many aspects of the shock tube data of Tsang and conclude that the absolute values of his rate constants are probably not in significant error.

The thermochemistry has been checked out by numerous experiments, and all evidence points to a low or near-zero barrier for rotation in the t-butyl radical.

The experimental data most suspect are the recombination rate constant measurements made by Metcalfe[26] using the rotating sector technique. The work has all the appearances of being carefully carried out; however, one can only express some measure of alarm at placing too much faith in an experimental technique that requires such an array of large correction factors. The correction factor for the first-order reaction alone accounts for a reduction in the rate constant by a factor

---

[26]E. Metcalfe, J. Chem. Soc., 1963, 3560.

of seven. An error of two powers of ten would, of course, be extreme; however, this is the factor required to bring the thermochemical data in line with the pyrolysis data.

From the foregoing presentation, we do not yet see a resolution of the discrepancy. A measurement of the recombination rate of t-butyl radicals at various temperatures would be helpful in resolving the discrepancy. A factor of ten error in this recombination rate (or in its extrapolation to high temperatures) plus a corresponding 2 kcal/mole error in ΔH_f(t-butyl) would probably resolve the disparity. Alternatively, a real activation energy of about 6 kcal for the recombination would also do it!

VLPP Pyrolysis of Metallo-Carbonyls

Lask and Wagner[27] showed that addition of trace amounts of metallo-organic compounds had a profound affect on the flame speed of a premixed air-hexane flame. Reductions of up to 30% in flame speed were produced by only 0.02% of lead tetraethyl or iron carbonyl when these compounds were premixed into the gas streams. There has been much speculation about reactions that cause this phenomenon, but, as yet, there have not been any clear-cut answers.

An answer to this question would perhaps permit important progress to be made toward better fire extinguishment through use of smaller amounts of material. Such factors are of special importance in space and aeronautics systems, because weight is at such a premium.

[27]G. Lask and H. Gg. Wagner, Eighth International Symposium on Combustion, Williams and Wilkins, Baltimore, Md., 1962, p.432.

Two significant modes of action seem important to us. The first is that maybe the materials undergo an initial partial decomposition to yield a metallo free radical. This free radical may then somehow step into and prevent, or partially disable, the chain branching process by a chemical reaction that produces products catalytically. The mechanism might be written

$$R + MX_n \rightarrow RH + (\text{Metallo Radical}) \qquad (19)$$

$$(\text{Metallo Radical}) \rightarrow MX_{n-1} + AB \qquad (20)$$

or

$$R + MX_n \rightarrow RX + MX_{n-1} \qquad (21)$$

or

$$MX_n \rightarrow MZ_{n-1} + X \qquad (22)$$

$$MX_{n-1} + Z \rightarrow (MX_{n-1}Z)^* \qquad (23)$$

$$(MX_{n-1}Z)^* \rightarrow MX_{n-1} + AB \qquad (24)$$

where M is the metal atom, R is a gas-phase free radical, X is CO or C_2H_5, and AB is an olefin.

In reactions (19) and (20), lead tetraethyl, for example, reacts with a free radical to yield ethylene and a lead triethyl radical. Reactions (23) and (24) might follow, and Z would be either oxygen or hydrogen peroxide.

In reactions (22), (23), and (24) we may have a possible mode of operation of the metallo-carbonyls, since it is well known that decomposition occurs very rapidly at temperatures of only 200 to 300°C. In flames, where the time scale is milliseconds, we can expect reactions to

go to completion at around 500 to 600°C. Again, upon production of a metallo radical, reactions with flame intermediates can be expected to be rapid.

In the above cited reactions, rapid catalytic removal of radicals or chain branching agents will lead to flame quenching.

The second basic mode of action of the metallo-organics is through surface reactions. In this instance, the assumption is that the metallo compound reacts and agglomerates to miniscule (oxide?) particles, and that the particle surfaces provide the centers for removal of active species from the flame.

For this second argument we have some special evidence derived from our studies on the pyrolysis of tertiary butyl hydroperoxide in VLPP systems.[12d] The pyrolysis was first carried out in a quartz reactor; there was no surface reaction. Products included acetone, an expected simple pyrolysis product, and isobutylene oxide, a product that can come only through free radical attack (presumably by OH reacting with one of the t-butyl hydrogens in the parent compound). The pyrolysis was next carried out in a metal reactor. In this case the products were dramatically different; they included isobutylene, t-butyl alcohol, and acetone. There was no isobutylene oxide. Evidently, the metal surface catalyzed the reaction through a route that did not yield free radicals. If such a process occurred in flammable systems, obviously the flame would be much weaker because free radicals are a mandatory component in flame propagation.

To learn more about such systems we performed some simple experiments on the pyrolysis of molybdenum carbonyl. The results of the brief study are given below.

C.3

We began also to do some experiments using iron carbonyl, but very rapid deterioration of the mass spectrometer functions (sensitivity and stability) prevented useful results from being obtained. We were also perturbed that the tubes containing our carefully prepared Xenon-iron carbonyl gas mixture began to be coated with brown crystalline deposits, possibly $Fe_2(CO)_8$.

In view of these difficulties and a low NASA priority for the work, no further research on this subject is contemplated under NASA sponsorship.

VLPP of $Mo(CO)_6$

Molybdenum carbonyl is a solid with a vapor pressure of about 300 μ Hg at room temperature. This is just sufficient to give a gas flow into our reactors of about 5×10^{14} molecules per second. Gases flow through a 4-mm stopcock and about 15 cm of 4-mm glass connecting tube to the 1-inch-long, 1/2-mm-diameter entrance capillary of the quartz reactor.

The quartz reactor is shaped like a hollow cylinder with a hemispherical cap on one end. Gases are introduced into the hemispherical cap end and leave by the other, flat end, which has a 3.84-mm aperture in it. The cylinder length is 8.3 cm, and the cap radius is 1.1 cm. The cylinder internal diameter is 2.2 cm. After emerging from the reactor, gases pass through a further tubular section of 5.5 cm length and 2.2 cm i.d. The exit aperture is a frustrated cone of base diameter 3.84 mm, length 0.6 mm, and a semi-angle of approximately 12°. Graphical

interpolation, using the tables of Iczowski, et al.,[28] gives a value of approximately 0.92 for the Clausing factor of the ractor escape aperture and a factor of about 0.99 correction for molecules that reenter the escape aperture after leaving. The overall Clausing factor is thus 0.91. The reactor escape rate constant is, for $Mo^{98}(CO)_6$, given by[12b]

$$k_e = 0.685\sqrt{T}$$

Experimental results are given in Table XX.

Table XX

PYROLYSIS OF MOLYBDENUM HEXACARBONYL

(Mass peak intensities in arbitrary units)

amu / Temp., Kelvins	C^+ 12	CO^{++} 14	O^+ 16	CO^+ 28	Mo^+ 98	$Mo(CO)_5^+$ 238	$Mo(CO)_6^+$ 266
377°	4.78 [a]	0.13	0.67	35.3	24.8	1.4	6.7
425°	4.55	0.18	1.4	38.0	27.6	1.4	7.0
473°	3.94	0.24	1.5	36.0	23.0	1.22	5.7
526°	10.07	1.53	5.0	307.0	0.72	0.045	0.22

[a] Corrections have been applied to the raw data to account for changes in spectrometer sensitivity and to subtract out residuals for all mass peaks. Data were measured from X-Y tracings of mass spectra.

Discussion

The data are conclusive in one significant feature, namely, that there is not very much decomposition at 473°K, but extensive decomposition at 526° K. The basic product is carbon monoxide. The $Mo(CO)_5$ mass peak is not significantly higher relative to $Mo(CO)_6$ than in the undecomposed compound,

[28] R. P. Iczowski, J. L. Margrave, and S. W. Robinson, J. Phys. Chem., 67, 229 (1963).

but obviously a data point intermediate between 473°K and 526°K would be needed to ascertain the possible existence of $Mo(CO)_5$ neutral gas identified by Pignataro and Lossing.[29]

We have estimated decomposition rate constants from the data at 473°K and 526°K. Results are given in Table XXI.

Table XXI

VLPP OF MOLYBDENUM HEXACARBONYL

RATE CONSTANTS (sec^{-1})

amu / Temp., Kelvins	98^+	238^+	266^+	Average
473°	2.1	2.2	3.0	2.4
526°	555	470	470	500

An Arrhenius plot of these data yields parameters of E = 51 kcal/mole and A = 10^{24} sec^{-1}--values that we reject out of hand as being unacceptable from a kinetic chemical point of view. Evidently a surface reaction has brought about a surface chain reaction of some sort that has given the exceptionally high apparent A-factor.

These results have special application to inhibition theory because autocatalytic surface producing reactions, of the type that such chemicals can bring about, must obviously be candidates for consideration in such systems.

---

[29]S. Pignataro and F. P. Lossing, J. Organometallic Chem., 11, 571 (1968).

VLPP of Cyclobutane

The thermal decomposition of cyclobutane has been shown to be a homogeneous, unimolecular reaction.[30-35] Although ethylene is the major product, there have been reports of the formation of small amounts of other alkenes.[31,33,34] Between 693 and 740°K, the high-pressure rate constant[31] is given by:

$$\log k_\infty = 15.6 - 62.5/\theta$$

where $\theta = 2.303\ RT$ (R in kcal deg^{-1} mole^{-1}). The rate constant has been shown to be independent of pressure above approximately 20 torr,[31-33] and several attempts have been made to apply unimolecular rate theory in the pressure dependent region.[31-33] Butler and Ogawa[33] measured the rate constant between 1.7×10^{-4} and 43 torr at 772°K. Using the parameters: $A_\infty = 2 \times 10^{15}$ sec^{-1}, $k_\infty = 4.9 \times 10^{-4}$ sec^{-1}, $s = 14$, $E_\infty = 61{,}700$ cal mole^{-1}, and collision diameter $\sigma = 5.5$ Å, they found that RRK theory fitted the data well down to 10^{-3} torr. Slater theory was found to give just as good a fit when n was taken to be 16. Below 1μ, the experimental rate

---

[30]C. T. Genaux and W. D. Walters, J. Amer. Chem. Soc., 73, 4497 (1951): F. Kern and W. D. Walters, Proc. Natl. Acad. Sci., (U.S.), 38, 937 (1952).

[31]C. T. Genaux, F. Kern, and W. D. Walters, J. Amer. Chem. Soc., 75, 6196 (1953).

[32]H. O. Pritchard, R. A. Sowden, and A. F. Trotman-Dickenson, Proc. Roy. Soc., A218, 416 (1953).

[33]J. N. Butler and R. B. Ogawa, J. Amer. Chem. Soc., 85, 3346 (1963).

[34]R. W. Vreeland and D. F. Swinehart, J. Amer. Chem. Soc., 85, 3349 (1963).

[35]R. W. Carr and W. D. Walters, J. Phys. Chem., 67, 1370 (1963).

constant was greater than the calculated, and a similar effect was noted by Vreeland and Swinehart[34] below about 20 μ. They used different parameters (A_∞ = 7.02 x 10^{15}, E_∞ = 63,200 cal $mole^{-1}$, s = 18, and σ = 5.8 Å) but obtained a curve very similar to Butler and Ogawa's. Vreeland and Swinehart suggested that cyclobutane could decompose by two competing paths:

(1) Simultaneous rupture of two bonds,

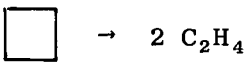

(2) Consecutive rupture, by way of the tetramethylene biradical,

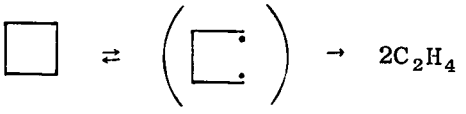

However, they could obtain no conclusive evidence for either mechanism. We conclude that the deviations of rate constants from expected values are due to a wall-promoted unimolecular reaction. See, for example, a paper by Maloney and Rabinovitch[36] on this subject.

Results

We have pyrolyzed cyclobutane in the VLPP apparatus and have plotted the results in Figure 36. The rate constants calculated from cyclobutane decay (k_C) are in good agreement with those calculated from ethylene formation (k_E) for each aperture setting.

---

[36]K. M. Maloney and B. S. Rabinovitch, J. Phys. Chem., 72, 4483 (1968).

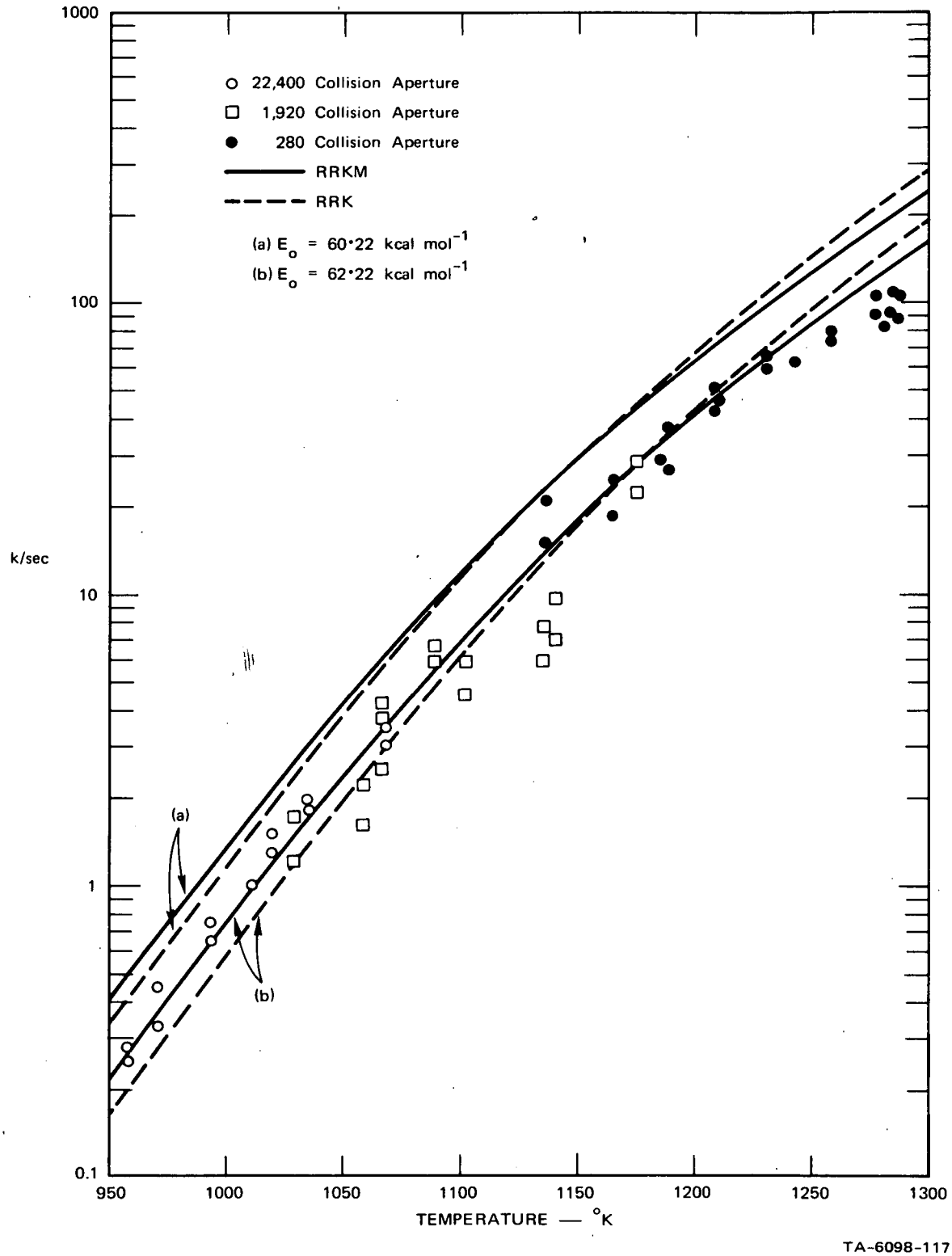

FIGURE 36 CYCLOBUTANE PYROLYSIS

The best fit of RRKM theory with our experimental results was obtained by using the value $E_0 = 62.22$ kcal mol^{-1}, which gives $E_\infty =$ 64.6 kcal mol^{-1} at 900^0K. In Figure 36 the theoretical curves are also shown for $E_0 = 60.22$ kcal mol^{-1}, which corresponds to the previously observed high-pressure activation energy[31] (E_∞) of 62.5 kcal mol^{-1}, although there is a difference of about 420^0K in the mean temperatures of previous measurements and those reported in this paper.

The pressure dependence of the rate constant in the 22,400-collision vessel is shown in Figure 37. Individual RRKM curves have been calculated according to the relation:

$$k = \int_{E_0}^{\infty} \frac{P(E)\ k(E)}{1 + k(E)/(\omega_1 + \epsilon \cdot \omega_2)}$$

where ω_1 = gas-wall collision frequency at temperature T, $\omega_1 = 4100\sqrt{T/M}$, and ω_2 = gas-gas collision frequency $\approx \frac{r_d}{\lambda} \cdot \omega_1$ (where λ = mean free path in cm). The best fit with experiment is found when $\epsilon = 0.1$, although the scatter is such that it could be anywhere in the range of 0.05 to 0.25. This ϵ is, of course, the mean relative collision efficiency of gas-gas collisions, gas-wall collisions being considered as totally efficient, and there is no evidence from the data that SF_6 is any more effective than cyclobutane in increasing the rate.

Pyrolysis of Ethyl Acetate

The rate constants for the pyrolysis

$$CH_3CO_2C_2H_5 \rightarrow CH_3CO_2H + C_2H_4$$

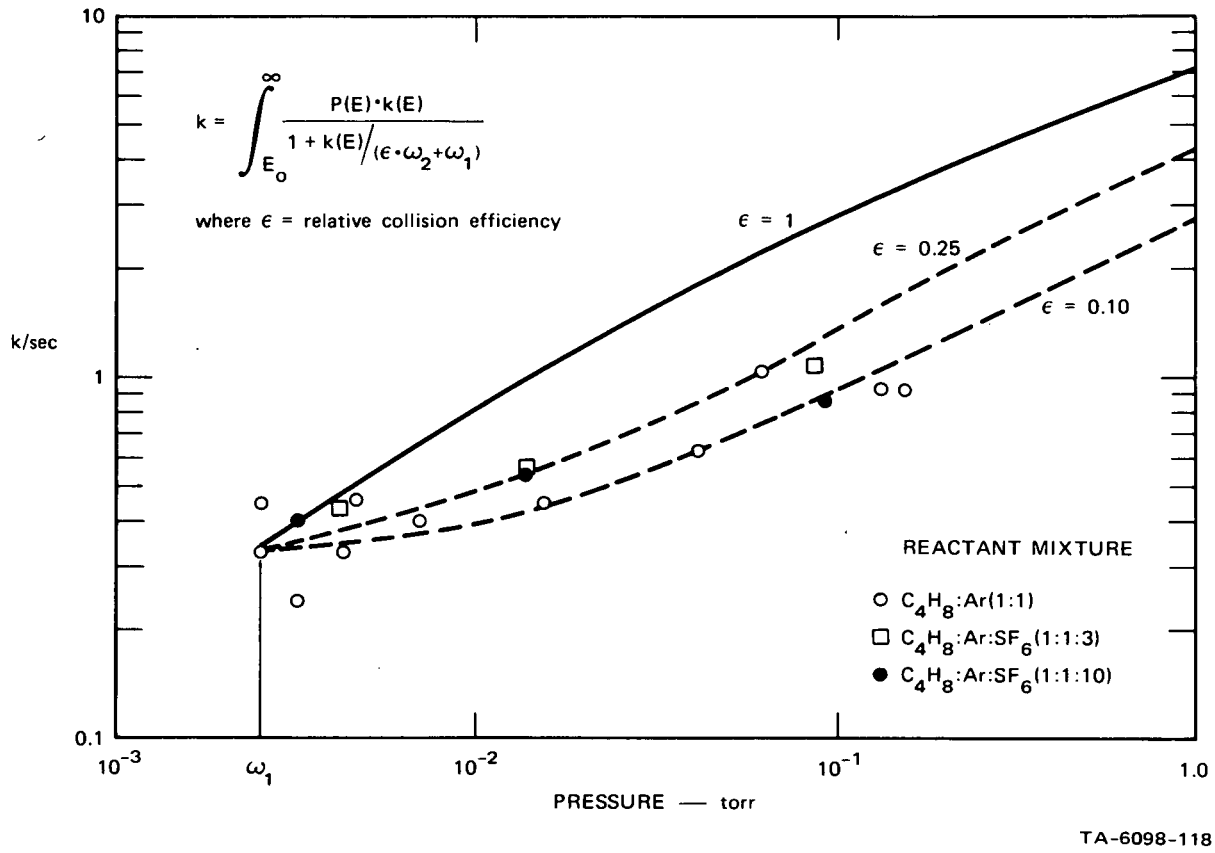

FIGURE 37 PYROLYSIS OF CYCLOBUTANE AT 969°K 22,400 COLLISION APERTURE

have been measured by Blades and Gilderson[37,38] and by Scheer, Kooyman, and Sixma.[39] The recommended value[40] for the high-pressure rate constant, in the range 770 to 880°K, is:

$$\log k_\infty = 12.59 - 48.0/\theta$$

where $\theta = 2.303\ RT$, as before. By measuring acetic acid formation or ester decay, or both, we can obtain values for the rate constant at low pressures and over a much larger temperature range.

We have pyrolyzed ethyl acetate in a VLPP reactor and find that there is good agreement between rate constants estimated from ethyl acetate decay (k_{ES}) and acetic acid formation (k_{AA}) in any particular reactor (Figures 38 and 39). Agreement between rate constants obtained at different apertures is also excellent.

A critical energy of 45.7 kcal mol^{-1} gave E_∞ = 48.1 kcal mol^{-1} at 900°K, in comparison with the reported value[29] of 48.0 kcal mol^{-1} at a mean temperature of 825°K. Both RRK and RRKM calculations gave a very good correlation with the experimental data when the above critical energy was used together with an A-factor of 12.6.[40]

---

[37]A. T. Blades, Can. J. Chem., 32, 366 (1954).

[38]A. T. Blades and P. W. Gilderson, Can. J. Chem., 38, 1407 (1960).

[39]J. C. Scheer, E. C. Kooyman, and F. L. Sixma, Rec. Trav. Chim. de Pays Bas., 82, 1123 (1963).

[40]S. W. Benson and H. E. O'Neal, "Kinetic Data on Gas-Phase Unimolecular Reactions," NSRDS-NBS21, National Bureau of Standards, Washington,D.C. (1970).

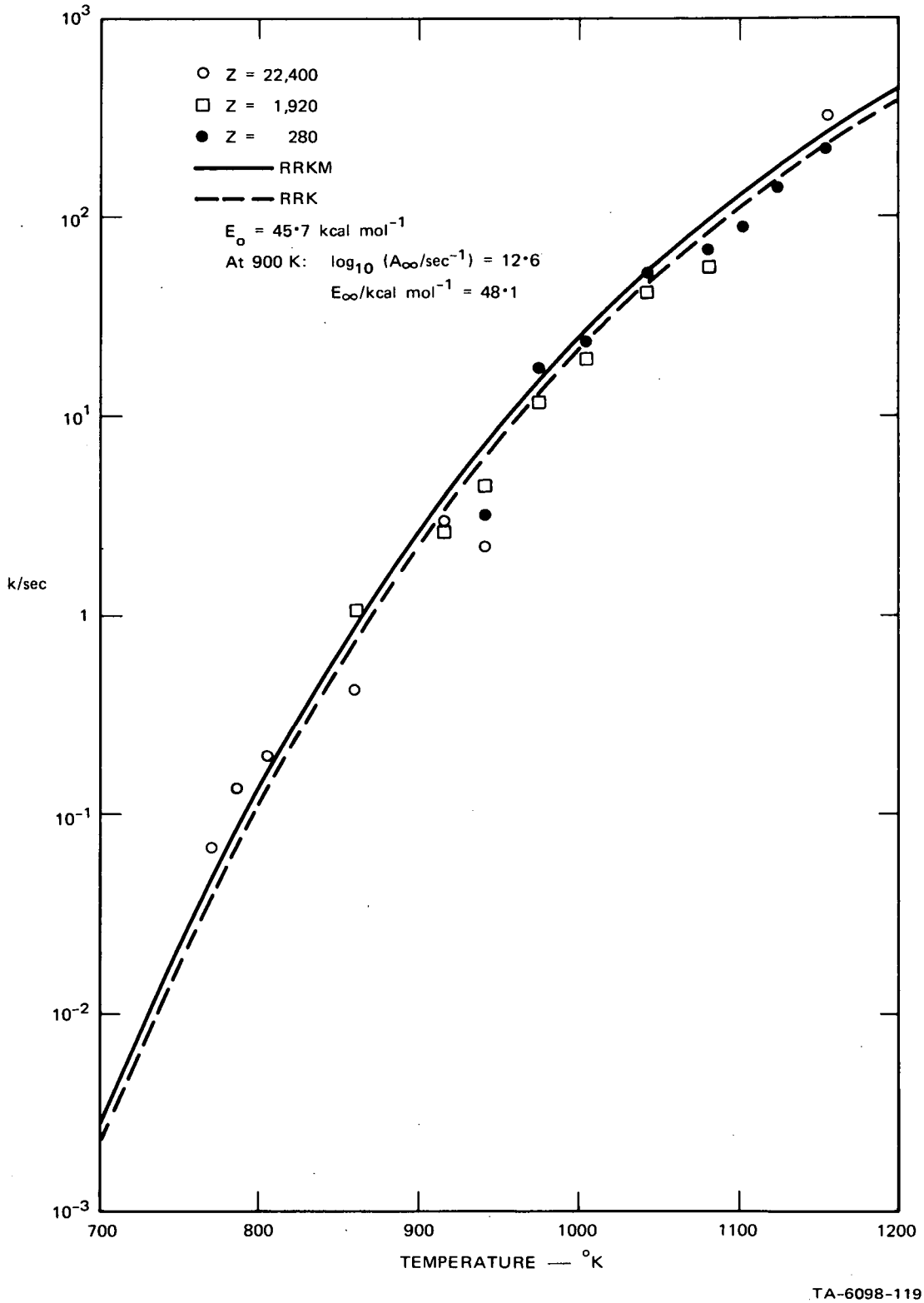

FIGURE 38 PYROLYSIS OF ETHYL ACETATE (ESTER LOSS)

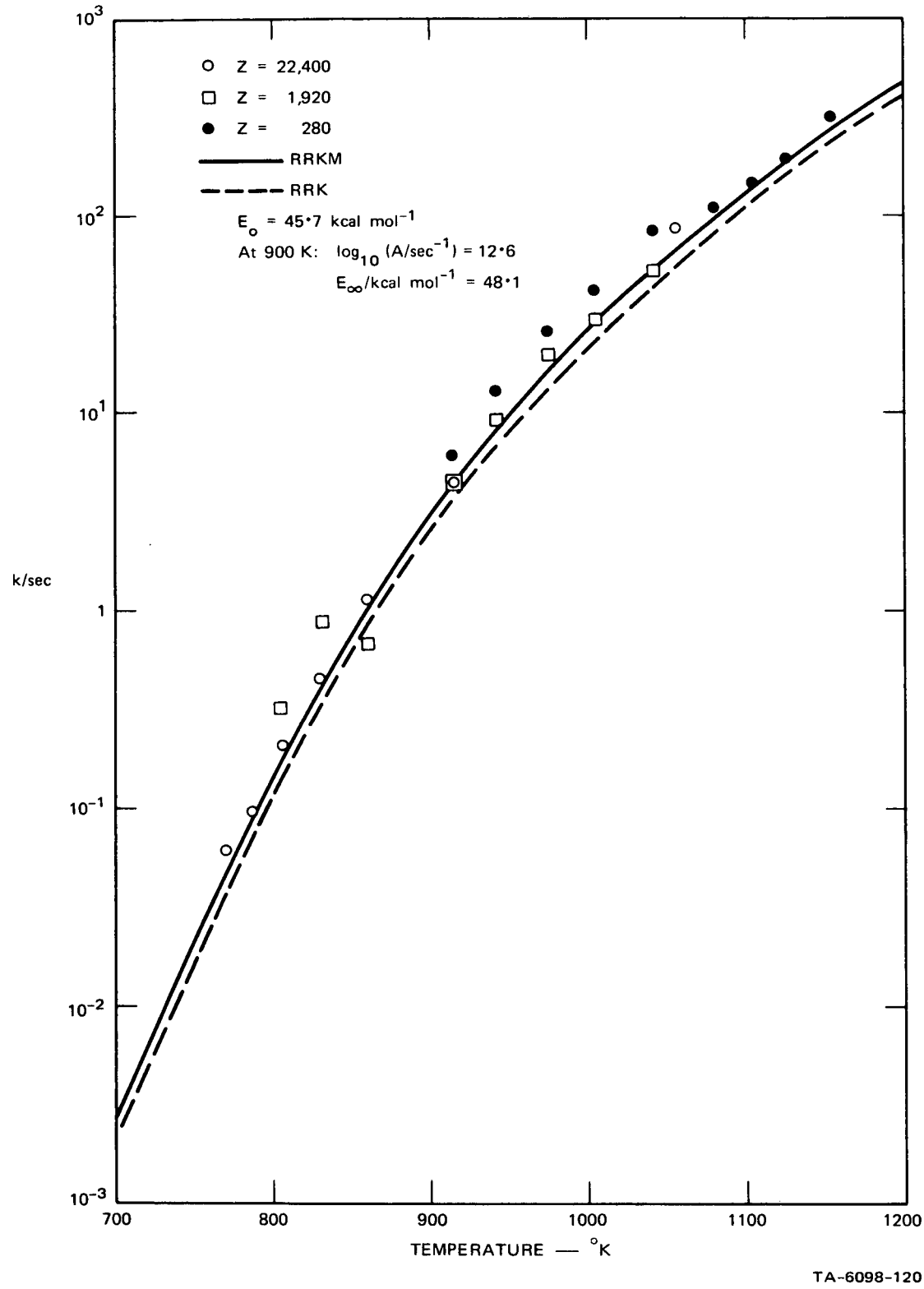

FIGURE 39 ETHYL ACETATE PYROLYSIS (ACETIC ACID FORMATION)

VIII MISCELLANEOUS STUDIES RELATED TO ABLATION CHEMISTRY

Some Current Problems in Oxidation Kinetics[41]

Experimental data on low-temperature ($< 150^{\circ}C$) and high-temperature ($> 250^{\circ}C$) oxidation were examined from the point of view of reported quantitative inconsistencies. Activation energies for $tBuO_2$ metathesis reactions with alkanes appear to be 7 kcal/mole higher than for comparable reactions of HO_2. Related isomerization reactions were examined in light of these differences without reaching any simple conclusions. The Russell mechanism for a 6-membered cyclic, transition state for termination of primary and secondary alkyl peroxy radicals was shown to be either inconsistent with thermochemical data or unique to solution reactions. Addition reactions of O_3 with olefins and acetylenes were shown thermochemically to have the possibility of following concerted and biradical pathways, respectively.

Reactions of SiO_2 + C in Ablating Chars

Below $1200^{\circ}K$, $SiO_2(s)$ and graphite do not react with each other at an appreciable rate. In the region of 1200 to $2000^{\circ}K$, however, a number of reactions occur with rates that depend mainly on the temperature but also on other experimental parameters.

From a kinetic point of view the most rapid reaction is:

$$SiO_2(s) + C(gr) \rightleftarrows SiO(s) + CO(g) \qquad (25)$$

---

[41] S. W. Benson, "Some Current Problems in Oxidation Kinetics," to be published in the Proceedings of the Symposium on The Mechanisms of Pyrolysis, Oxidation, and Burning of Organic Materials, October 26-29, 1970, National Bureau of Standards, Gaithersburg, Maryland.

At these high temperatures SiO(s) is unstable with respect to disproportionation:

$$2\ SiO(s) \rightleftarrows SiO_2(s) + Si(s) \qquad (26)$$

We can estimate the thermochemistry of the net reaction as[42]

$$\tfrac{1}{2}\ SiO_2(s) + C(gr) \rightleftarrows \tfrac{1}{2}\ Si(s) + CO(g) \qquad (27)$$

$$\Delta H_{1500} = -80.2\ \text{kcal/mole}$$

K_p is $10^{-5.62}$ atm at 1200°K; $10^{-2.62}$ atm at 1500°K; and 2 atm at 2000°K.

The reaction thus provides an extremely powerful, endothermic, cooling mechanism in the range 1500 to 2000°K with an efficiency limited only by the kinetics of the process. The kinetics of these reactions have been studied from an engineering standpoint by Blumenthal, Santy, and Burns,[43] who measured the rate of CO evolution from SiO_2 + C mixtures. They found the rates to be somewhat sensitive to the particle sizes, more so at the lower temperatures (1600°K), and to proceed to near completion, according to reaction (27), in excess C(gr). Half-lives at 1800°K were from 3 to 6 minutes.

The authors also showed that $Si + SiO_2 \rightarrow 2\ SiO$ proceeds at a measurable rate above 1500°K, whereas $SiC(s) + SiO_2(s)$ produces volatile products above 1500°K. These latter products probably are SiO(g) + CO(g),

$$SiC(s) + 2\ SiO_2(s) \rightarrow CO(g) + 3\ SiO(g) \qquad (28)$$

---

[42]All data from JANAF, unless otherwise stated.

[43]J. M. Blumenthal, M. J. Santy, and E. A. Burns, J. AIAA, 4, 1053 (1966).

Reaction (28) is endothermic by 307 kcal as written, or 77 kcal per mole of gas formed.

At temperatures where Si(s) has a mobile surface layer (i.e., >1500°K), the overall reaction of SiO_2 and C becomes:

$$SiO_2(s) + C(gr) \rightleftarrows CO(g) + SiO(g) \qquad (29)$$

This reaction is endothermic by 161 kcal, or 81 kcal per mole of gas formed.

At higher temperatures in excess C(gr), the commercial process for making carborundum has the stoichiometry:

$$SiO_2(s) + 3C(gr) \rightarrow SiC(s) + 2CO(g) \qquad (30)$$

with $\Delta H_6(1500^\circ K) = 115$ kcal and $K_{p1500} = 10^{5.22}$ $(atm)^2$, or $P_{CO(1500)} \simeq 50$ atm.

In a typical ablating system containing excess C, one would expect reaction (30) to represent the behavior of the upper part of the char layer. However, excess SiO_2 in the system will tend to change the stoichiometry over to that of reaction (29).

Some directly related studies on the ablative-type system were performed by Ladacki,[44] using an arc-image furnace. He mounted a Pyrex dome over the ablating sample and found deposits of SiO_2 + SiC from Refrasil-phenolic char mixtures and from SiC + SiO_2 mixtures. Neither SiC alone or graphite plus phenolic char gave any deposits. Pure

[44]M. Ladacki, J. AIAA, 4, 1445 (1966).

quartz gave a thin yellow film, presumably of $SiO + SiO_2$. It appears that the SiC deposit must come from the exothermic reaction of SiO with CO at the cooler Pyrex wall. Other experiments with $SiC + SiO_2$ suggest that this reaction may be faster than the $SiO_2 + C$ reaction.

The reactions of $3SiO + CO \rightarrow 2SiO_2 + SiC$ have been reported earlier.[45] It appears that SiO(g) is a very important component of any SiO_2 + graphite system at temperatures above 1300°K and that its formation is accompanied by very effective cooling.

Figure 40 is a van't Hoff plot of the equilibrium constant for reaction (29). The ordinate is 1/2 log K_p, which is equal to the partial pressures of CO and SiO in atmospheres in a closed equilibrium system. $P_{CO}\left(= P_{SiO}\right)$ changes from about 1 torr at 1500°K to 1 atm at 2000°K.

In this same temperature range, the gas-phase species C(g), SiC(g), SiO_2(g), Si_2(g), and Si(g) are all negligible compared with SiO and CO.

Pyrolysis of Hydrocarbons

Our experimental studies have shown that there is a 67% mass yield of very high-boiling, high-molecular-weight, tarry vapors from epoxy novolac. These vapors must undergo further pyrolysis in the hotter parts of the char layer. This conclusion is in accord with observations of density changes in practical heat shields.[46]

---

[45] J. D. Baird and J. Taylor, Trans. Faraday Soc., 54, 526 (1958).

[46] M. Ilmat, "Evaluation of the Thermophysical Properties of the Appollo Heat Shield," Final Report by AVCO Corporation under Contract NAS9-6940 (1967).

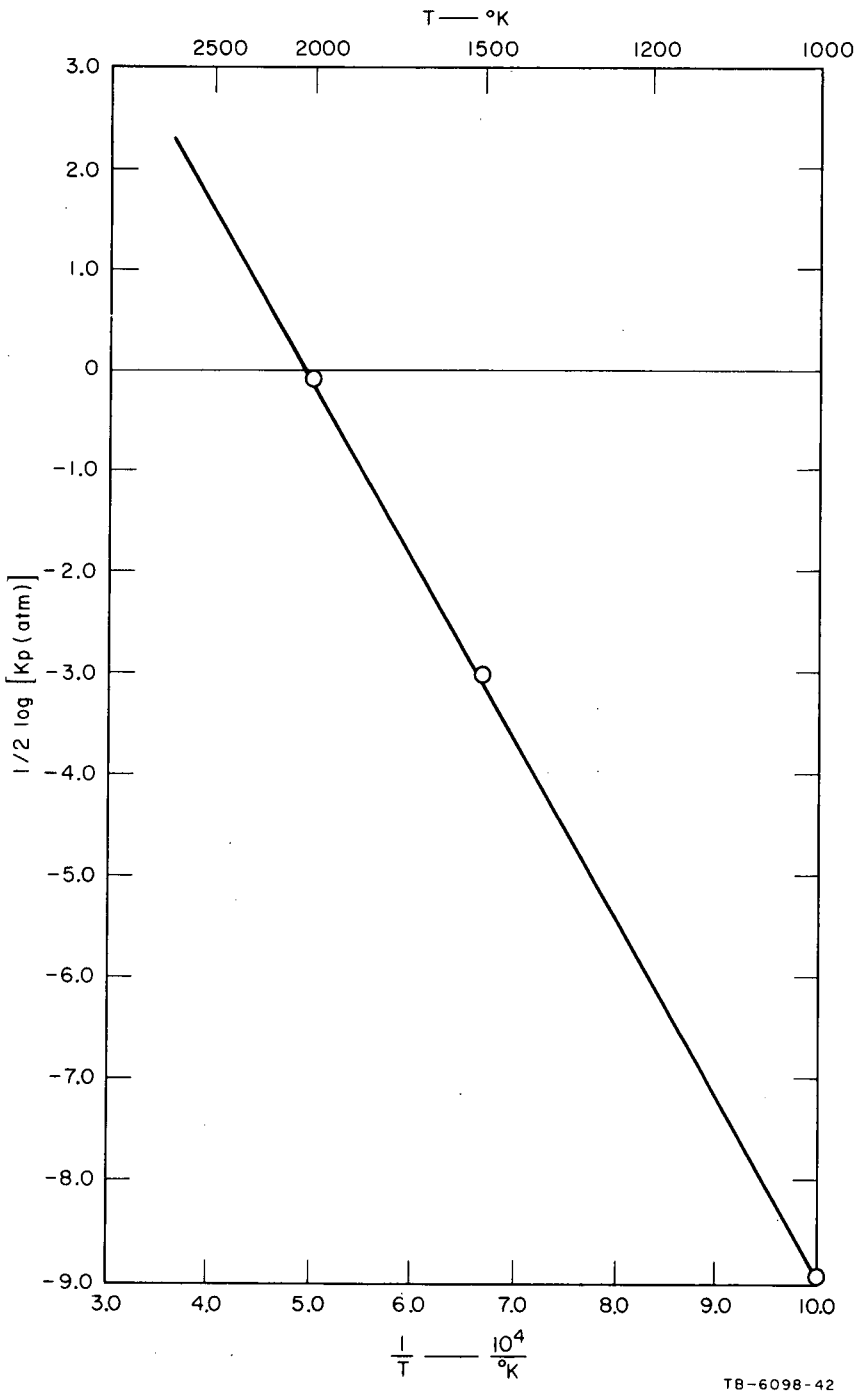

FIGURE 40 VAN'T HOFF PLOT FOR THE REACTION $SiO_2(S) + C(gr) \rightleftharpoons SiO(g) + CO(g)$. ($P_{CO} = P_{SiO} = K_p^{1/2}$.)

We may now put in some numbers relating to hydrocarbon decomposition rate and combine these with a simple model of the char layer to yield further information relevant to char-forming ablative materials.

Assuming viscous flow through the char layer, one can calculate that the flow velocity of the low-molecular-weight gases through the char is about 10^2 cm/sec. This calculation is based on a recession rate of 10^{-2} cm/sec and an estimated porosity of 10%, which gives an estimated residence time of about 10 msec in the char zone. The low-molecular-weight gases will act as a carrier for the high-molecular-weight gases, since the latter constitute less than 10 mole % of the total gas evolution.

We can estimate an upper limit for the stability of aliphatic hydrocarbons and ethers from knowledge of their bond strengths. The Arrhenius parameters for their rates of pyrolysis fall roughly in the same range with A-factors of about 10^{17} sec^{-1}; bond energies are about 80 kcal. At $800^{\circ}K$, the half-life of such molecules is about 1 day, while at $1000^{\circ}K$ it is 2 sec and only $10^{-2.5}$ sec at $1200^{\circ}K$. High-boiling materials are thus not likely to decompose appreciably before they pass the $1000^{\circ}K$ zone; however, at $1200^{\circ}K$ they will decompose to a distance of a few millimeters into the char.

Unsaturated molecules with bonds weakened by allylic or benzylic stabilization will also decompose at rates similar to the saturated molecules. The bond energies in these unsaturated molecules are lower by about 12 kcal/mole, but since this is almost completely compensated for by lower A-factors ($\sim 10^{15}$ sec^{-1}), their net pyrolysis rate at $1000^{\circ}K$ is perhaps 2 to 3 times faster than the saturated aliphatics.

Aromatics with much higher bond strengths ($DH^0 \sim 96$ kcal) will not approach comparable dissociation rates until the temperature is 200^0 higher.

Metathetical reactions with free radicals such as H, CH_3, and OH will compete with unimolecular pyrolysis. We can estimate half-lives, $t_{1/2}(MH)$ of molecules, MH, with respect to such reactions from known rate constants:

$$H + MH \rightarrow H_2 + M^{\bullet} \quad (31)$$

$$CH_3 + MH \rightarrow CH_4 + M^{\bullet} \quad (32)$$

$$OH + MH \rightarrow H_2O + M^{\bullet} \quad (33)$$

$$t_{1/2}(MH + H) \frac{1}{k_{31}(H)}, \quad t_{1/2}(MH + CH_3) \sim \frac{1}{k_{32}(CH_3)}, \text{ etc.}$$

Radical concentration may be calculated from equilibrium data, e.g.,

$$\tfrac{1}{2} H_2(g) \rightleftarrows H(g)$$

$$C(s) + \tfrac{3}{2} H_2(g) \rightleftarrows CH_3(g)$$

Assuming $H_2(g) \sim 0.1$ atm, we can estimate H(g) at 1000^0K as 10^{-11} mole/liter, 10^{-9} mole/liter at 1250^0K, and $10^{-7.3}$ mole/liter at 1500^0K. $CH_3(g)$ will be $10^{-11.5}$ mole/liter at 1000^0K, 10^{-10} mole/liter at 1250^0K, and $10^{-9.2}$ mole/liter at 1500^0K (calculated from JANAF Tables). These values, together with the much larger A-factors for H-atom reactions, favor reaction (31) as the major radical-molecule reaction in the char layer. The concentrations of OH turn out to be much too small, relative to H or CH_3, to be of importance.

At 1000^0K, $t_{1/2}(MH + H)$ for the atomic hydrogen reaction turns out

to be $\sim$ 10 sec; it is about 10^{-3} sec at 1500°K. Thus we see that radical metathetical reactions become important above 1400°K, whereas pyrolysis reactions are important starting at about 1200°K.

The radicals produced by pyrolysis will undergo further very rapid pyrolysis either to produce olefins plus smaller radicals or to react with the char. We have accumulated large amounts of evidence indicating that both of these paths are important.

Radical pyrolyses typically have high-pressure A-factors of 10^{14} sec^{-1} and activation energies of about 40 kcal. At 1200°K the half-life is $\sim 10^{-7}$ sec, and even if it is in its second-order regime, the half-life will still be less than 10^{-4} sec. This means that once a large molecule has undergone an initial unimolecular split, it will rapidly decompose to smaller and smaller fragments to give small free radicals and molecules such as H_2, CO, CO_2, C_2H_2, C_2H_4, and H_2O, and solid carbon.

Radicals probably react with the char by addition reactions to form strong chemical bonds and moieties that can lose H_2, H, or small radicals on further pyrolysis. Small olefins may survive ato 1800°K. Large olefins undergo pyrolytic reactions at lower temperatures, giving rise to allenes or dienes that can add to the char at free radical sites.

The present analyses suggest that further study of the kinetics in the char zone is important if one is to understand and eventually control the stability of the char zone. Our experimental studies show that, at very low pressures, heterogeneous processes can have rates far higher than the normal pyrolysis rates. Further work is needed to evaluate the effects of pressure on reaction rates at temperatures above 1300°K.

The Kinetics of Flame Processes

Most thermal theories conclude that flame velocities are weakly coupled to the kinetics of the flame process. There is an approximate square root dependence of flame speed on rate constants. If we make allowance for the diffusion of free radicals and molecular species across the flame front, we introduce a slightly stronger dependence on the reaction kinetics. In principle, it should be possible to predict flame velocities and the effects of inhibitors from a quantitative knowledge of the kinetics steps in the flame (and preflame) regions. Unfortunately, this knowledge is usually incomplete and seldom quantitative. The largest gaps in our present understanding are those related to the absolute values of the rate constants for bimolecular reactions. In the propane-air flame, to take an example, the initial high-temperature ($> 600^{0}K$) reaction is to produce propylene and H_2O_2.[47]

$$C_3H_8 + O_2 \rightarrow C_3H_6 + H_2O_2 + 3 \text{ kcal}$$

This is approximately thermoneutral and has only a small entropy change (+ 6 gibbs/mole). The driving force for the combustion is provided by the subsequent decomposition of H_2O_2 to H_2O. The overall reaction is:

$$C_3H_8 + \tfrac{1}{2} O_2 \rightarrow C_3H_6 + H_2O + 28 \text{ kcal}$$

The appreciable entropy change (+ 19 gibbs/mole) contributes to the reaction driving force.

[47] R. R. Baldwin, D. E. Hopkins, and R. W. Walker, Trans. Faraday Soc., 66, 189 (1970), and a paper given at a meeting on Oxidation, Liverpool (April 1970).

The propagation mechanism for the reactions is:

$$HO_2^{\bullet} + C_3H_8 \rightarrow \dot{C}_3H_7 + H_2O_2 \quad (34)$$

$$\dot{C}_3H_7 + O_2 \rightarrow C_3H_6 + H\dot{O}_2 \quad (35)$$

$$H_2O_2 + M \rightarrow 2\dot{O}H + M \quad (36)$$

$$HO^{\bullet} + C_3H_8 \rightarrow \dot{C}_3H_7 + H_2O \quad (37)$$

The decomposition of the H_2O_2, which is important in the degenerate chain branching, becomes important only above $800^{\circ}K$, the approximate ignition limit for the system.

The above mechanism leaves open the question of the original initiation source for the system. Above $1200^{\circ}K$ it is most probably the unimolecular pyrolysis of the hydrocarbons. However, once the flame is ignited there will be diffusion current of radicals from the high-temperature region that will tend to maintain a sufficient initiation rate if chain branching occurs as it almost always does in an O_2 system.

The slow reactions in the flame propagation are reactions (34) and (36) above. The rates of these steps will be most important in determining combustion velocities. The rate constant k_{36} has been measured, but k_{34} has not. It will, in addition, be important to try to measure the rate of pyrolysis of the parent hydrocarbon, since this may be of importance in determining the sensitivity of the propane-air mixture to ignition.

The present discussion omits the secondary oxidation of the initial product C_3H_6. This is undoubtedly important, since it gives rise to the very stable allyl radicals and allene, which will tend to inhibit

burning. The VLPP technique is well suited to such studies, and we will try to measure the rates of oxidation of both C_3H_6 and allyl radicals in later studies. Our present efforts are addressed to the parent hydrocarbon pyrolysis and to peroxy radical reactions.

IX CONCLUSIONS AND RECOMMENDATIONS FOR FUTURE WORK

From our studies we have made some qualitative predictions about the chemical behavior of certain types of ablative materials. Future work may be expected to emphasize quantitative aspects of prediction, based on surer knowledge of the chemical profiles in real systems. Of special relevance in future studies will be the role of heterogeneous and free radical reactions of all types. Our experiments have shown that heterogeneous chemical effects can be extremely important at temperatures as low as 1000°K. Future SRI programs for NASA will be directed toward understanding the natures of certain heterogeneous chemical reactions of solids. Quite possibly, these heterogeneous reactions will be initiated by homogeneously formed free radicals. We can now readily predict the basic processes of many types of homogeneous reactions. The world of heterogeneous reactions is, by comparison, one of almost total darkness. For this reason, we believe that future research should give strong emphasis to problems of heterogeneous chemistry.